2016

Pure and Binary Adsorption of Methane and Nitrogen on Silicalite

Prahar S. Vaidya
Cleveland State University, p.s.vaidya@vikes.csuohio.edu

PURE AND BINARY ADSORPTION OF METHANE AND NITROGEN ON SILICALITE

PRAHAR S. VAIDYA

Bachelor of Technology in Chemical Engineering
Gujarat Technological University
May 2012

Submitted in partial fulfilment of requirements towards the degree of
MASTER OF SCIENCE in Chemical Engineering
at the
CLEVELAND STATE UNIVERSITY
May 2016

We hereby approve this thesis

For

PRAHAR S. VAIDYA

Candidate for the Master of Science in Chemical Engineering degree for the

Department of Chemical and Biomedical Engineering

And the

CLEVELAND STATE UNIVERSITY

College of Graduate Studies by

Thesis Chairperson, Dr. Orhan Talu

Department of Chemical and Biomedical Engineering May 3, 2016

Thesis Committee Member, Dr. Dhananjai B. Shah

Department of Chemical and Biomedical Engineering May 3, 2016

Thesis Committee Member, Dr. Jorge E. Gatica

Department of Chemical and Biomedical Engineering May 3, 2016

May 3, 2016

Date of Defense

ACKNOWLEDGEMENTS

Although only my name appears on the cover of this dissertation, a great many individuals have contributed to its existence. I owe my gratitude to all those individuals who have made this dissertation possible and because of whom my graduate experience has been one that I will cherish forever.

First and foremost, I want to thank my advisor Professor Orhan Talu for his patience, guidance, encouragement, and support throughout my time learning under him. I appreciate all his contributions of time, ideas, and funding to make my masters experience productive and stimulating. It has been a pleasure to work under him and I have been amazingly fortunate to have an advisor who gave me the freedom to explore on my own, and at the same time the guidance to recover when my steps faltered. The joy and enthusiasm he has for his research was contagious and motivational for me, even during tough times along with pursuit of masters.

Next, I would like to thank my committee, Dr. Dhananjai B. Shah and Dr. Jorge E. Gatica for their input and critique of my thesis. They provided beneficial contributions to the final draft of my thesis and valuable resources during the writing of my thesis. I thank Dr. Shah for his advice on several technical issues at various stages of this project. Dr. Gatica has been kind to help me with data analysis and I am also thankful to him for encouraging the use of correct grammar and consistent notation in my writings and for carefully reading and commenting on countless revisions of this manuscript. Special mention needs to be made of all my lab mates Matthew, future Doctor Aaron, for their help

in the lab and experimental work. I won't forget to mention few other class mates Josh, Stephen, and Eric, who have helped me stay sane through these difficult years. Their support and care helped me overcome setbacks and stay focused on my graduate study. I greatly value their friendship and I deeply appreciate their belief in me. I am also grateful to the all the faculty and staff of the Chemical and Biomedical Engineering department that helped me adjust to a new country and making the graduate studies at Cleveland State University a pleasant experience.

The financial support in form of graduate research assistantship through the Chemical and Biomedical Engineering department made my graduate studies possible. Ms. Becky Laird and Ms. Darlene Montgomery, department's administrative assistants, were always a great help to get through various administrative hassles at the university. Without their help, this work would not have been completed. Additionally, I wish to thank Mr. David Epperly and Mr. Jim Barker for providing help in necessary improvement to the apparatus.

Most importantly, none of this would have been possible without the love and patience of my family. My family to whom this dissertation is dedicated to, has been a constant source of love, concern, support and strength all these years. Their faith in me was perpetual as many students like me dream to pursue their higher education in United States but most of them fail to fulfil this dream. I would like to express my heart-felt gratitude to my family. I have to give a special mention for the support and encouragement by Urvika Shukla throughout this endeavor.

PURE AND BINARY ADSORPTION OF METHANE AND NITROGEN ON SILICALITE

PRAHAR S. VAIDYA

ABSTRACT

Separation processes comprise a large portion of the activity in the chemical and petrochemical industries. For the chemical, petroleum refining, and materials processing industries as a group, separation processes are considered to be critical. Almost all the applications of chemical industries involves mixtures, so innovation in separation technology not only enhances productivity and global competitiveness of U.S. industries, but is also critical for achieving the industrial energy and waste reduction goals. Traditionally, air separation to produce nitrogen and oxygen and to separate nitrogen from methane was practiced by cryogenic distillation, which involved expensive high pressure units and large requirement of energy.

The separation of nitrogen from methane is becoming increasingly important for upgrading LGF (Landfill gas), coal gas, and natural gas. Natural gases contain significant amounts of nitrogen. From the environmental perspective, Methane is the most important non-CO_2 greenhouse gas responsible for global warming with more than 10 % of total

greenhouse gas emissions. Adsorption separation techniques are used widely among other separation processes as they tend to utilize fewer resources and are highly energy efficient. By considering the advantages of adsorption processes over other separation processes, it is of great interest to characterize the adsorption properties of microporous and nanoporous solid materials for their potential use as an alternative to the conventional catalytic separation process, and storage applications. Despite the advantages of using adsorption for methane upgrading, methane-nitrogen separation has been found particularly difficult because of the lack of satisfactory adsorbent. The equilibrium selectivity favors methane over nitrogen (or high methane/nitrogen selectivity) for all known adsorbents. Therefore, it is one of the objective of this study to check the potential application of silicalite adsorbent in natural gas upgrading.

Plenty of data is available in the literature for pure component but not for the binary mixtures as it is very time consuming and involves tedious calculations for quantifying binary adsorption measurement. According to some statistics, there are more models to predict multicomponent adsorption than accurate data to test them. So the effort made here was to complete measurements of the binary adsorption isotherms, compare those with Ideal Adsorbed Solution Theory (IAST) predictions and the experimental data available in the literature.

This study reviews one of the most commonly used technique (i.e. volumetric measurement) for pure and binary adsorption isotherm measurement for methane and nitrogen on silicalite adsorbent. This method involves measuring the pressure change in a known volume of gas subjected to adsorption. As the gas is adsorbed and allowed to reach equilibrium, the measured decrease in the system pressure yields the amount of gas

adsorbed under the given conditions. Pure adsorption equilibria for the gases listed above was measured at three different temperatures (283.15 K, 308.15 K and 338.15 K). The virial equation of state was used to correlate the experimental data, to calculate the Henry's law constants and the heats of adsorption at zero loading. Ideal separation factor (selectivity) was obtained from the experimental pure adsorption isotherms by using the virial isotherm model. Binary adsorption behavior for methane and nitrogen mixture, covering the whole concentration range at 308.15 °K and at 504 kPa was determined experimentally. The corresponding x-y diagrams and selectivity were obtained from these data. The experimental results were compared with the results predicted from a mixture adsorption model, IAST. It was found that IAST successfully predicted the total amount adsorbed throughout the concentration range. There is a considerable deviation in selectivity as well as partial amount adsorbed for both the species at higher pressure. The reason is attributable to the fact that selectivity is much more sensitive to uncertainties in the measurement.

Keywords: Methane • Nitrogen • Adsorption • Silicalite • Henry's law constant • Heat of adsorption • Binary adsorption Isotherm • Ideal adsorbed solution theory (IAST)

TABLE OF CONTENTS

ABSTRACT v

LIST OF TABLES xiii

LIST OF FIGURES xiv

LIST OF ABBREVIATIONS xviii

CHAPTER I INTRODUCTION 1

1.1 Adsorption 5

1.1.1 History 5

1.2 Zeolite 7

1.2.1 History 8

1.2.2 Composition and Structures 9

CHAPTER II THEORY 12

2.1 Adsorption Fundamentals 12

2.2 Adsorption Thermodynamics 14

2.3 Gibbs Dividing Surface 18

2.4 Phase Rule 22

2.5 Fundamental Property Relations 24

2.6 Solution Thermodynamics and Phase Equilibrium Relations 26

2.7 Gibbs Adsorption Isotherm.....31

2.8 Thermodynamic Consistency and Gibbs-Duhem Equation for Adsorbed Phase.....33

2.9 Pure Component Adsorption Model 34

2.9.1 The Langmuir Model.....35

2.9.2 The Virial Model 36

2.10 Isosteric Heat of Adsorption.....38

2.11 Spreading Pressure Calculation.....40

2.11.1 Pure Component 41

2.11.2 Binary Mixture 42

2.12 Binary Mixture Adsorption Model.....43

2.12.1 Ideal Adsorbed Solution Theory (IAST).....43

CHAPTER III EXPERIMENTAL.....47

3.1 Apparatus 47

3.1.1 Feed/Storage Section.....48

3.1.2 Adsorption/Desorption & Exit Section 50

3.1.3 Bypass and Analysis Section.....52

3.2 Operating Procedure 54

3.2.1 Pre-Experimental Measurements 54

3.2.1.1 Void Volume Determination.....54

3.2.1.2 Gas Chromatograph Calibration 57

3.2.2 Experimental Procedures.....60

3.2.2.1 Column Activation.....60

3.2.2.2 Experimental Protocol for Pure Component Adsorption Isotherm 61

3.2.2.3 Calculating Pure Component Adsorption 62

3.2.2.4 Experimental Protocols for Binary Gas Adsorption Isotherm 63

3.2.2.5 Calculating Binary Absorption Isotherm 64

3.3 Details of Adsorbent 66

3.4 Details of Adsorbates.....68

CHAPTER IV RESULTS AND DISCUSSIONS.....70

4.1 Pure Component Adsorption Isotherms.....71

4.2 Modeling of Pure Component Adsorption Isotherms.....76

4.2.1 Langmuir Adsorption Isotherm Regression Results 76

4.2.2 Virial Adsorption Isotherm Regression Results 79

4.2.3 Comparison between both the Models 82

4.3 Isosteric Heat of Adsorption 84

4.4 Spreading Pressure 85

4.5 Binary Adsorption Isotherm Results 87

4.5.1 Measurement of Binary Adsorption Equilibria 87

4.5.2 Binary Equilibrium Data 88

4.5.3 Analysis of Binary Equilibrium Data 90

4.5.3.1 X-Y Plot 90

4.5.3.2 Variation in Amount Adsorbed With Gas Phase Composition 91

4.5.3.3 Variation in Amount Adsorbed With Equilibrium Gas Phase Pressure 95

4.5.3.4 Variation in Selectivity with Equilibrium Gas Phase Pressure 97

4.5.3.5 Surface Response Plot for Total Amount Adsorbed 98

4.5.3.6 3D Plot for Selectivity 100

4.5.3.7 Variation in Selectivity with Equilibrium Gas Phase Composition 101

4.5.3.8 Thermodynamic Consistency.....102

4.6 Literature Review and Comparison 105

CHAPTER V SUMMARY AND CONCLUSIONS 113

5.1 Pure Component Adsorption Equilibrium Measurements Using Volumetric System.....113

5.2 Binary Adsorption Equilibrium Measurements Using Volumetric System 114

REFERENCES 116

APPENDIX.....122

APPENDIX A Error Analysis and Uncertainties in Primary Data Measurement 123

APPENDIX B Calibration Data for Gas Chromatograph 124

APPENDIX C Matlab Code for Binary Prediction from IAST.....125

LIST OF TABLES

Table 3.1	Experiments performed using the volumetric system	47
Table 3.2	Inside volume of different sections	56
Table 3.3	Temperature dependency of second virial coefficient for various gases	68
Table 3.4	Physical properties of gases	69
Table 4.1	Experimental adsorption isotherm data for methane on silicalite	73
Table 4.2	Experimental adsorption isotherm data for nitrogen on silicalite	74
Table 4.3	Uncertainty in pure component adsorption isotherms obtained from volumetric system	75
Table 4.4	Langmuir parameters for methane, nitrogen on silicalite	77
Table 4.5	Virial parameters for methane and nitrogen on silicalite	79
Table 4.6	Comparison of Residual Sum of Square Error for two different regression models	83
Table 4.7	Binary equilibrium data for CH_4 + N_2 mixture on silicalite at 308.15 K	89
TABLE B.1	Results of GC Calibration for CH_4+N_2 Mixture on Silicalite	124

LIST OF FIGURES

Figure 1.1 Relative energy use by various separation processes 2

Figure 1.2 Secondary building unit 10

Figure 1.3 Sodalite unit with Si, Al atoms 11

Figure 1.4 (a) Zeolite A (b) Faujasite-type zeolite X and Y formed by sodalite cages 11

Figure 2.1 The potential energy between two atoms separated by distance r 14

Figure 2.2 The six main types of gas Physisorption isotherm, according to IUPAC classification 16

Figure 2.3 Density profiles next to a solid surface 19

Figure 2.4 Illustration of density profiles and the Gibbs dividing surface near a flat surface 21

Figure 2.5 Calculation of mixture adsorption equilibria from pure component spreading pressures 46

Figure 3.1 Feed/storage Section 49

Figure 3.2 Adsorption/ Desorption & Exit section 51

Figure 3.3 Bypass/ Analysis section 53

Figure 3.4 K-factor for methane changes with its area fraction 59

Figure 3.5 Ramp and soak implemented by temperature controller 60

Figure 3.6 Framework topology of ZSM-5. The 5-ring polyhedron is connected into chains which form the ZSM-5 structure with the 10-membered openings of the linear channels 66

Figure 3.7 Idealize channel system in silicalite 67

Figure 4.1 Methane adsorption isotherms on silicalite 71

Figure 4.2 Nitrogen adsorption isotherms on silicalite 72

Figure 4.3 Model Predictions and Experimental Data for Pure methane 78

Figure 4.4 Model Predictions and Experimental Data for Pure nitrogen 78

Figure 4.5 Virial Regressions and experimental data for Pure methane 80

Figure 4.6 Virial Regressions and experimental data for Pure nitrogen 81

Figure 4.7 Isosteric heat of adsorption for CH_4, N_2 on silicalite 85

Figure 4.8 Spreading pressure of methane & nitrogen on silicalite at 308.15 K 86

Figure 4.9 X-Y plot of CH4 + N2 mixture at 308.15 K and 504 kPa.....91

Figure 4.10 Total amount adsorbed with gas phase mole fraction of methane at 308.15 K 92

Figure 4.11 Amount adsorbed in terms of methane with change in gas phase mole fraction of methane at 308.15 K 94

Figure 4.12 Amount adsorbed in terms of nitrogen with change in gas phase mole fraction of methane at 308.15 K 94

Figure 4.13 Variation in total amount adsorbed with change in gas phase pressure at constant composition and temperature 95

Figure 4.14 Partial amount adsorbed of Methane with change in partial pressure at constant composition and temperature 96

Figure 4.15 Partial amount adsorbed of nitrogen with change in partial pressure at constant composition and temperature 96

Figure 4.16 Selectivity in terms of methane with the change in pressure 97

Figure 4.17 Change in total amount adsorbed with gas phase pressure and composition for CH_4+N_2 mixture in silicalite at 308.15 K 99

Figure 4.18 Change in selectivity with gas phase composition and pressure for CH_4+N_2 mixture in silicalite at 308.15 K 100

Figure 4.19 Selectivity in terms of methane with the change in gas phase composition 101

Figure 4.20 The integrand in spreading pressure calculations for binary adsorption at constant composition and temperature 103

Figure 4.21 The integrand in spreading pressure calculations for binary adsorption at constant pressure and temperature 104

Figure 4.22 Pure methane adsorption isotherms on silicalite and comparison with literature data 106

Figure 4.23 Pure nitrogen adsorption isotherms on silicalite and comparison with literature data 108

Figure 4.24 Amount adsorbed with change in gas phase composition data and their comparison with Tezel et al. [37].....110

Figure 4.25 X-Y diagram and comparison with Tezel et al. [37].....111

Figure 4.26 Selectivity Vs Gas phase mole fraction and comparison with Tezel et al. [37].....111

LIST OF ABBREVIATIONS

A	Specific are of adsorbent, m^2kg^{-1}
a	Specific area of adsorbent per mole of adsorbate, m^2 mol^{-1}
$\%A_i$	Percentage area obtained for methane
B	Langmuir parameter, kPa^{-1}
B_i	Second virial coefficient for gas species i, cc mol^{-1}
B_{i-j}	Cross virial coefficient cc mol^{-1}
B_{mix}	Second virial coefficient for gas mixture, cc mol^{-1}
C	Number of Chemical Species
C_i	Third virial coefficient kg^2 mol^{-2}
D_i	Fourth virial coefficient, kg^3 mol^{-3}
F	Number of thermodynamic freedom
f_i^o	Fugacity of species i at its standard state, kPa
$\hat{f}_i$	Fugacity of the species i in the adsorbate mixture, kPa
$\widehat{f_i^g}$	Fugacity of the species i in the bulk gas phase, kPa
g	Molar Gibbs' free energy j mol^{-1}
${g_i}^0$	Gibbs' free energy of species i at its standard state (same T and spreading pressure as that of the mixture), J mol^{-1}
$\bar{g}_i$	Partial molar Gibbs' free energy of species i in the adsorbate mixture, J mol^{-1}
$\bar{g}_i^{id}$	Partial molar Gibbs' free energy of species i in an ideal adsorbate mixture, J mol^{-1}

q	Limiting isosteric heat of adsorption, kJ mol^{-1}
H	Henry's law constant
$K - Factor$	K-factor for GC analysis
L	Distance from solid surface where adsorbed phase density is equal to bulk-gas phase density, m
M	Molar thermodynamic property, m
m	Mass of the solid
$V_{unknown}$	Unknown volume in helium expansion experiments, cc
V_{known}	Known inside volume of different sections in experimental section, cc
x_i	Adsorbed phase mole fraction of species i
y_i	Gas phase mole fraction of species i
z	Distance from solid surface, m
Z	Compressibility factor for the adsorbed phase

GREEK LETTERS

$S_{1,2}$	Selectivity of the adsorbent for species 1 over species 2
μ_i	Chemical potential of species i in adsorbed phase, J mol-1
$\mu_i{}^g$	Chemical potential of species i in gas phase, J mol-1
Γ^{abs}	Absolute amount adsorbed per unit area of adsorbent, mol m-2
Γ^{ex}	Excess amount adsorbed per unit area of adsorbent, mol m-2

ψ	Reduced spreading pressure, mol kg-1
γ_i	Activity coefficient of species i in the adsorbed phase
χ	Number of phases
μ	Chemical potential, J mol-1
μ_i	Chemical potential of species i, J mol-1
π	Spreading pressure, N m-1
υ	Molar volume of the gas, cc mol^{-1}

CHAPTER I

INTRODUCTION

This chapter briefly explain, what is adsorption? Advantages of adsorption, History of adsorption, difference between Physical adsorption and chemisorption, history of zeolite.

Separation processes comprise a large portion of the activity in the chemical and petrochemical industries. For the chemical, petroleum refining, and materials processing industries as a group, separation technologies are critical for improving energy efficiency. Almost all the applications of chemical industries involves mixtures and therefore Separation processes crosscut all manufacturing industries and account for approximately 4,500 trillion Btu/yr. (TBtu/yr.), or about 22% of all in-plant energy use in the United States. Innovations in separation technologies not only enhance productivity and global

competitiveness of U.S. industries, but also critical for achieving the industrial energy and waste reduction goals [4].

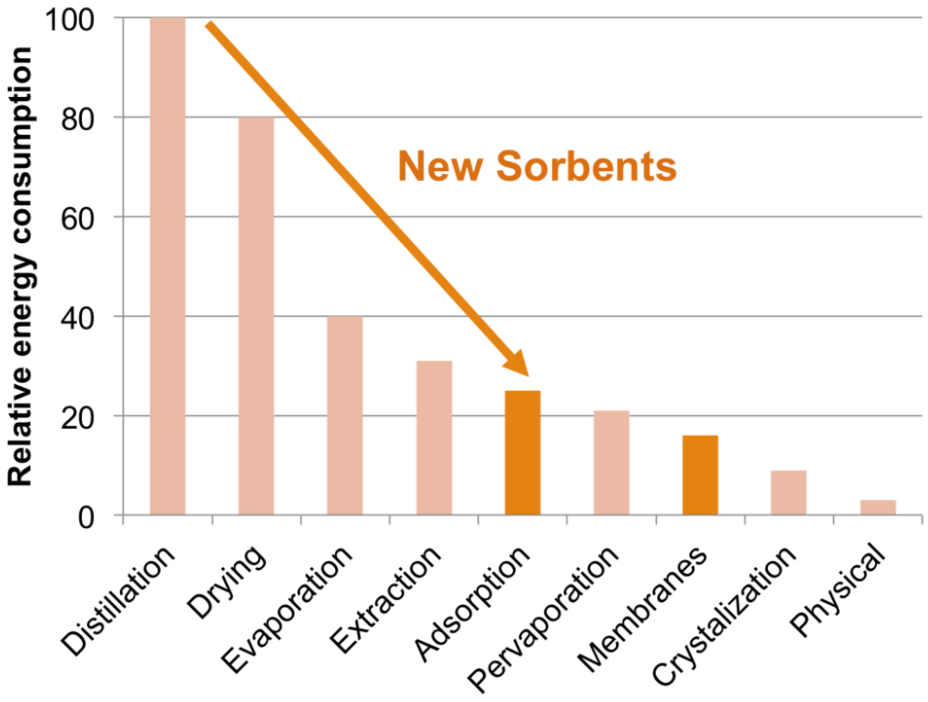

Figure 1.1. Relative energy use by various separation processes [67]

As described by the Figure 1.1 industrially well-established separation techniques like distillation, evaporation and drying technologies requires high energy. They are thermally driven (based on the heats-of-vaporization of the components) and respectively account for 49%, 20%, and 11% of the industrial separations energy consumption. Extraction, absorption, adsorption on the other hand are physical property-based operations and tend to utilize fewer resources including energy, below 3% of industrial separation consumption and are highly efficient [4]. The unique advantage of adsorption is the selectivity that can be manipulated by adsorbent solid. Therefore it is of great interest to characterize the adsorption properties of microporous and nanoporous material.

From the environmental perspective, Methane is the most important non-CO_2 greenhouse gas responsible for global warming with more than 10 % of total greenhouse gas emissions. Which has a detrimental effect on the ozone layer in the atmosphere and therefore it has a major contribution to global warming of our planet. Despite the small amounts of methane released to the atmosphere, the greenhouse warming potential of this gas is much higher than that of carbon dioxide (approximately 20% more potent by weight than carbon dioxide), so any reduction in methane emissions is very important in atmosphere reconstruction [8, 9].

The separation of nitrogen from methane is becoming increasingly important for upgrading LGF (Landfill gas), coal gas, and natural gas. Natural gases contain significant amounts of nitrogen. To be able to use it as an alternative to the fossil fuel and in order to meet the pipeline quality for minimum heating value specifications (typically 950 BTU/ft^3 or < 4% inert for US pipeline specifications), it must be upgraded in terms of methane. This is the situation with majority of natural gas reserves in United States. Different sources have reported that around 14% (or about 19 trillion cubic feet) of known reserves in the US are sub-quality due to high nitrogen content and needs upgradation. Effectively capturing methane from landfill gas can reduce the factors affecting human being and can be used as a major fossil fuel alternative [8, 31, 45]. Methane being primary component of landfill gas and if uncontrolled, this gas can cause nuisance odors, stress on vegetation, smog, risk of fire/explosion, and health and safety concerns because of methane content. In 2013, the methane produced by United States landfill sites contains enough energy in the range of 16 billion kilowatt-hours (depending on the composition) which is capable of powering 1,180,000 homes & heating 746,000 homes a year. This effort can save CO_2

emissions from 253 million barrels of oil or 12.2 billion gallons of gasoline consumed. In 2013 United States have around 621 operating projects of landfill gas from which 22 are in Ohio [67].

In case of enhanced oil recovery where nitrogen is injected into the reservoir increases the level of nitrogen contamination in the natural gas (or petroleum gases) recovered from the reservoir above the naturally occurring concentration. Another application for this separation is the recovery of methane from coalmines where nitrogen concentration is also high. Typically, the low-quality natural gas obtained from coal has contamination of nitrogen around 20% needs to be upgraded to 5–10% nitrogen. The only technology that is being mostly used for nitrogen removal from methane till date is cryogenic distillation, which is highly energy-intensive and costly. The combined costs of liquefaction and subsequent re-compression of the low pressure product make this an expensive process. It is economical only for large, highly contaminated gas. Since a high feed pressure is already available, pressure swing adsorption (PSA) is considered as a potential technology. Separation by PSA can be accomplished in either equilibrium or kinetic method [31, 71]

Despite the advantages of using adsorption for methane upgrading, this separation has been found particularly difficult because of the lack of satisfactory adsorbent. Potential adsorbent needs to have high nitrogen/methane selectivity. The equilibrium selectivity favors methane over nitrogen (or high methane/nitrogen selectivity) for all known adsorbents, such as activated carbon, silica gel, activated alumina, large-pore zeolites and molecular sieves. That is why the development of such adsorbents and its adsorption property is desirable.

1.1 Adsorption

Adsorption is defined as a process in which a fluid, when exposed to a solid substance, tends to be attracted by its particles. So fluid density near the vicinity of solid interface increases as we move closer to the solid-fluid interface. In this process solid called adsorbent, and the adsorbed fluid on the solid surface is called adsorbate and bulk fluid phase that is in contact with solid is called adsorptive.

1.1.1 History

The phenomena of adsorption was first discovered by Scheele in 1773. The ability of charcoal to remove colors of tartaric acid solutions was first investigated by Lowitz in 1785 [39, 40]. Systematic studies of adsorption and exothermic nature of adsorption was noted by De Saussure started in 1814 [15, 16]. He came to the conclusion that all types of gases are taken up by porous substances sea-foam, cork, charcoal, asbestos, and this process is accompanied by the evolution of heat. Thus, he discovered the exothermic character of adsorption processes, and he was the first to pay attention to the commonness of adsorption. The term ‘adsorption’ was proposed by du Bois-Reymond but introduced into literature by Kayser [29, 30]. During the next few years, the terms ‘isotherm’ and ‘isothermal curve’ were used to describe the results of adsorption measurements at constant temperature. Kayser also developed some theoretical concepts which became basic for the

monomolecular adsorption theory. Some more investigation studies of slower uptake of hydrogen by carbon were reviewed by J. W. McBain [13, 14, 44].

Now Adsorption occurs due to two major underlying Mechanism and fundamental difference between these two is the existence of electron transfer which results in chemical bonds.

I. Physisorption: Also known as physical adsorption, this phenomena occurs due to forces involved in physical adsorption are Van Der Waals forces (dispersion-repulsion) and electrostatic forces between guest molecule (adsorbate fluid) and adsorbate solid surface.

II. Chemisorption: The forces involved in chemisorption are similar to those in chemical species. It is characterized by formation of surface compounds in various stoichiometric ratios due to formation of chemical bonds.

Contrary to Physisorption, chemisorption occurs only as a monolayer. In Physisorption the entire solid surface available, while Chemisorption occurs at active sites which can form a chemical bond with guest molecules. Physical adsorption can be compared to the condensation process of the adsorptive and it is a reversible process that occurs at all temperature. Chemisorption occurs usually at temperatures much higher than the critical temperature. Under favorable conditions, both processes can occur simultaneously or alternately. Physical adsorption is accompanied by a decrease in free energy and entropy of the adsorption system and, thereby, this process is exothermic. Physisorption is rather small at low partial pressure and large at high partial pressure. The total amount of material adsorbed in Physisorption is high. Whereas, Chemisorption is large at low partial pressure and increasing slightly with increasing partial pressure and

total amount adsorbed in Chemisorption per weight of material is low. Physisorption has low heat of adsorption in range of 1/3 to 1/2 times of total latent heat of evaporation. While in Chemisorption it is ranging between 2 to 3 times of latent heat of evaporation. This work concentrates on Physisorption only.

1.2 Zeolite

An Adsorption process to be developed on a commercial scale requires availability of suitable adsorbent with large surface area per mass and most importantly at a reasonable lower cost so out total cost of operation will remain in a profitable range. This stimulated fundamental research in the field of adsorption which led to development of novel adsorbents. Only four types of generic sorbents have dominated the commercial use of adsorption: activated carbon, zeolites, silica gel, and activated alumina [27, 70].

A commercial adsorbent should have following qualities: availability in large scale, high selectivity, high capacity for the gases for which are going to get processed, ability to regenerate and reusable, chemically inert, low cost etc. Characteristics of the adsorbate-adsorbent pairs and selection of the appropriate working pair are the most important task of the adsorption. Adsorbents are characterized first by surface properties such as available surface area and polarity.

1.2.1 History

A Swedish scientist named by Baron Cronstedt about 200 years ago in 1756 came up with a name “ZEOLITE”. The name actually came from Greek, Zeo, to boil, and Lithos, a stone. Natural occurring zeolites usually contain impurities and an irregular chemical composition that limit their usefulness as industrial application. In 1905 in Germany, a synthetic zeolite with a larger capacity compared to natural zeolites was manufactured, which allowed for the first commercial use of zeolites as water softener. Two years later also in Germany, natural zeolites were used to create the first “self-acting” laundry detergent. By 1945, Richard Barrer classified zeolite minerals into three classes depending on the size of the molecules which can adsorb rapidly, slowly, or not appreciably at room temperature or above. However, zeolites did not find any significant commercial use until Mordenite, a synthetic zeolites was discovered and developed by him in 1948 by means of high temperature and pressure. From 1949 through the early 1950s, the commercially significant zeolites A, X, and Y, were synthesized from readily available raw materials at much lower temperature and pressure. Linde Air Products Division of Union Carbide Corporation in 1960’s perfected synthesis of X and Y zeolites which have larger pore size than most of the known natural zeolites, which allowed the use in processing larger molecules. In addition, they had larger pore volume which gives higher capacity [42, 70, 71].

1.2.2 Composition and Structures

Zeolites are porous crystalline aluminosilicates of alkali and alkali earth metals such as sodium, potassium, and calcium. The zeolite framework consists of an assemblage of SiO_4 and AlO_4 tetrahedral joined together through the sharing of oxygen atoms. This will create an open crystal lattice containing pores of molecular diameter into which guest molecule can penetrate. Zeolites differ from other adsorbents because their uniform crystal lattice provides a well-defined pore size for molecules to travel through while also allowing them to act as effective molecular sieves. The stoichiometry of zeolite assembly can be represented as below,

$$M^{x}/_{n}[(AlO_2)_x((SiO_2)_y]zH_2O \quad (1.1)$$

Where x and y are integers with y/x ratio equal or greater than 1 but there is no upper limit, n is the valance of cation M, and z is the numbers of water molecules in each unit cell. Each aluminum atom introduced one negative charge on the framework which must be balanced by exchangeable cation. If the framework structure of zeolite remains constant, the cation exchange capacity is inversely related to Si/Al ratio. A lower Si/Al ratio gives a higher cation exchange capacity and increases the zeolites ability to adsorb polar molecules such as water. Examples of commonly used exchangeable cations include the ions Na^+, K^+, and Ca^{2+}. The type and size of the exchangeable cation determines the pore size and properties of the zeolite. Fine-tuning of adsorptive and catalytic properties can be achieved by the adjustment of size and valence of the exchangeable cation. The adsorption property shows a systematic transition from the aluminum rich sieves, which

has very high affinity for water and other polar molecules, to the microporous silicalite which is an aluminum free for of zeolite which are essentially hydrophobic and suitable for removal of organic molecules from aqueous solution and from moist gases.

The structure of zeolite are built up from the assemblages of secondary building units (SBU's), which are polyhedral made up of several SiO_4 and AlO_4 tetrahedral. These secondary units are linked in 3-D space to create a porous crystalline structure. Secondary building units and some of the commonly occurring polyhedral, shown in the Figure 1.2, illustrate silicon and aluminum atoms at the apices with lines representing oxygen bridges between them that show the diameter of an oxygen atom.

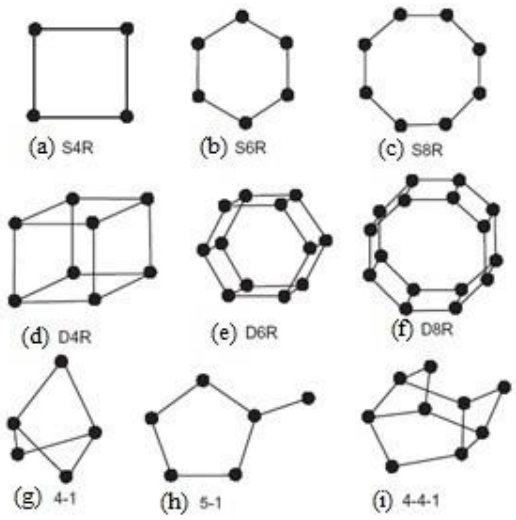

Figure 1.2. Secondary building unit [11]

Sodalite unit shown in Figure 1.2 formed from S4R and S6R units joint with each other in 3-D space (Figure. 1.2. (a) and Figure.1.2. (b) respectively). Eight sodalite (β cages) units form the eight-membered oxygen ring of Type A zeolites and are connected by D4R units (Figure. 1.2. (d)) with the final crystal shown in Figure 1.4. (a). Ten sodalite units organized in a different fashion in 3-D space form the twelve-membered oxygen ring

of Type X and Y zeolites (Figure: 1.4. (b)) and are connected by D6R units (Figure 1.2.(e)). The Si/Al ratio is what differentiates Type X and Y zeolites as Type X zeolites have a ratio between 1 and 1.5, while Type Y zeolites have a ratio between 1.5 and 3.

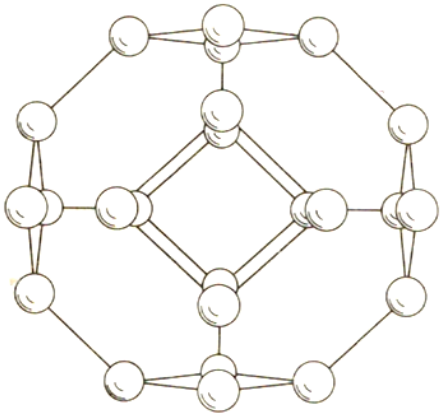

Figure 1.3. Sodalite unit with Si, Al atoms [61]

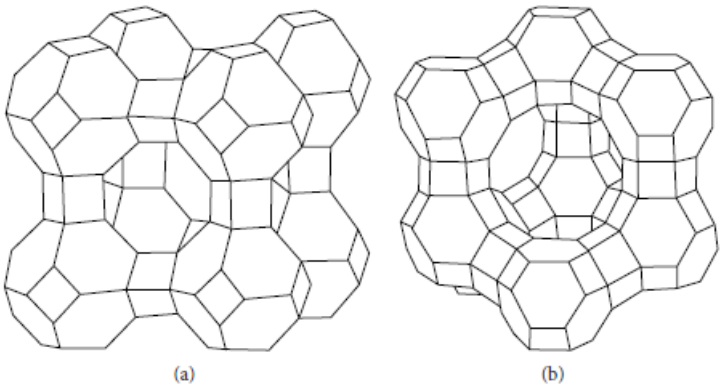

Figure 1.4. (a) Zeolite A (b) Faujasite-type zeolite X and Y formed by sodalite cages [41]

Till date more than 150 synthetic zeolite types are known. Types A and X are synthetic mordenite and their ion-exchanged varieties are most important commercially used zeolites. Of the 40 or so naturally occurring zeolites the most important commercially used are chabazite, faujasite and mordenite. Specifics about the adsorbent used in this study is discussed in Chapter III [19, 49, 56, 58, 71].

CHAPTER II

THEORY

The literature pertaining to the sorption of gases by solids is now so vast that it is impossible for any, except those who are specialists in the experimental technique, rightly to appraise the work, which has been done, or to understand the main theoretical problems which require elucidation.

– J. E. Lennard-Jones, 1932 [36]

2.1 Adsorption Fundamentals

As explained in previous chapter Adsorption is accumulation of fluid molecules at a surface. This accumulation is because of attraction between adsorbent and adsorbate molecules is a due to intermolecular interactions, which are caused by a combination of permanent dipoles, permanent quadrupoles, induced dipoles, and London dispersion forces. Permanent dipoles occur in polar molecules as a result of uneven distribution of

charge in the electron cloud. The best example for this phenomena is adsorption of ammonia & water on Zeolite NaX as they both possess large dipole moment [20]. Polar molecules can also induce an uneven charge distribution (i.e. polarity) in nonpolar molecules if they are close enough to interact for example, methane has no dipole moment but when subjected to electric field it gets polarized. Nonpolar molecules do not have permanent poles when their charge is averaged over time. However, at any moment they will have a dipole due to instantaneous location of electrons that has the potential of inducing a dipole on another nonpolar molecule, creating London Dispersion forces. Repulsion forces occur when molecules are too close to each other and their electron clouds start overlapping with each other. When adsorption occurs, there is equilibrium between these repulsion forces and the forces of attraction. As illustrated in Figure 2.1, potential energy diagram for adsorption that shows potential energy (sum of all the interactions that exist between the adsorbate fluid and adsorbent solid) as a function of the distance of the adsorbate molecule from the adsorbent surface. The high positive repulsive potential energy near the adsorbent surface is where the electron cloud overlap would occur. The depth of the potential well, U, is dependent on density and crystal structure of the adsorbent and the polarizability and molecular size of the adsorbate. In other words it will reflect how attractive the adsorbate is to the surface of adsorbent. The larger the potential energy difference, the greater the adsorbate would be attracted to the surface. At zero Kelvin where there is no kinetic energy, a molecule would settle at the bottom of the well. At all other finite temperatures, the molecule will oscillate around the minimum potential energy and occasionally escaping to the bulk phase from the surface where, by definition adsorption potential is zero [52, 56, 66, 71].

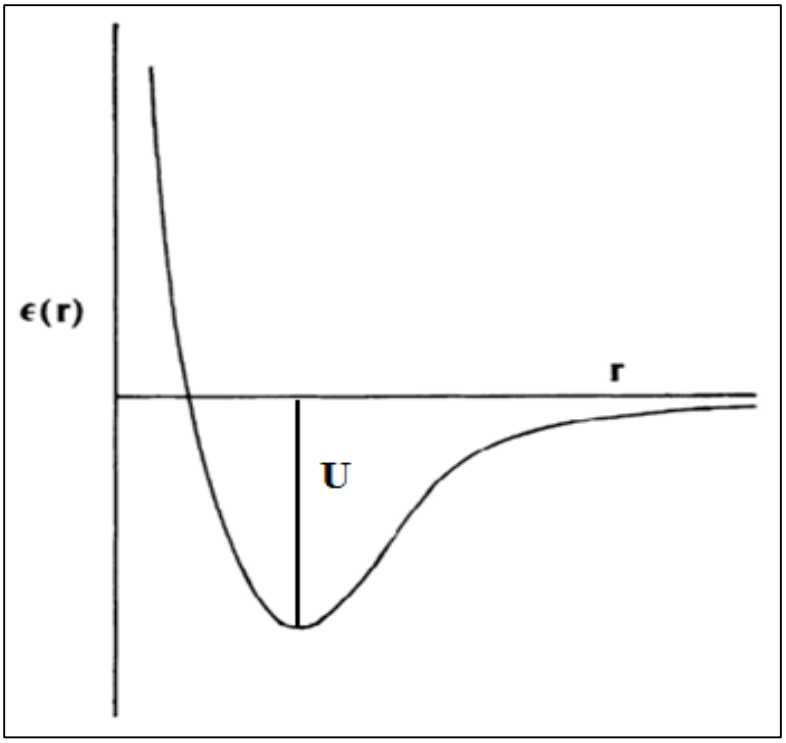

Figure 2.1.The potential energy between two atoms separated by distance r [71]

2.2 Adsorption Thermodynamics

The amount of gas adsorbed, n^a, for given mass of solid, m^s, is dependent on the equilibrium pressure, *P*, temperature, *T*, the nature of the Solid-Gas System. Thus we can write;

$$n^a/_{m^s} = f(P, T, gas - solid\ system) \tag{2.1}$$

For a given adsorbate molecules on a particular solid at a constant temperature we can write the adsorption isotherm equation as;

$$n^a/_{m^s} = f(P)_{T,gas-solid\ system} \tag{2.2}$$

If the gas is below its critical temperature, isotherm is usually shown as reduced pressure as;

$$n^a/_{m^s} = f\left(P/_{P^0}\right)_T \tag{2.3}$$

Where, the standard pressure P^0 is the saturation vapor pressure of the adsorptive at *T*. Equations (2.2) and (2.3) represent the adsorption isotherm which is a relationship between the amount adsorbed by unit mass and the equilibrium pressure or relative pressure, at known constant temperature. The experimental adsorption isotherms are presented in a graphical form. Although experimental adsorption isotherms measured on wide variety of gas-solid systems, display a very wide range of forms, but the majority of the isotherms which results from physical adsorption may be grouped into six categories in IUPAC classification. The first five types (I to V) of classification were originally proposed by Brunauer et al. [7] and also referred as Brunauer classification (1945). The IUPAC 1985 classification of physisorption isotherms are shown in Figure 2.2 below,

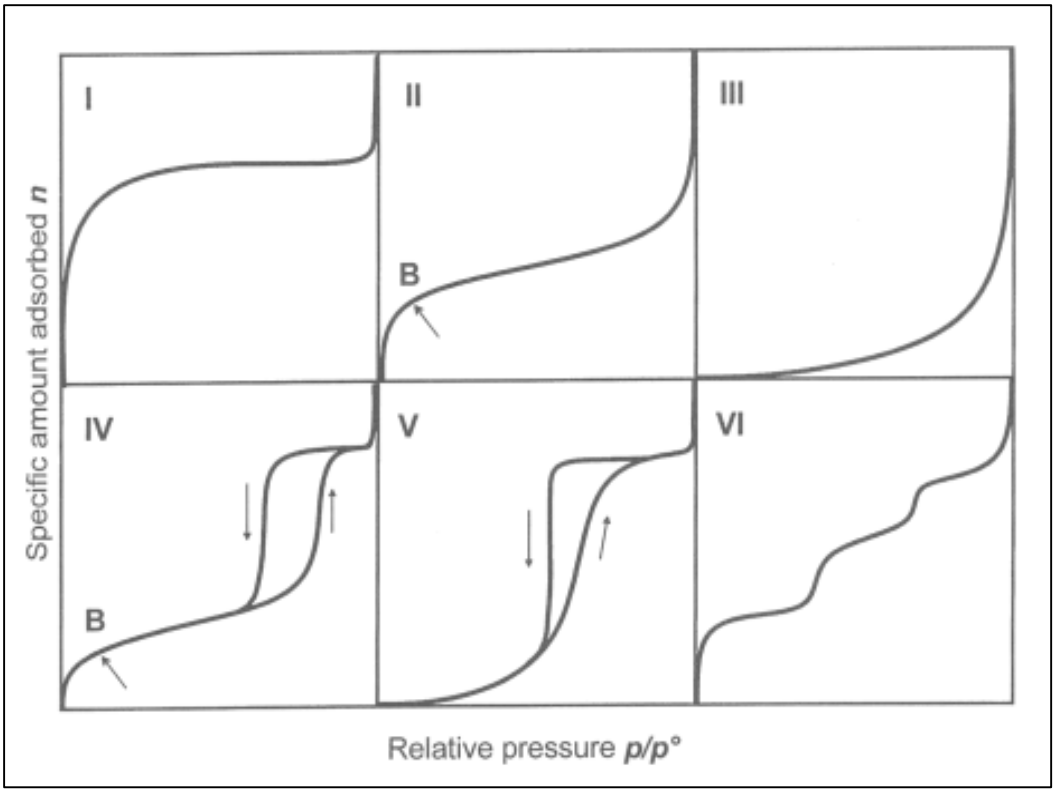

Figure 2.2. The six main types of gas Physisorption isotherm, according to IUPAC classification [55]

Type I, most commonly observed isotherm shapes is concave to the relative pressure axis. It rises sharply at low relative pressure and reaches a plateau. The amount adsorbed for unit mass of solid approaches limiting value as $P/P^0 \rightarrow 1$ due to finite capacity of micropore solid. They are characteristic of microporous solid in which pores are no more than a few molecular diameters in width and they cannot accommodate more than a single layer on their walls and thus plateau corresponds to the completion of the monolayer. From Type I isotherm we can estimate the total micropore volume. The Type II isotherm is also concave to the pressure axis and then almost linear and finally convex to pressure axis which is a result of formation of a second adsorbed layer whose thickness increases

progressively with increase in relative pressure until $P/P^0 \rightarrow 1$. It indicates that the solid is non-porous. From Type II isotherm of a given gas-solid system, it is possible to calculate monolayer capacity of the solid, which in turn used to derive the value of specific surface area [23]. Type III isotherms is convex to the pressure axis over the complete range. The uptake at relatively low pressure is small due to the fact that the adsorbate-adsorbent forces are weak but once a molecule has become adsorbed, the adsorbate-adsorbate forces will promote the adsorption of the further molecules. Occurrence of this type of isotherm is somewhat uncommon. Type IV isotherm, whose initial region is very similar to Type II isotherm, tends to level off at higher relative pressure. It exhibits a hysteresis loop. The lower branch of loop represents measurement obtained by progressive addition of gas and upper region represents the withdrawal. This behavior is because of filling and emptying the mesopores of adsorbent solid by capillary condensation, which is a phenomena occur in the smaller pores where vapor will be able to condense to liquid due to lower equilibrium vapor pressure (P) than saturation vapor pressure ($P°$). Mesopore range of pore size is usually taken to be that range which gives rise to a type IV isotherm. Type V isotherm is initially convex to pressure axis and level off at higher relative pressure which is similar to the Type III isotherm in a way of weak interaction between adsorbate-adsorbent and similar to Type IV isotherm in a way of filling & emptying the mesopores because of capillary condensation. This is the rarest observed pattern. Type VI isotherm, sometimes called stepped isotherm is a result of layer by layer adsorption on highly uniform surface [55].

When a gas (adsorbate) in contact with solid (adsorbent), its density is not uniform near the vicinity of the solid. The density and composition profile of the adsorbed phase in microporous solid can't be directly measured by any experimental method. It is not

possible to clearly identify the distance from the surface where the density is equal to the bulk gas phase. Gibbs developed a hypothetical two-dimensional mathematical surface which divides the adsorbate and the adsorptive [5, 25, 62].

2.3 Gibbs Dividing Surface

The adsorb phase properties can only be measured as a difference between pure solid in the absence of any surrounding fluid. Amount adsorbed is absolutely zero when there is no fluid surrounding the solid by definition. But some other property like chemical potential of the solid is not zero. Because of this reason the change in total thermodynamic properties are always in the form of a difference with the pure solid as a reference state. Adsorbed phase is also not autonomous. It can only exists in an equilibrium with its bulk fluid phase [2]. The interfacial region is in dynamic equilibrium with the fluid phase and there is a constant exchange of molecules between the interfacial region and the bulk fluid phase. The density close to the solid surface is not uniform as illustrated in Figure 2.3. From the given Figure 2.3 some of the observations that we can make are as followed [5, 25, 62]:

1. The disturbances in density decay to mean fluid density at a distance sufficiently far away from the surface,
2. The actual distance, denoted by “L” where the density decays to fluid density is not known and/or clearly defined,

3. This distance depends on thermodynamic properties of the system such as pressure, and temperature. The value of L increases as the bulk fluid density increases at constant temperature. It also decreases with increasing temperature.

4. The density profile indicates layering of molecules, it means the density is not necessarily higher than bulk fluid at all locations. The density between layers can be actually lower than the bulk fluid density.

5. The density is highest in the first layer if the fluid wets the surface,

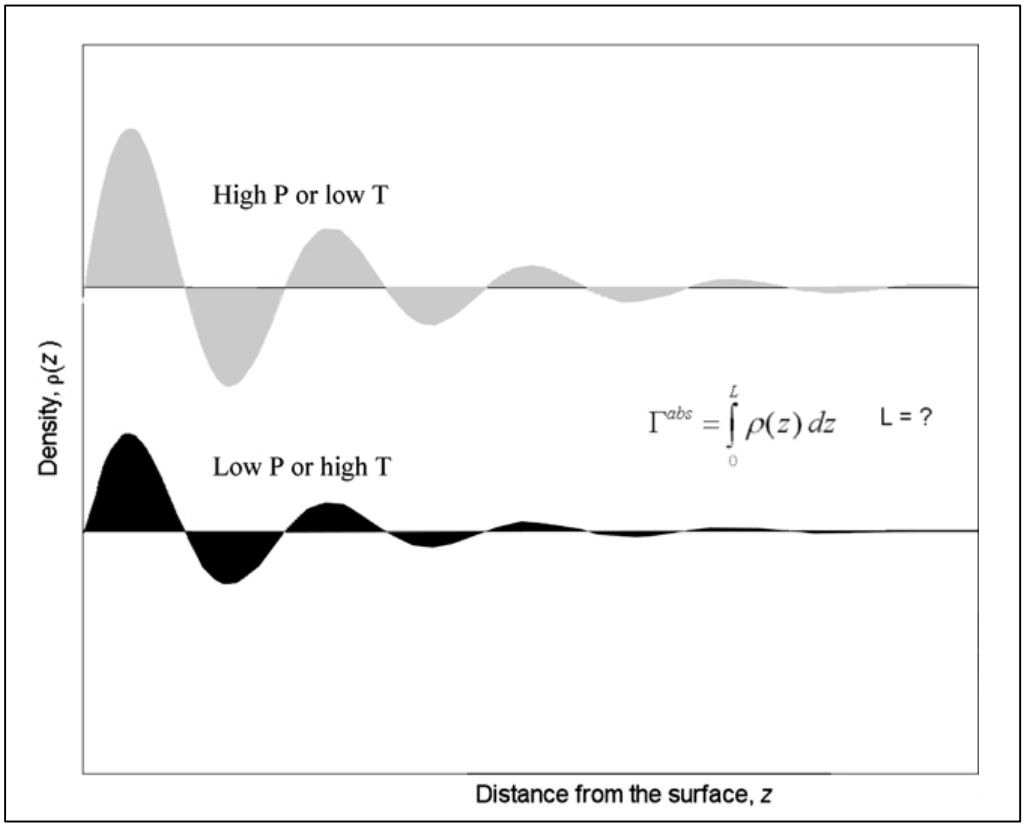

Figure 2.3. Density profiles next to a solid surface [24, 62].

Considering these observations, it is impossible to estimate the “absolute” amount adsorbed, which is defined in literature as the area under the density profile [62]. On a unit area basis the absolute amount adsorbed is defined as,

$$\Gamma^{abs} = \int_0^L \rho(z)\, dz \tag{2.4}$$

Here, $\rho(z)$ is the density of the gas at any distance z from the interfacial surface. L is the distance from the surface when density of the gas is equal to the density of the bulk fluid density. In Equation (2.4) the upper limit for integration L is not clearly defined. Furthermore, L is a function of temperature and pressure, which complicates the use of absolute amount adsorbed definition.

Understanding these difficulties, Gibbs (1928) [21] was first to formalize a thorough thermodynamic treatment of adsorption phenomena. His mathematical transformation relies upon the meaning of a "Dividing Surface" between the Solid and the Fluid phase. "Surface" is utilized as a part of a general sense and it doesn't suggest any shape. This surface divides two bulk regions, from which the solid occupies one side of this numerical surface and fluid occupies the other. In the Gibbs meaning of Dividing Surface, the fluid phase properties are thought to be steady and equivalent to their values far from the surface. The actual changes happening in the interfacial region are attributed to a 2D adsorbed phase. Mathematically, the adsorbed phase is a surface, thus it does not have a volume. All Thermodynamic properties are referred to as "*Gibbs surface excess*" properties. With Gibbs definition, the amount adsorbed is related to the shaded areas in Figure 2.3 by;

$$\Gamma^{ex} = \int_0^\infty (\rho(z) - \rho^g)\, dz \tag{2.5}$$

Where, ρ^g is the density of the bulk gas phase and Γ^{ex} is the excess amount adsorbed per unit area. Equation (2.5) circumvents the problematic upper limit from specific distance L to infinite. Here there is no net contribution towards the amount adsorbed and thus we can write the excess amount adsorbed as followed;

$$N^{ex} = A \int_0^{\infty} (\rho(z) - \rho^g)\, dz \tag{2.6}$$

Where, A is the specific area of the adsorbent means area per unit mass and N^{ex} is excess amount adsorbed per unit mass of solid.

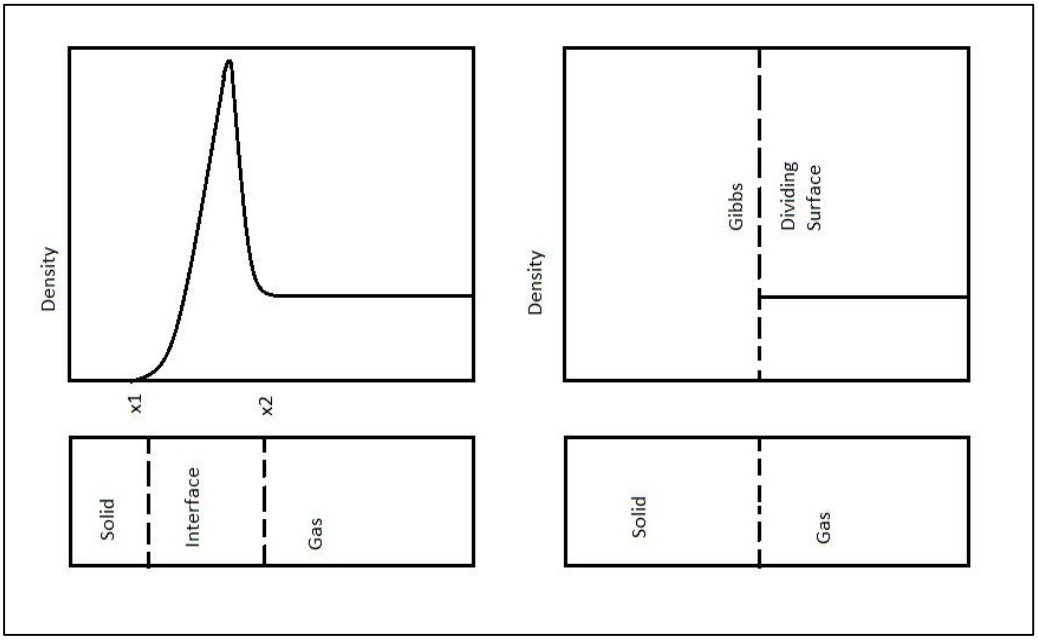

Figure 2.4.Illustration of density profiles and the Gibbs dividing surface near a flat surface [55].

Gibbs does not suggest any experimental method to locate the dividing surface. It is a purely mathematical definition. But practical use of thermodynamic relations requires that (1) either area is measured, or (2) it is calculated from other measurable quantities. The

excess amount actually means extra amount of fluid available near the immediate vicinity of the surface. Again, Gibbs' definition is purely a transformation of complex surfaces to thermodynamically equivalent simple system [25, 55].

2.4 Phase Rule

Two phases, bulk gas phase and adsorbed phase must be arbitrarily fixed by their own sets of intensive properties to get into the state called Equilibrium. By definition equilibrium means equality of

1. Thermal potential (or temperature)
2. Mechanical potential (or pressure) and
3. Mass potential (or Chemical potential)

The equality of thermal potential is obvious in which both the phases must be at same temperature, otherwise, heat transfer will occur and the system will not be called in equilibrium. Equality of chemical potential means each species in both the phases must not transfer any net mass.

The problem arises when we try to equate the mechanical potential. Mechanical gradient which is pressure as an intensive variable is meaningless in case of Adsorbed phase as it is two-dimensional. In two-dimensional adsorbed phase. Extensive variable like pressure and volume are not appropriate coordinates [68]. To define adsorbed phase properly and to fix its state, an intensive variable called *Spreading Pressure* is used [59].

The spreading pressure is the negative of the familiar surface tension and has units of dynes per centimeter or Nm^{-1}. In physical adsorption, it is positive (even for a multilayer adsorption). Therefore the system does work on the surrounding during the conceptual process of increasing the area of the adsorbent. There is no experimental technique for measuring the spreading pressure directly for a microporous solid, similar to the mechanical measurement of the surface tension of a liquid. It is therefore important to distinguish the thermodynamic variable spreading pressure from its interpretation by a particular physical model. Mechanical work term for adsorbed phase per mole of solid is thus given as $\pi * a$, analogous to the intensive variable for the work term $P * V$ in the bulk phase. This thermodynamic spreading energy can always be calculated from the experimental adsorption isotherm and is independent of any particular physical model of the adsorbed phase.

Due to extra intensive variable caused by lack of mechanical equilibrium and specific area of adsorbent becomes an additional thermodynamic variable thus the phase rule for the adsorption is [62, 68]

$$F = C - P + 3 \tag{2.7}$$

Where, F = number of degree of freedom

C = number of chemical species

P = number of phases

In the Equation (2.7) adsorbent is not counted as a separate component as it is assumed to be thermodynamically inert. Thus for binary gas adsorption equilibria (C = 2) there are three degree of freedom.

2.5 Fundamental Property Relations

The thermodynamic of physical adsorption has been thoroughly studied by Hill [26]. There are mainly three underlying assumptions on top of which the thermodynamic equation of adsorbed phase are based, and those three assumption are as followed and which were restated by Myer and Prausnitz [47] and O. Talu [62, 63, 65]:

1. The adsorbed phase is assumed to be thermodynamically inert; that means the thermodynamic property changes like change in internal energy, during the adsorption process is considered to be negligible as compared to that of the adsorbate.

2. Temperature invariant area possessed by adsorbent is same for all the adsorbates. This assumption might be wrong for the molecular sieve adsorbent where, the area available for adsorption depends upon the size adsorbate molecule.

3. By applying Gibbs Definition of Adsorption, we were able to circumvent the problem of defining the boundary between the adsorbed and gas phase in a system to which thermodynamic equations need to apply. The solution was the construction of a mathematical dividing surface between the two phases. One is gas phase persists unchanged up to solid surface and abnormality in the properties of interfacial region are attributed to the mathematical surface, which is then treated as a two dimensional phase

with its own properties. The basic fundamental property relation for adsorbed phase is defined as followed;

$$d\,(N \cdot u) = T \cdot d(N \cdot s) - \pi \cdot d(N \cdot a) + \sum \mu_i \cdot dN_i \tag{2.8}$$

Or

$$du = T \cdot ds - \pi \cdot da + \sum \mu_i \cdot dx_i \tag{2.9}$$

Where, N is the total number of moles adsorbed per unit mass of the solid adsorbent, u is molar internal energy, T is temperature, s is molar entropy, π is spreading pressure, a is area of adsorbent per unit mass per unit moles adsorbed (N), μ_i is the chemical potential of i^{th} component and N_i is the number of moles of i^{th} component adsorbed per unit mass of the solid adsorbent and x_i is the mole fraction of the component *i* in the adsorbed phase.

So we can write from the Equation (2.9) that variable π (spreading pressure) is defined by,

$$\pi = -\left(\frac{\partial u}{\partial \mathrm{a}}\right)_{S,x_i} \tag{2.10}$$

The molar enthalpy 'h' for the adsorbed phase is then,

$$h = u + \pi \cdot \mathrm{a} \tag{2.11}$$

Resulting in the following equation;

$$dh = du + d(\pi \cdot \mathrm{a}) \tag{2.12}$$

$$dh = \{T \cdot ds - \pi \cdot da + \sum \mu_i \cdot dx_i\} + \pi \cdot da + a \cdot d\pi \tag{2.13}$$

$$dh = T \cdot ds + a \cdot d\pi \ + \sum \mu_i \cdot dx_i \tag{2.14}$$

Using Legendre transformation the Gibbs free energy g of the adsorbed phase is;

$$dg = -s \cdot dT + a \cdot d\pi \ + \ \Sigma \, \mu_i \cdot dx_i \tag{2.15}$$

This definition of the total Gibbs free energy of the adsorbed phase has an advantage that total free energy of the system may be written as,

$$G = \sum \mu_i \cdot dN_i \tag{2.16}$$

2.6 Solution Thermodynamics and Phase Equilibrium Relations

The following definitions are based upon the solution thermodynamics first derived by Myers and Prausnitz [47].The theory of solution thermodynamic was first extended to adsorption by them and detail derivation of these equation was given by Van ness [68]. Similar to the bulk gas phase fugacity for the adsorbate can be defined by replacing P with f. Partial molar Gibbs free energy for the adsorbate in the mixture at constant temperature can be written as;

$$d\mu_i = \ d\bar{g}_i = R \cdot \ T \cdot \ d \ ln\widehat{f_i} \tag{2.17}$$

$$\lim_{\pi \to 0} \frac{\hat{f}_i}{{f_i}^0\{\pi\}} = 1 \tag{2.18}$$

Here, in Equation (2.18) ${f^0}_i$ is the fugacity in the gas phase of pure component *i* at the same temperature and spreading pressure as that of the mixture.

With the similar definition of the fugacity of the pure component and a component in the mixture, the activity coefficient for a species *i* in the adsorbate mixture is defined by the following Equation (2.19);

$$\gamma_i = \frac{\hat{f}_i}{x_i \cdot {f_i}^0\{\Psi\}} \tag{2.19}$$

By limiting the value of fugacity in Equation (2.19), the activity coefficient will be unity as π approaches zero.

$$\lim_{\pi \to 0} \gamma_i = \lim_{\pi \to 0} \frac{\hat{f}_i}{x_i \cdot {f_i}^0} = \lim_{\pi \to 0} \frac{{\hat{f}_i}/{x_i \cdot \pi}}{{{f_i}^0}/{\pi}} = 1 \tag{2.20}$$

Which leads us to

$$\bar{g}_i - {\bar{g}_i}^{id} = R \cdot T \cdot ln\gamma_i \tag{2.21}$$

Here in Equation (2.21) superscript "*id"* means Gibbs free energy for ideal solution in adsorbed phase. Integrating this equation at constant temperature and spreading pressure from pure component species *i* to a state of mixture containing x_i mole fraction of i^{th} component;

$$\bar{g}_i - {\bar{g}_i}^0 = R \cdot T \cdot ln\frac{\widehat{f}_i}{{f_i}^0} \tag{2.22}$$

Suppose the solution is ideal then we can deduce from Equations (2.21) and (2.22);

$$\bar{g}_i^{id} = {g_i}^0 + R \cdot T \cdot ln\, x_i \tag{2.23}$$

$$\bar{g}_i = {g_i}^0 + R \cdot T \cdot \ln(x_i \cdot \gamma_i) \tag{2.24}$$

It must be noted that in Equation (2.24) $\bar{g}_i$ is the partial molar property with respect to g and therefor;

$${g_i}^0 = x_i \cdot \bar{g}_i \tag{2.25}$$

Multiplying both the sides of Equation (2.24) with x_i and summarize it over all the species i will give us following Equation (2.26);

$$g - \sum_i x_i \cdot {g_i}^0 = R \cdot T \cdot \sum_i x_i \cdot \ln(x_i \cdot \gamma_i) \tag{2.26}$$

In this Equation (2.26) the LHS is the molar Gibbs free energy of mixing at constant temperature, spreading pressure (π) and mole fraction (x_i) and thus we can write it as superscript m and The activity coefficient for mixed adsorbed phase are included in the formulation is to account for the phase non-ideality;

$$g^m\{T, \pi, x_i, \ldots..\} = R \cdot T \cdot \sum_i x_i \cdot \ln(x_i \cdot \gamma_i) \tag{2.27}$$

In general, for any molar property M, any extensive change on mixing is defined as followed;

$$M^m\{T, \pi, x_i, \ldots\} = M\{T, \pi, x_i, \ldots\} - \sum_i x_i \cdot {M_i}^0\{T, \pi\} \tag{2.28}$$

In Equation (2.28) ${M_i}^0$ is the standard state defined as molar value of the proper for pure species *i* at same spreading pressure (π) and temperature *T* as that of the mixture. *M* is the molar value of the property for the mixture.

With the activity coefficient γ_i defined as in Equations (2.26) and (2.27), change in other thermodynamic function upon mixing are obtained as followed;

$$h^m(T,\pi,x_i,\dots) = -T^2\left\{\frac{\partial\left({}^{g^m}/_{T}\right)}{\partial T}\right\}_{x_i,\pi} = -R\cdot T^2\sum_i x_i\cdot\left(\frac{\partial \ln\gamma_i}{\partial T}\right)_{\pi,x_i} \quad (2.29)$$

$$a^m(T,\pi,x_i,\dots) = a\{T,\pi,x_i\} - \sum_i x_i\cdot {a_i}^0\{T,\pi\} = R\cdot T\sum_i x_i\cdot\left(\frac{\partial \ln\gamma_i}{\partial \pi}\right)_{T,x_i} \quad (2.30)$$

Combining Equations (2.29) and (2.30) and we will get

$$\mu_i(T,\pi,x_i) = {g_i}^0(T,\mu) + R\cdot T\cdot\ln(\gamma_i\cdot x_i) \quad (2.31)$$

In Equation (2.31) ${g^0}_i$ is the standard state molar Gibbs free energy of component *i*. Since there are only two degree of freedom in the adsorption of a pure component, the pressure P in the gas phase is uniquely determined by specifying temperature T and spreading pressure π of the system. Considering the equilibrium of pure component *i* adsorbate at temperature T and spreading pressure π and thus the vapor phase, we can write equation for ${g_i}^0$ as followed,

$${g_i}^0(T,\pi) = {g_i}^0(T) + R\cdot T\cdot\ln {P_i}^0(\pi) \quad (2.32)$$

In Equation (2.32) ${g_i}^0$ is the standard state molar Gibbs free energy of the component *i* at the perfect gas state and at the temperature of the system. In Equation (2.32) it is assumed

that gas phase is ideal, which is an excellent approximation at relatively low pressure. We can combine Equations (2.31) and (2.32) to get the Equation (2.33) stated below,

$$\mu_i(T, \pi, x_i) = g_i{}^0(T) + R \cdot T \cdot \ln(P_i{}^0) + R \cdot T \cdot \ln(\gamma_i \cdot x_i) \tag{2.33}$$

In the similar manner chemical potential for the component *i* in the mixture in gas phase with the same reference state will be;

$$\mu_{i,g}(T, P, y_i) = g_i{}^0(T) + R \cdot T \cdot \ln(P \cdot y_i) \tag{2.34}$$

When someone uses equilibrium criterion that chemical potential in adsorbed phase is equal to the chemical potential in the gas phase, the Equation (2.34) will yield to the equation of equilibrium for mixed gas adsorption;

$$P \cdot y_i = P_i{}^0(T, \pi) \cdot x_i \cdot \gamma_i(T, \pi, x) \tag{2.35}$$

Equation (2.35) is analogous to the modified Raoult's law for liquid-Vapor equilibrium. At higher pressure Equation (2.35) can be written with slight modification but in a similar way just by adding vapor phase fugacity coefficient Φ_i at pure state and in the mixture at constant temperature,

$$P \cdot y_i \cdot \Phi_i = P_i{}^0(T, \pi) \cdot \Phi_i{}^0 \cdot x_i \cdot \gamma_i(T, \pi, x) \tag{2.36}$$

Where, $\Phi_i{}^0$= Vapor phase fugacity coefficient of pure *i* at the standard state.

Φ_i= Vapor phase fugacity coefficient of component *i* in the mixture.

Using the same proposition the molar area of mixed adsorbate can be written as [62, 63];

$$\frac{1}{N_t} = \sum_i \frac{x_i}{{N_i}^0(T,\pi)} + \sum_i x_i \cdot \left(\frac{\partial \ln \gamma_i}{\partial \left(\frac{\pi A}{RT}\right)} \right)_{T,x_i} \tag{2.37}$$

Here in Equation (2.37) N_t is total number of moles adsorbed mixture, ${N^0}_i$ is numbers of moles of *i* adsorbed at pure standard state i.e. at the same temperature T and spreading pressure π as that of the adsorbed mixture.

2.7 Gibbs Adsorption Isotherm

The Gibbs adsorption isotherm can be written from the total Gibbs free energy *g* of the adsorbed phase [63]. Chemical potential for the component *i* in the surface phase given in terms of the bulk gas phase properties is,

$$-{a_i}^0 \cdot d{\pi_i}^0 + d{\mu_{i,a}}^0 = 0 \tag{2.38}$$

Here in Equation (2.38) ${a_i}^0$ $(m^2 \cdot mol^{-1})$ is the area per mole of the adsorbed gas, ${\mu_i}^0$ $(j \cdot mol^{-1})$ is the chemical potential of the pure component *i* in the adsorbed phase and ${\pi_i}^0$ $(j \cdot m^{-2})$ is the spreading pressure at ${a_i}^0$. The specific area in the above Equation (2.38) can be written as;

$${a_i}^0 = A/{N_i}^0 \tag{2.39}$$

Where A is the specific surface are $(m^2 \cdot kg^{-1})$of the adsorbent and ${N_i}^0$ $(mol \cdot kg^{-1})$ is amount adsorbed for component *i*. At equilibrium the chemical potential of component *i* in the adsorbed phase is equal to the chemical potential in the gas phase and we can write

chemical potential of component *i* in the surface phase in terms of bulk gas phase properties.

$$d\mu_{i,g}{}^{0} = d\mu_{i,a}{}^{0} \tag{2.40}$$

Supposedly if the gas phase is ideal, then chemical potential of the component *i* in the mixture of the gas phase can be written as;

$$d\mu_{i,g}{}^{0} = R \cdot T \cdot d\ln\left(P_i{}^{0}\right) \tag{2.41}$$

Summarizing all the Equations from (2.38) to (2.41) will give us;

$$-a_i{}^{0} \cdot d\pi_i{}^{0} + R \cdot T \cdot d\ln\left(P_i{}^{0}\right) = 0 \tag{2.42}$$

$$-A \cdot d\pi_i{}^{0} + N_i{}^{0} R \cdot T \cdot d\, ln\left(P_i{}^{0}\right) = 0 \tag{2.43}$$

The integral form of above Equation (2.43) can be written as follows,

$$\pi_i{}^{0} = \frac{R \cdot T}{A} \int_{0}^{P_i{}^{0}} N_i{}^{0} \cdot d\ ln(\ P_i{}^{0}) \tag{2.44}$$

This is called Gibbs adsorption isotherm in adsorption literature [17, 59]. In Equation (2.44) $P_i{}^{0}$ is the equilibrium pressure of pure component *i.* It gives spreading pressure, $\pi_i{}^{0}$ as a function of $P_i{}^{0}$ for a system where $N_i{}^{0}$ is a known function of $P_i{}^{0}$.

At constant temperature, for the mixture having *i* components in it, Equation (2.42) can be written as;

$$-a \cdot d\pi + \sum_i x_i \cdot R \cdot T \cdot d\ln(P) = 0 \tag{2.45}$$

By substituting $a = {}^{A}/_{N_t}$ in Equation (2.45) will lead us to,

$$-A \cdot d\pi + \sum_i R \cdot T \cdot N_i \cdot d\ln(y_i \cdot P) = 0 \tag{2.46}$$

2.8 Thermodynamic Consistency and Gibbs-Duhem Equation for Adsorbed Phase

The fundamental relation of adsorption thermodynamics is the Gibbs adsorption isotherm (van ness 1969) [68] which was defined earlier as [47, 56, 65, 68, 71];

$$-a \cdot d\pi + \sum N_i \cdot d\mu_i = 0 \tag{2.47}$$

At constant spreading pressure the above Equation (2.47) becomes;

$$\sum x_i \cdot d\mu_i = 0 \tag{2.48}$$

Substitute Equation (2.33) in Equation (2.48) will give us;

$$\sum x_i \cdot d\ln \gamma_i = 0; \tag{2.49}$$

Equation (2.49) is Gibbs-Duhem relation for the adsorbed phase at constant temperature and spreading pressure. As the spreading pressure can't be controlled, a more general relation for adsorbate mixture under isothermal condition can be written as follows [63];

$$\sum x_i \cdot d\ln \gamma_i = d\left(\frac{\pi \cdot A}{R \cdot T}\right)\left(\frac{1}{N_t} - \sum_i \frac{x_i}{N_i{}^0}\right) \tag{2.50}$$

The last term in Equation (2.50) represents the molar area for mixing. The thermodynamic consistency check can be performed by evaluating the left hand side and the right hand side of Equation (2.50).

2.9 Pure Component Adsorption Model

Whether the adsorption isotherm has been determined experimentally or theoretically from molecular simulation, the data points must be fitted with analytical equations for interpolation, extrapolation, and for the calculation of thermodynamic properties by numerical integration or differentiation. Many theories and models have been developed to interpret these types of isotherms. A detail discussion of various models used to interpret each type of isotherm have been given by various authors like Gregg and Sing [23]. There are mainly three different approaches on which most of the isotherm models are based upon. (1) Mechanistic models postulating microstructures of adsorbed phase, (2) Equation of state models originating from 1 2D gas like behavior and (3) Pore filling models are based upon Polanyi [50, 51] theory treating the adsorbed phase as highly compressed gas. The first two approaches are used in this study.

2.9.1 The Langmuir model

The Langmuir isotherm [33-35] is originally a kinetic model which is the most widely used and cited isotherm in the literature. It is a mechanistic model. This model was original developed to represent Chemisorption on a set of localized adsorption sites and that is why it is more appropriate to chemisorption. In a physisorbed layer molecules are highly mobile and resemble more closely a two dimensional gas [55, 56]. Nevertheless, Langmuir isotherm captures all essential characteristics of Type I isotherm. This model stipulates that there are fixed number of localized adsorption sites and each site can hold one adsorbate molecule. All sites are energetically equivalent and there is no interaction between the adsorbed molecules on neighbor sites. Langmuir isotherm is actually based upon the concept of dynamic equilibrium which means that rate of evaporation (desorption) is equal to the condensation (adsorption). The final isotherm equation is given as [6, 33-35, 71],

$$\Theta = \frac{N}{N^{\infty}} = \frac{b \cdot P}{1 + b \cdot P} \tag{2.51}$$

In Equation (2.51), Θ is fraction of surface covered, N is number of moles adsorbed per gram of adsorbent, P is the pressure and N^{∞} and b are Langmuir parameters and both have important physical significance. b is the slope of the isotherm when pressure is very small and it is an indication of affinity of the solid for gas molecules. It is related to positive value of the adsorption energy. N^{∞} is the saturation limit of the isotherm for large values of pressure which is indication of monolayer or micropore capacity. Langmuir parameters can

be obtained from experimental data by linear regression with the following Equation (2.52) [55],

$$\frac{P}{N} = \frac{1}{b \cdot N^{\infty}} + \frac{P}{N^{\infty}} \tag{2.52}$$

Dual Site Langmuir (DSL) model is a modification of this actual model to account for heterogeneity. In this model the total amount adsorbed is a result of net contribution for adsorption on two patches with different adsorption energies and capacities. DSL is commonly used in process simulation due to its flexibility in representing wide range of isotherms [43].

2.9.2 The Virial Model

A 2D equation of state mode, the virial isotherm equation truncated at an appropriate point has been used successfully to represent pure gas isotherm data and gives excellent fit at low and moderate pressure range. The General Virial equation can be applied to find the virial constant from the data regression, which can further be used in mixture adsorption prediction [3];

$$Z = \frac{\pi \cdot a}{R \cdot T} = \left(1 + \frac{B'}{a} + \frac{C'}{a^2} + \frac{D'}{a^3} + \cdots\right) \tag{2.53}$$

In the Equation (2.53), π is spreading pressure, a is area per mole, B', C', D' are interaction parameters. After rearrangement, and taking the derivative at constant temperature, will lead us to the virial equation of state for the adsorbed phase;

$$\left(\frac{\partial \pi}{\partial a}\right)_T = -R \cdot T\left(\frac{1}{a^2} + \frac{2 \cdot B'}{a^3} + \frac{3 \cdot C'}{a^4} + \cdots\right) \tag{2.54}$$

$$\ln P = constant\ (T) - \ln A + \frac{2 \cdot B'}{a} + \frac{3 \cdot C'}{2 \cdot a^2} + \frac{4 \cdot D'}{3 \cdot a^3} + \cdots \tag{2.55}$$

$$P = N_i\left(\exp\left\{constant\ (T) - \ln A + \frac{2 \cdot B'}{A}N_i + \frac{3 \cdot C'}{2 \cdot A^2}{N_i}^2 + \frac{4 \cdot D'}{3 \cdot A^3}{N_i}^3 + \cdots\right\}\right) \tag{2.56}$$

Which will reduce to the following Equation (2.57);

$$P = N_i \cdot e^{(K(T) + B(T) \cdot N_i + C(T) \cdot {N_i}^2 + D(T) \cdot {N_i}^3 + \cdots)} \tag{2.57}$$

In Equation (2.57), B, C, and D…are the virial coefficients representing the two body, three body and four body interactions in the adsorbed phase respectively. The Henry's law constant (H) is related to the gas-solid interaction. Equation (2.57) provides basis and useful means of evaluating Henry's law constant (H).

Henry's Law constant is related to the slope of the isotherms at the origin. It is a very important thermodynamic property, related to the interaction of the molecules with the surface. However, with strongly adsorbed components, it is difficult to determine the Henry's Law constant directly from the limiting slope of the isotherm. A plot of $ln\left(\frac{P}{N_i}\right)$ versus N_i should be linear at concentrations below Henry's Law limit. The extrapolation of this plot to zero-adsorbed phase concentration provides the simplest way of evaluating the Henry's Law constant from isotherm data. From the Equation (2.57),

$$ln\left(\frac{P}{N_i}\right) = K + B \cdot N_i + C \cdot {N_i}^2 + D \cdot {N_i}^3 \tag{2.58}$$

$$H = \lim_{P \to 0} \frac{N_i}{P} = e^{-K} \tag{2.59}$$

From isothermal data, the parameters in the virial isotherm equation (Equation (2.57)) can be expressed as a function of temperature as follows;

$$K(T) = k_0 + \frac{k_1}{T}; \tag{2.60}$$

$$B(T) = b_0 + \frac{b_1}{T} + \frac{b_2}{T^2} + \cdots \tag{2.61}$$

$$C(T) = c_0 + \frac{c_1}{T} + \frac{c_2}{T^3} + \cdots; \tag{2.62}$$

$$D(T) = d_0 + \frac{d_1}{T} + \frac{d_2}{T^3} + \cdots \tag{2.63}$$

2.10 Isosteric Heat of Adsorption

Isosteric heat of adsorption is one of the basic quantities in adsorption studies, which is defined as the ratio of the infinitesimal change in the adsorbate enthalpy (∂H) to the infinitesimal change in the amount adsorbed (∂n). It is a negative of a specific adsorption enthalpy. It provides useful information about the nature of the solid surface and the adsorbed phase. The information regarding the heat released is important in kinetic studies because, when heat is released due to adsorption, the released energy is partly absorbed by the solid adsorbent and partly released to the surroundings. The portion absorbed by the solid increases the particle temperature, which slows down the adsorption kinetics because the mass uptake is controlled by the rate of cooling of the particle [17].

The heat of adsorption profile reveals the type of heterogeneity in the solid adsorbent and the degree of gas-solid interactions, and it may vary with loading. An increase in heat of adsorption with gas loading is characteristic of non-heterogeneous adsorbents (e.g. graphitized carbon) with constant gas-solid energies of interaction. The increase is due to cooperative interactions between adsorbed molecules. A decrease in the heat of adsorption with gas loading is characteristic of highly heterogeneous adsorbents (e.g. activated carbon) with a wide distribution of gas-solid interaction energies. A constant heat of adsorption with gas loading indicates a balance between the strength of cooperative gas-gas interactions and the degree of heterogeneity of gas-solid interactions.

The heats of adsorption is used in the calculation of energy balances in packed columns. As most columns operate adiabatically, the heat of adsorption determines the temperature profile inside the column. The heat of adsorption is another measure of how much energy is required to regenerate the column, which is the major operating cost for thermal swing- adsorption (TSA) columns. It can be calculated from the temperature variation of isotherms, without using a calorimetric instrument. The Clausius-Clayperon equation has long been used for the evaluation of the heat of adsorption from the adsorption isotherm data assuming ideal behavior of the adsorbate molecules in their gaseous phase. The equation can be written as follows [18, 46, 53],

$$\bar{H} = -R \cdot T^2 \left[\frac{\partial \ln P}{\partial T}\right]_n \tag{2.64}$$

Or,

$$q^{ig} = -R \cdot \left[\frac{\partial \ln P}{\partial\left({}^{1}/_{T}\right)}\right]_{n} \tag{2.65}$$

Equation (2.65) is derived with the assumption that the volume change of the adsorbed phase is negligible, which is not true at high pressure. Therefore Equation (2.65) is further modified as described by Chakrabarty et al. [10]; i.e.

$$q = -R \cdot \left[\frac{\partial \ln P}{\partial\left({}^{1}/_{T}\right)}\right]_{n} + T \cdot (v_g - v_a) \cdot \left(\frac{dP}{dT}\right) \tag{2.66}$$

In Equation (2.66) the second term is the compression of the bulk gas phase due to volume change in the adsorbed phase. To calculate the Isosteric heat, the virial equation of state (Equation (2.57)) can be applied as follows;

$$q = -R \cdot \left[\frac{\partial \ln P}{\partial\left({}^{1}/_{T}\right)}\right]_{n} = -R \cdot (k_1 + b_1 \cdot N_i + c_1 \cdot {N_i}^2 + d_1 \cdot {N_i}^3 + \cdots) \tag{2.67}$$

2.11 Spreading Pressure Calculation

The spreading pressure is not a measurable property but can be calculated from macroscopically measured quantities by the integration of the Gibbs adsorption isotherm. The final integrated equation depends upon the path used in equilibrium measurements. Therefore the value of the spreading pressure is unique at every point in the phase diagram since it is an independent intensive property of the surface phase.

2.11.1 Pure Component

As described earlier, the Gibbs adsorption isotherm for a pure component is,

$$\frac{A \cdot d\pi_i{}^0}{R \cdot T} = N_i{}^0 \cdot dln\left(P_i{}^0\right) \tag{2.68}$$

If Equation (2.68) is integrated from zero pressure to the equilibrium pressure of component *i*, $P_i{}^0$ the spreading pressure, $\pi_i{}^0$ at constant temperature for the adsorbed phase can be obtained as;

$$\pi_i{}^0 = \frac{R \cdot T}{A} \int_0^{P_i{}^0} N_i{}^0 \cdot dln\left(P_i{}^0\right) \tag{2.69}$$

Rearranging Equation (2.69) yields;

$$\psi = \frac{A \cdot \pi_i{}^0}{R \cdot T} = \int_0^{P_i{}^0} N_i{}^0 \cdot dln\left(P_i{}^0\right) \approx f(\ P_i{}^0) \tag{2.70}$$

Since $N_i{}^0$ is the number of moles of *i* adsorbed at $P_i{}^0$, in other words, the adsorption isotherm for pure component *i*, Equation (2.70) can be used to calculate $\pi_i{}^0$ from the experimental adsorption isotherm data for pure component *i*.

With the Virial EOS (Equation (2.57)) used in this study, the spreading pressure expression is implicit in amount adsorbed and it can be written as [62],

$$\psi = \frac{\pi_i{}^0 \cdot A}{R \cdot T} = N_i{}^0 + \frac{B \cdot (N_i{}^0)^2}{2} + \frac{2 \cdot C \cdot (N_i{}^0)^3}{3} + \frac{3 \cdot D \cdot (N_i{}^0)^4}{4} \tag{2.71}$$

2.11.2 Binary Mixture

For the calculation of the experimental activity coefficient for a binary mixture, the spreading pressure of the mixture must be calculated. From Equations (2.45) and (2.46), an equation for the spreading pressure at constant temperature can be derived as follows;

$$\frac{d\pi \cdot A}{R \cdot T} = N_1 \cdot dln(P \cdot y_1) + N_2 \cdot dln(P \cdot y_2) \tag{2.72}$$

If the total pressure of the system is held constant Equation (2.72) becomes;

$$\frac{d\pi \cdot A}{R \cdot T} = N_1 \cdot dln(y_1) + N_2 \cdot dln(y_2) \tag{2.73}$$

Integrating Equation (2.73) from π_1, spreading pressure of the component 1 at the same temperature and gas pressure which is least adsorbed, to π, the spreading pressure of the mixture of interest, and right hand side Equation (2.73) from $y_1 = 1$ to $y_1 = y_1$, Equation (2.73) can be rewritten as follows;

$$\frac{\pi \cdot A}{R \cdot T} = \left.\frac{A \cdot \pi}{R \cdot T}\right|_{y_1=1} + \int_{y_1=1}^{y_1=y_1} N_1 \cdot dln(y_1) + \int_{y_1=1}^{y_1=y_1} N_2 \cdot dln(y_2) \tag{2.74}$$

Equation (2.74) can be used when the system pressure is low in the range of an ideal gas. If the system pressure is high enough, the non-ideality of the gas can be included through the fugacity coefficient. The spreading pressure with the real gas equation is then;

$$\frac{\pi \cdot A}{R \cdot T} = \left.\frac{\pi \cdot A}{R \cdot T}\right|_{y_1=1} + \int_{y_1=1}^{y_1=y_1} N_1 \cdot dln(\Phi_1 \cdot y_1) + \int_{y_1=1}^{y_1=y_1} N_2 \cdot dln(\Phi_2 \cdot y_2) \tag{2.75}$$

For the binary mixture, the spreading pressure for the gas mixture can be calculated from Equation (2.75). All that is needed is the binary experimental data at constant temperature and pressure for the entire range of gas composition.

2.12 Binary Mixture Adsorption Model

The experimental measurement of multicomponent adsorption is time consuming due to the large number of variables involved. The problem of predicting binary and multicomponent adsorption from single component adsorption data has, therefore, attracted significant attention. In addition, binary measurements are complicated because the amount of each component adsorbed in a porous solid cannot be directly measured. The partial amounts are calculated as differences from fluid phase material balances. A rigorous thermodynamic of multicomponent adsorption based on solution thermodynamic was presented by Myers and Prausnitz (1965) [47].

2.12.1 Ideal Adsorbed Solution Theory (IAST)

Proposed in 1965 by Myers and Prausnitz [47], Ideal Adsorbed Solution Theory (IAST) provides a link between pure component and multicomponent adsorption. This theory is based upon the solution thermodynamics and most of its equations resemble those of Vapor-liquid equilibria. If we assume that the adsorption is thermodynamically ideal

then it is possible to derive the equilibrium relationships for the mixture adsorption, from pure component isotherms of the same gases which comprise the mixture, without postulating any specific model for the adsorbed phase activity coefficient. IAST requires two relationships: one for the intensive property (i.e. adsorbate composition) and another for the total amount adsorbed. For the first relationship, the equality of chemical potential is assumed, while for the second relation it can be assumed that, in the ideal adsorption case, the total partial molar adsorbed area is additive. Therefore, the equation of equilibrium for a mixed gas adsorption (Equation (2.35)), the system can be assumed to behave ideally, i.e. $\gamma_i = 1$. At equilibrium the chemical potential (Equation (2.35)) of the component *i* in each phase can be written at constant temperature as;

$$P \cdot y_i = x_i \cdot P_i^{\,0}(\pi_i, T) \tag{2.76}$$

Here $P_i^{\,0}(\pi_i, T)$ is the equilibrium gas pressure of the pure component *i* adsorbed at the same temperature (T) and spreading pressure (π) as those of the mixture. $P_i^{\,0}$ is the fictitious pressure analogous to the vapor pressure of the pure component in vapor–liquid equilibrium. It is the pressure that species *i* adsorbed alone would exert, at the same *P*, *T* and the spreading pressure π as that of the mixture The mixture predictions by this model are obtained by carrying out the mixing process at a constant spreading pressure (π) and temperature (T), i.e.

$$\pi_1 = \pi_2 = \pi \tag{2.77}$$

Therefore, in an ideal adsorbed solution, there will be no enthalpy change and no area change upon mixing so Equations (2.29) and (2.30) can be written as;

$$h^m = 0 \quad and \quad a^m = 0 \tag{2.78}$$

Combining Equations (2.76) to (2.78) with the Molar property M (Equation (2.28)), provides a route for the calculation of the number of moles adsorbed in an ideal mixture,

$$\frac{1}{N_t} = \frac{x_1}{{N_1}^0} + \frac{x_2}{{N_2}^0} \tag{2.79}$$

Here ${N_1}^0$ is the amount adsorbed for component 1 at spreading pressure (π) and temperature (T) which is defined as the standard state.

Under isothermal condition, Equations from (2.76) to (2.79) provide seven equations as with nine unknowns $(P, x_{1,}, x_2, y_1, y_2, {P_1}^0, {P_2}^0, \pi_1, \pi_2)$. Therefore, in this theory if two unknowns are specified, for instance are P and y_1, all other mixture properties (including the total amount adsorbed) can be calculated by solving Equations (2.80)-(2.86) simultaneously. This relation is shown in a Figure 2.5 [47, 48];

$P \cdot y_1 = x_1 \cdot {P_1}^0(\pi_1, T)$	Eq. (2.76) for component 1	(2.80)
$P \cdot y_2 = x_2 \cdot {P_2}^0(\pi_2, T)$	Eq. (2.76) for component 2	(2.81)
${N_1}^0 = f\,({P_1}^0, T)$	Pure component 1 isotherm	(2.82)
${N_2}^0 = f\,({P_2}^0, T)$	Pure component 2 isotherm	(2.83)
$\frac{1}{N_t} = \frac{x_1}{{N_1}^0} + \frac{x_2}{{N_2}^0}$	Eq. (2.79) for ideal mixture	(2.84)
$x_1 + x_2 = 1;\ y_1 + y_2 = 1$	Binary condition for adsorbed phase & gas phase composition	(2.85)
$\pi_1({P_1}^0, T) = \pi_2({P_2}^0, T)$	Definition of standard state	(2.86)

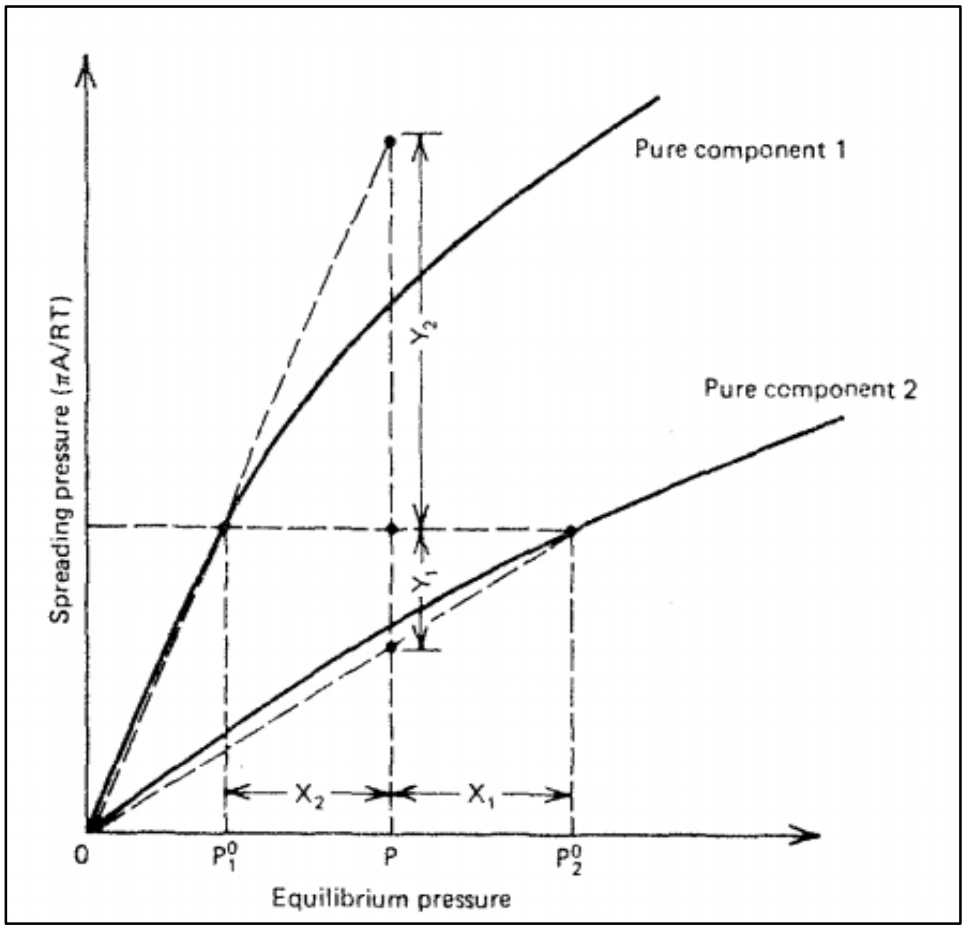

Figure 2.5. Calculation of mixture adsorption equilibria from pure component spreading pressures [47].

CHAPTER III

EXPERIMENTAL

3.1. Apparatus

The experimental system is a manual unit, designed for measurement of both pure component and multicomponent adsorption experiments using a pre-calculated amount of gases charged into the system. Table 3.1 lists the details of the pure and binary adsorption experiments performed on the system.

Table.3.1 – Experiments performed using the volumetric system

Gas	Type	Temperature (K)
Methane (CH_4)	Pure	283.15, 308.15, 338.15
Nitrogen (N_2)	Pure	283.15, 308.15, 338.15
Methane (CH_4)+Nitrogen (N_2)	Binary	308.15

Major tubing used in the system is 1/4” stainless steel except the gas sampling lines and pressure transducers lines, which are 1/8” inside diameter. The gas is mixed and circulated by a pump through a loop consisting of an adsorption column, a large tank, a small tank, a flow controller, a GC sampling valve (Auto sampling valve which is mounted in GC itself), and a circulation pump for binary measurements. Pure component measurements do not require circulation. The system is mainly composed of three sections:

3.1.1 Feed/storage section.

3.1.2 Adsorption/Desorption & exit section.

3.1.3 Bypass and analysis section.

3.1.1 Feed/Storage Section

A detailed schematic diagram of feed section is shown in Figure 3.1. The feed section consists of two different gas manifolds which are connected to nitrogen (grade: 5.0, >99.999% pure), helium (grade: 4.7, >99.997% pure) and methane (grade: 4.7, >99.997% pure). Nitrogen/helium and methane were filled into the system through a three way valve F1, which switches between Gas manifolds.

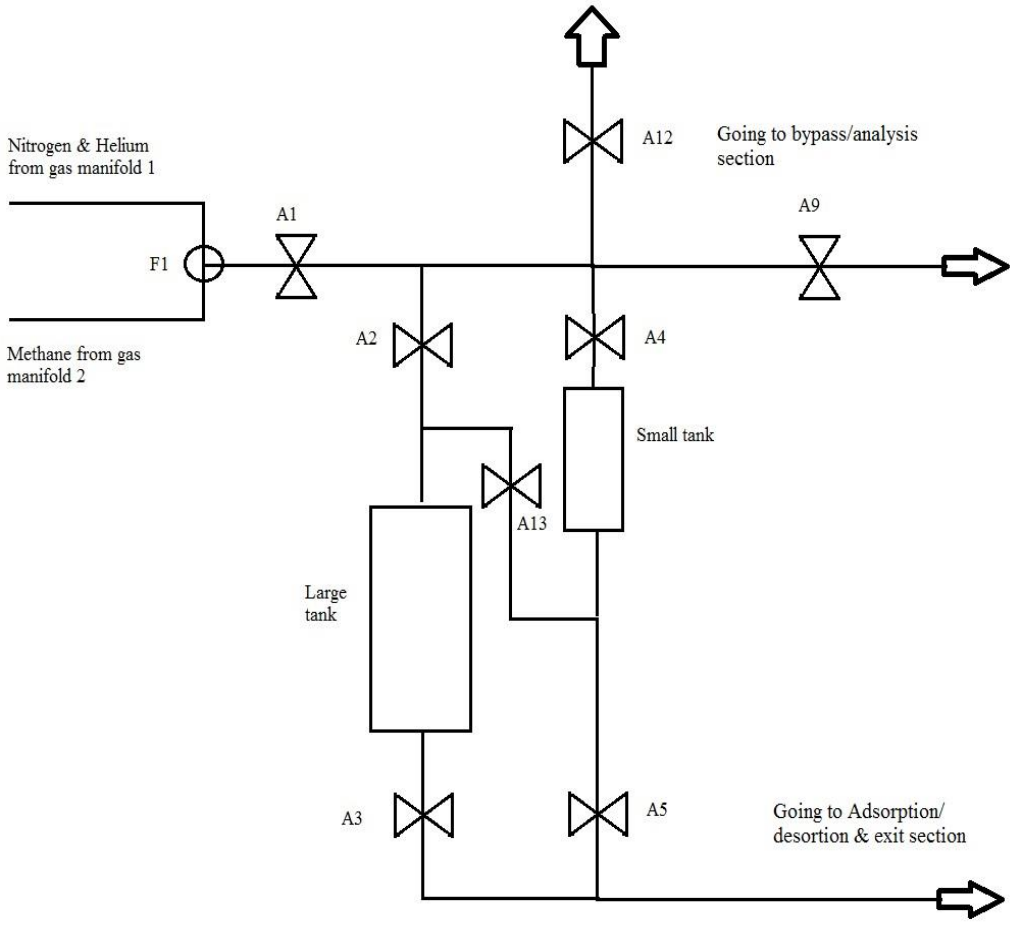

Figure 3.1.Feed/storage Section

All three way valves used to switch between gases while charging into the system are Swagelok SS-41XSP. The flow rate of gases while charging the system was controlled by lab size Omega (Model: FMA-2-DPV) mass flow controller. The range for the flow controller (model: FMA 123) was 0-100 SCCM. The mass flow controller was calibrated before the actual measurements were taken using a bubble flow meter (not shown in Figure 3.1).

This section also contains two tanks, one is a small tank having volume of 95.60 cc (±1.46 cc) and a large tank having volume of 162.21 cc (±2.51 cc). All the unknown internal volumes measurements were performed using a helium expansion technique at room temperature and are within 1% accuracy and 2% Coefficient of Variation. Both tanks are maintained in a constant temperature water bath which is measured using J-type thermocouple on a lab size temperature readout Omega (model: DP82). All the main valves used in this section were "B-type" bellow valve, NUPRO SS-4BK, which have precision-formed metal bellows for positive isolation from the surroundings.

3.1.2 Adsorption/Desorption & Exit Section:

A detailed schematic of the adsorption-desorption & exit sections is shown in Figure 3.2. This section consists of a changeable 1/2" 316 stainless steel adsorption column in between valve A6 and A7. A total 5.1619 grams of silicalite adsorbent, purchased from UOP LLC, Illinois (Lot# 917797020012) in 1/16" pellets form, were placed in the column. In order to carry out experiments at isothermal conditions, the column is kept in a thermostatic water-bath during the experiments.

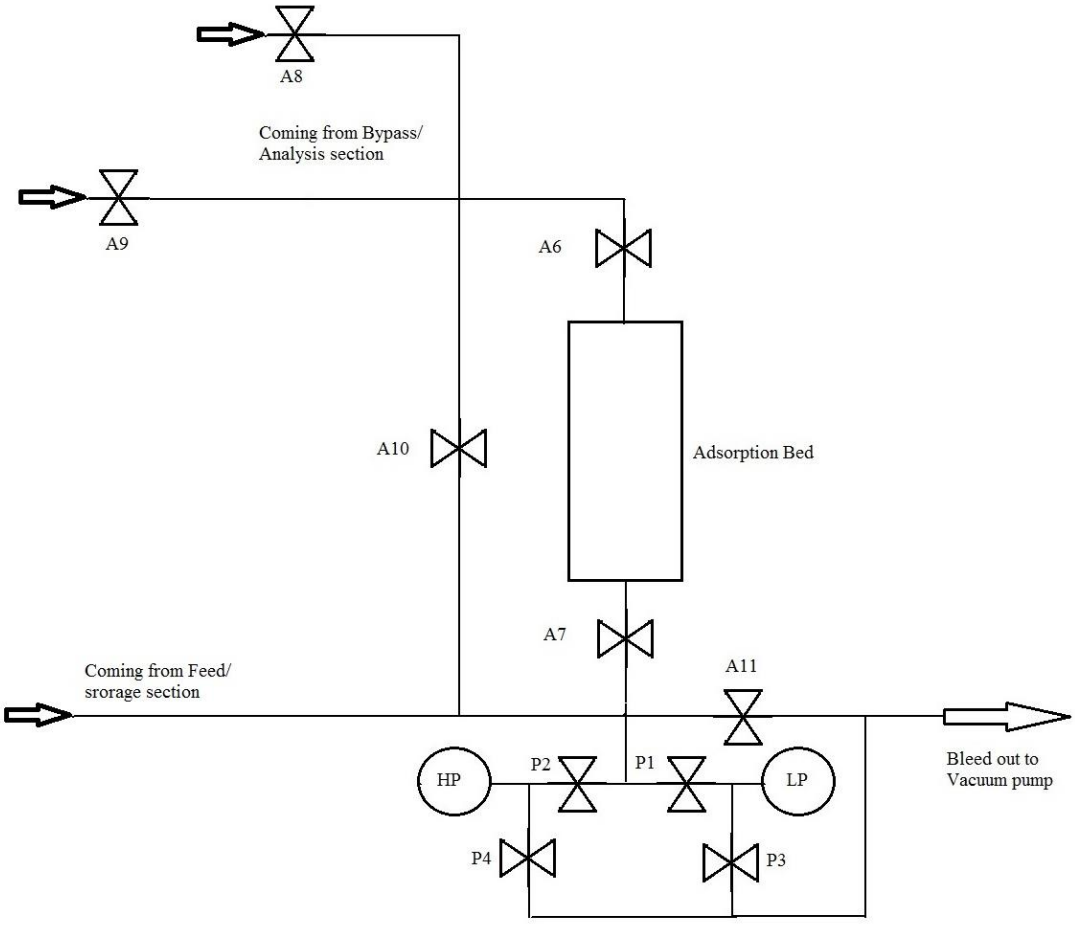

Figure 3.2.Adsorption/ Desorption & Exit section

The water bath is connected to a Fisher Scientific Refrigerating/Heating water circulator (model: 9005) (not shown in Figure 3.2), which can stabilize the temperature of the column within ±0.1 °C. There is a J-type thermocouple inserted into the column and connected to the temperature read-out to measure the column temperature.

This section also contains two pressure transducers to measure pressure of different sections at various times. This pressure transducers are surrounded with four pressure gauge valves (P1, P2, P3, P4), which are "H-TYPE" compact rugged bellow valves, NUPRO SS-2H. Other than these four vales, all other valves used are same as those used in other sections, "B-TYPE" bellow valves, NUPRO SS-4BK. High pressure levels are measured with a sensotec pressure transducer (model: TJE/713-10) ranging from 0-100 psi (±0.1 psi), while low pressure levels are measured with a sensotec pressure transducer (model: TJE/713-26) ranging from 0-15 psi (±0.01 psi). Both the pressure read-outs used in the system are sensotec (model: 60-3147-01). At the farmost end, after the exit valve, A11, there is a laboratory size vacuum pump Welch duo-seal (model: 1400) connected to a dispose exhaust stream to enable bleeding out the system down to 0.01 psi.

3.1.3 Bypass and Analysis Section

This section is mainly used when dealing with binary gas adsorption. This section consists of mainly of a high pressure rotary vane pump, ASF Thomas Memmingen (model: M42), for better mixing and circulation through the system. As it was discussed above, this section contains a mass flow controller Omega (model: FMA-2-DPV) to maintain and

control the gas flow rate through the system during helium activation/ regeneration and gas circulation. This section includes a sampling valve for a gas chromatograph system equipped with a thermal conductivity detector. The Hewlett Packard gas chromatograph (model: 7890A) with a 3 feet long Supelco molecular sieve 5A column is used to analyze the gas sample. The sampling valve is automatic and placed inside the gas chromatograph to sample a given amount of gas mixture (0.5 CC) into the gas chromatograph carrier gas. The carrier gas used for the analysis was helium (grade: 4.7, >99.997% pure) brought in to the chromatograph from the second gas manifold through moisture trap.

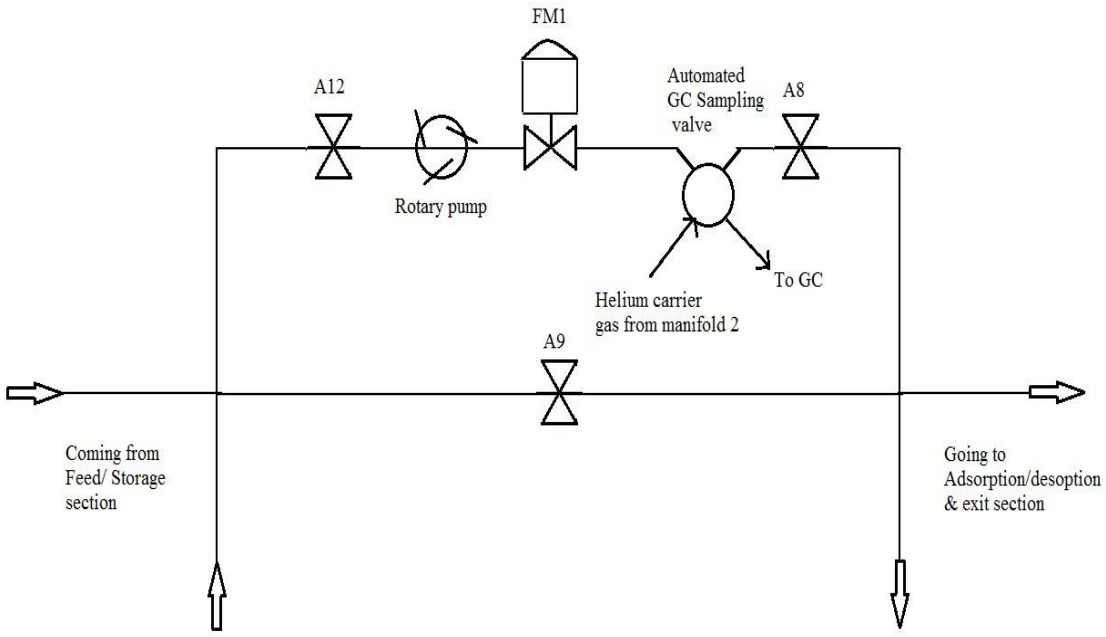

Figure 3.3. Bypass/ Analysis section

3.2. Operating Procedure

The apparatus described in the previous section was used to determine both pure component and multicomponent adsorption isotherms. In this section, the experimental protocols and techniques are described.

3.2.1 Pre-Experimental Measurements

Before staring the experiments (i.e. pure component and binary mixture adsorption isotherms) the internal volume of the various sections are needed to perform mass balances, which, in-turn is used to calculate amount adsorbed. GC calibration is needed to calculate the gas phase mole fraction after the equilibrium in binary adsorption measurements.

3.2.1.1 Void Volume Determination

In this system, only the volume of the exit section was previously determined by mercury displacement and helium burette techniques. The inside volumes of other sections were measured by helium expansion at the room temperature. Inside volumes are necessary to calculate the number of moles of gas adsorbed via a material balance. Helium expansion is a method to measure the internal volume of a system, by charging helium into the known reference section and expanding it to the target section. The volume of the target section can be calculated from material balances.

First, an unknown volume section of apparatus is completely evacuated then helium is charged into a known volume V_{known} at a pressure of P_{charge}. It is then expanded into one of the unknown volume $V_{unknown}$ in the system. The final equilibrium pressure P_{final} is measured. At the sub atmospheric pressure, usually ranging from 0-15 psi and around atmospheric temperature, there is no significant non-ideality for helium and hence ideal gas law can be applied to calculate the unknown volume from known volume measurements. The number of moles charged at the beginning into the system will remain the same after the expansion, so material balance can be written as follows,

$$N_{charge} = \frac{P_{charge} \cdot V_{known}}{R \cdot T_{charge}} = \frac{P_{final} \cdot (V_{known} + V_{unknown})}{R \cdot T_{final}} \qquad (3.1)$$

While measuring the column void volume, adsorption of helium around sub atmospheric pressure and ambient temperature can be neglected [62]. The calculation of volume of a column with helium expansion technique is similar to that of the isotherm measurement, but the only difference is that the gas adsorbed is assumed to be zero. The results of the volume calculations are summarized in Table 3.2 below,

Table 3.2.Inside volume of different sections

	Section	Enclosed by valves	Volume(cc)	Standard Deviation	CV%
Vol-1	Inlet	A1+A2+A4+A9+ A12	20.05	0.24	1.2
Vol-2	Bypass	A6+A8+A9+A10	9.96	0.15	1.5
Vol-3	Exit	A3+A5+A10+A7+ A11+P1+P2	14.48	0.28	2.0
Vol-4	Pump	A12+A18	27.83	0.017	0.1
Vol-5	B-tank/saturator	A2+A3 +A13	162.22	2.51	1.5
Vol-6	S-tank	A4+A5+A13	95.60	1.46	1.5
Vol-7	Low-P	P1+P3	6.57	0.13	2.0
Vol-8	High-P	P2+P4	6.44	0.10	1.5
Vol-9	Bed (full)	A6+A7	24.08	0.52	2.2
Vol-10	Bed (empty)	A6+A7	25.75	0.45	1.7

3.2.1.2 Gas Chromatograph Calibration

In binary gas adsorption isotherm measurements, it is necessary to determine the gas phase composition at the end of the experiment (when the system is at equilibrium), to perform a material balance and calculate the partial adsorption isotherms. Before starting multicomponent experiments, it is necessary to calibrate the GC responses for the gases of interest.

The manual volumetric system with the known volumes was used to make gas mixtures of known composition. To prepare a mixture, gas species 1 is charged to pressure P_1 in either of the tanks with volume V_1 and gas species 2 to a pressure of P_2 into another tank with volume V_2. The moles of each species can be calculated using a virial EOS with the second virial coefficient. The second virial coefficient B_i for a gas species i can be calculated from the Equation (3.2) listed below (reference DIPPR® physical properties database),

$$B_i = \frac{a_i}{1} + \frac{b_i}{T} + \frac{c_i}{T^3} + \frac{d_i}{T^8} + \frac{e_i}{T^9} \tag{3.2}$$

The molar volume ϑ_i of a gas species i at pressure P_i and temperature T can be calculated from the Equation (3.3) given by Van Ness et al. (1987); [68]

$$\vartheta_i = \frac{R \cdot T}{2 \cdot P_i} \cdot \left(1 + \sqrt{1 + \frac{4 \cdot B_i \cdot P_i}{R \cdot T}} \right) \tag{3.3}$$

The number of moles, n_i, of gas species *i* charged into the system can be calculated from Equation (3.4),

$$n_i = \frac{V_i}{\vartheta_i} \tag{3.4}$$

The charge is then thoroughly mixed using the gas circulation pump. The mole fraction of species *i* in the gas mixture is then,

$$y_i = \frac{n_i}{n_1 + n_2} \tag{3.5}$$

A small quantity of the known mixture was then injected into GC for analysis. The GC itself was optimized for the appropriate flow rate of carrier gas, column operation temperature, run time, etc. Under all optimized conditions two clear and separate peaks are obtained, one for each of the species in the binary gas mixture. The area under these peaks are calculated using the chromatograph integrator. These peak areas (A_i) are proportional to the amount of the corresponding species (n_i) injected. For instance total amount injected is n_t and y_i is the mole fraction of corresponding species,

$$\%A_i \, \alpha \, n_i \implies \%A_1 \, \alpha \, n_t . y_1 \approx \%A_2 \, \alpha \, n_t . y_2 \, ; \tag{3.6}$$

Let K_i be the proportionality constant between area fraction ($\%A_i$) and mole fraction (y_i). From the experiments performed, it is clear that K-factor (K_i) depends upon both the area fraction ($\%A_i$) and the mole fraction (y_i) of the gases in the mixture. While doing these calibration and actual binary experiments, the injection pressure of the sample was maintained constant at 15 psi to ensure that the amount of sample going into the GC column is constant.

$$\%A_i = \frac{y_i}{y_i + K_i \cdot y_j} \tag{3.7}$$

Rewriting Equation (3.7) in terms of proportionality coefficient K_i;

$$K_i = \frac{y_i - \%A_i \cdot y_i}{y_j \cdot \%A_i} \tag{3.8}$$

After doing calibration at several different mixture composition and plotting K-factor in terms of Methane (K_1) against its area fraction ($\%A_1$), third degree polynomial relationship for K-factor and area fraction has been derived and can be shown by following Equation (3.9),

$$K_1 = 0.3861 * \%A_1{}^3 - 0.9352 * \%A_1{}^2 + 0.8102 * \%A_1 + 1.1453 \tag{3.9}$$

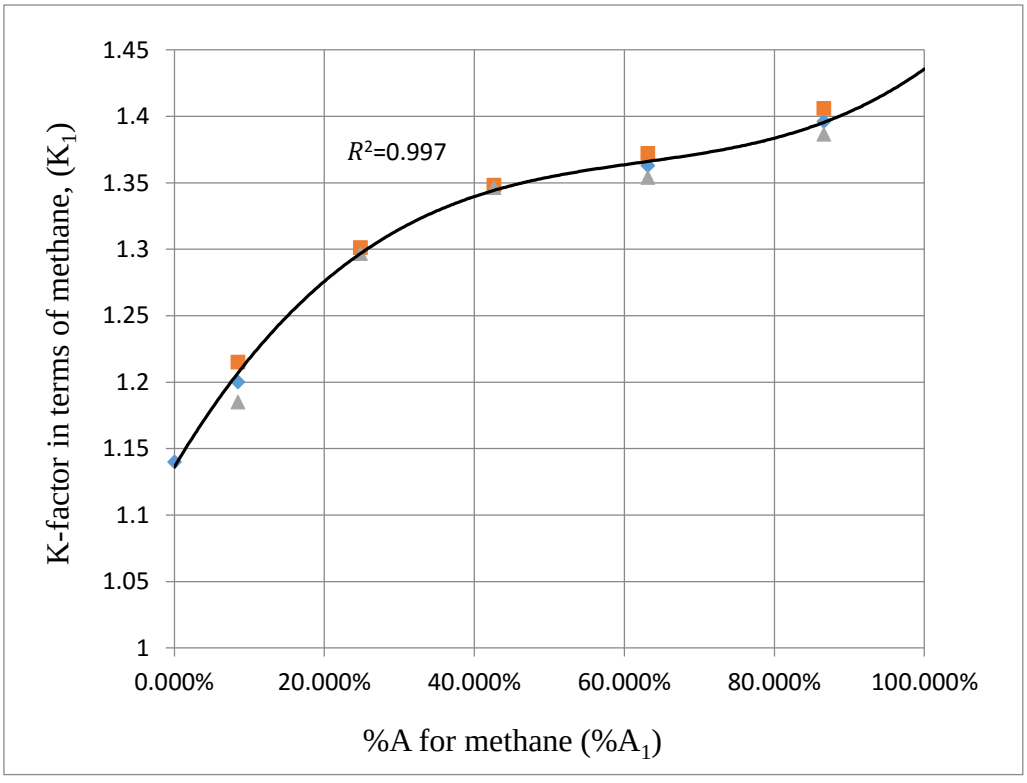

Figure 3.4. K-factor for methane changes with its area fraction

3.2.2 Experimental Procedures

3.2.2.1 Column Activation

The zeolite in the column is first activated under vacuum with a small helium flow at elevated temperature. Column is heated with a Glas-Col heating jacket (model: 100B TM518) which was controlled by lab size temperature controller Omega (model: CN2011 TC-D3).

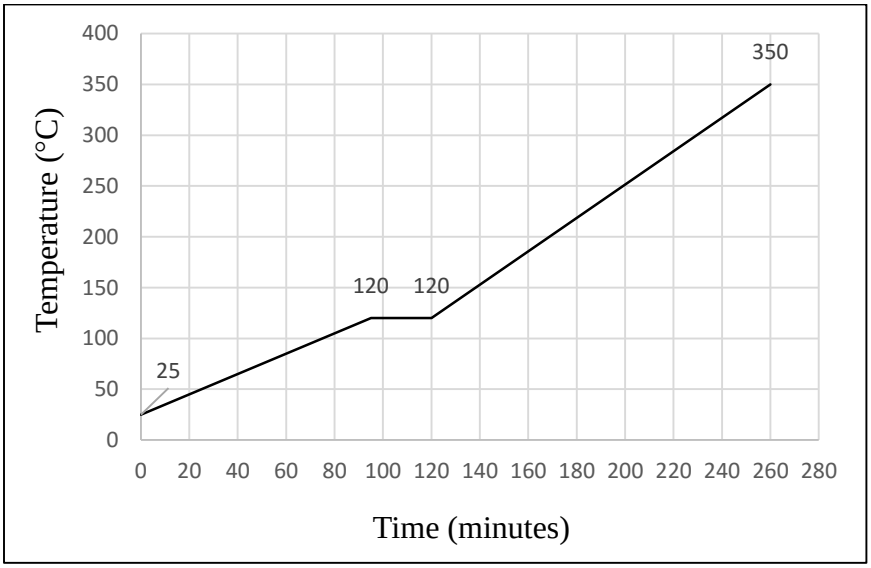

Figure 3.5. Ramp and soak implemented by temperature controller

Initially the heating rate was 1°C/ min up to 120 °C and after that it goes up to 350°C in 4 hours and 20 minutes. The ramp and soak method as shown in the Figure 3.5 is implemented by the temperature controller. During activation helium flow was set to 20 sccm/min and pressure (with full vacuum application) is 0.02 psi. The conditions are

maintained overnight to make sure column adsorbent is completely regenerated. After leaving the system overnight, the column was isolated after evacuation and then cooled down to the atmospheric temperature by removing the heating jacket.

3.2.2.2 Experimental Protocol for Pure Component Adsorption Isotherm

For pure component adsorption isotherm, one or both the storage tanks were filled with the desired gas. The pressure and temperature was recorded after sufficient time is allowed for constant pressure reading (e.g. 10 minutes). This measurement is necessary to calculate initial number of moles of gas in the system. The gas is then allowed to expand into the adsorbent column by opening valve A7. A transient pressure drop will occur due to adsorption and column temperature will also rise momentarily as adsorption is an exothermic phenomenon. After the pressure and temperature of the system is stabilized indicating equilibrium is achieved, pressure reading for gas phase was recorded along with the temperature reading at different location of the system. In most of the pure component experiments, equilibrium is assured by negligible pressure fluctuation within 30 minutes. After finishing first set of expansion, the adsorption column was isolated by closing valve A7 and the system was recharged with the same gas multiple times, depending upon the pressure range and readings necessary to represent isotherm. Maximum 6-7 points are measured before the column is regenerated. This is necessary to necessary to minimize error in measurements since the calculation procedure is stepwise causing accumulation of uncertainty.

3.2.2.3 Calculating Pure Component Adsorption

It is a similar concept as measuring unknown void volume. The only modification made in the material balance was inclusion of amount adsorbed to calculate pure component adsorption isotherm. At the beginning of the experiment a known volume of system, V_{charge} was filled with the gas of interest to a pressure of P_{charge}. Since the gas was adsorbed in the column, the mole balance can be written as;

$$n^{ads}|_{eq-1} \cdot m + n_{bed}|_{eq-1} + n^{initial}\Big|_{charge} = n^{final}\Big|_{eq} + n^{ads}|_{eq} \cdot m \quad or \qquad (3.10)$$

$$n^{ads}|_{eq-1} \cdot m + \frac{V_{bed}}{\vartheta_{bed}}\Big|_{eq-1} + \frac{V^{initial}}{\vartheta^{initial}}\Big|_{charge} = \frac{V^{final}}{\vartheta^{final}}\Big|_{eq} + n^{ads}|_{eq} \cdot m \qquad (3.11)$$

In Equations (3.10) and (3.11), V^{final} is the total gas phase volume accessible to gas at the equilibrium and *m* is the mass of solid adsorbent, $n^{ads}|_{eq-1}$ is the moles of gas adsorbed during the previous equilibrium step and $n_{bed}|_{eq-1}$ is the moles of gas in the void volume of the bed but remains unabsorbed during the previous equilibrium step. This Equation (3.11) directly yields amount of gas adsorbed at equilibrium for the most recent charge, $n^{ads}|_{eq}$, when molar volume of charge, $\vartheta^{initial}$ and molar volume at equilibrium, ϑ^{final} can be calculated from the Equation (3.3).

3.2.2.4 Experimental Protocols for Binary Gas Adsorption Isotherm

For binary measurement each storage tank is filled with a different gases of interest. Both the pressure and temperature readings for various sections were noted to calculate initial moles of each gases present in the system. After the charge step both the gases were circulated at high flow rate (about 100 sccm/min) for about 30 minutes through the column bypass with the help of the pump to ensure thorough mixing before introducing to column adsorbent. It is necessary to flush pressure transducer lines (1/8" I.D. tubing) because it might happen that gases inside those lines are not mixed properly in normal mixing procedures. Pressure transducer lines were flushed several times by pressurizing gas mixture by closing valve A3. After proper mixing was assured, gas mixture was then circulated through the column by opening both the valve A6 and A7 with column bypass valve A10 closed. As the pure component adsorption, a sudden pressure drop will occur due to adsorption along with the slight temperature rise. Initially in the first stage the gas mixture was set to higher flow rate for about 1 hour; then to a medium flow rate about the same time and in the last stage gas mixture was set to the lowest flow rate for 30 minutes. After the pressure and temperature of the system is stabilized, means equilibrium is achieved, circulation of the gas mixture was stopped to get the pressure reading for gas phase along with the temperature reading at different location of the system. In most of the binary adsorption experiments, equilibrium is assured by negligible pressure fluctuation within 2 hours after starting the gas flow across the column.

After equilibrium pressure is measured, the column is isolated by closing valves A6 and A7. Again flow of the gas mixture is set across the column bypass by opening column bypass valve A10. The composition of the gas phase mixture was analyzed using a gas chromatograph.

Only one experiment per day is possible in case of binary experiment because of a large error that would be introduced in material balance calculations. That is why the solid adsorbent is regenerated before the experimental protocol is repeated for another experiment next day.

3.2.2.5 Calculating Binary Absorption Isotherm

For instance gas species 1 be charged to a pressure P_1 into known volume V_1 in the system and species 2 be charged to a pressure P_2 into volume V_2 of the system. The moles of each individual species charged n_1 and n_2 can be calculated from Equation (3.4).

The mixture is then equilibrate with the adsorbent. Let V_{eq} be the volume accessible to gas at the equilibrium condition and pressure at equilibrium be P_{eq}. The gas phase composition was analyzed by gas chromatograph. The area under the peak for each species A_1 and A_2 are obtain using integrator. Using the K-factor definition (Equation (3.8)), the equilibrium gas phase mole fraction $y_{1,eq}$ and $y_{2,eq}$ are then calculated.

$$y_{1,eq} = \frac{\%A_1 \cdot K_1}{1 - \%A_1 + \%A_1 \cdot K_1} \tag{3.12}$$

$$y_{2,eq} = 1 - y_{1,eq} \tag{3.13}$$

After getting gas phase mole fraction at equilibrium, it is required to calculate total number of moles of gas mixture at equilibrium. Which can be calculated by Equation (3.4).

$$n_{eq} = \frac{V_{eq}}{\vartheta_{eq}} \tag{3.14}$$

The molar volume, ϑ_{eq} for the gas mixture at equilibrium can be calculated from Equation (3.3) using temperature and pressure at equilibrium. However the only difference will be requirement of the second virial coefficient for the mixture, B_{mixt}. Second virial coefficient is pair interaction between two molecules and in binary mixture containing species 1 and 2, there are three types of two molecule interaction are possible. For each of these interaction, 1-1, 2-2, 1-2, there is a corresponding second virial coefficient B_{1-1}, B_{2-2} and B_{1-2}. The second virial coefficient for the mixture is a quadratic function of the mole fraction $y_{1,eq}$ and $y_{2,eq}$

$$B_{mixt} = {y_{1,eq}}^2 \cdot B_{1-1} + 2 \cdot y_{1,eq} \cdot y_{2,eq} \cdot B_{1-2} + {y_{2,eq}}^2 \cdot B_{2-2} \tag{3.15}$$

In this work, the cross virial coefficient is approximated by hard-sphere model with

$$B_{1-2} = \left(\frac{(B_{1-1})^{\frac{1}{3}} + (B_{2-2})^{\frac{1}{3}}}{2} \right)^3 \tag{3.16}$$

Once the total moles at equilibrium, n_{eq} , were known, a mass balance was performed on individual species to calculate partial amount adsorbed , ${n_1}^{ads}$ and ${n_2}^{ads}$.

$$n_1 = {n_1}^{ads} \cdot m + n_{eq} \cdot y_{1,eq};\ n_2 = {n_2}^{ads} \cdot m + n_{eq} \cdot y_{2,eq} \tag{3.17}$$

3.3 Details of Adsorbent

Silicalite as a 1/16" pellets (around 20% binder) form is used in this study. Silicalite is a member of pentasil zeolites which comprise a family of silica-rich zeolite with structure base on the double five-ring unit shown in Figure 3.6. Silicalite is the aluminum free end member of the ZSM-5 family of zeolite. It is one of the most important synthetic zeolites widely used as a selective adsorbent. Dealumination of certain silica rich zeolites can be achieved by acid treatment. ZSM-5 structure is formed from linkage of secondary building unit (SBU) as shown in Figure 3.6. It should be also evident from Figure 3.6 that this SBU can be readily viewed as a pair of five 1-unit that can be interconnected to form a layer as outlined in Figure 3.6. Silicalite structure us exactly same as ZSM-5 except that aluminum (Al^{+3}) are replaced by silicon atoms (Si^{+4}). The framework outlines a three dimension system of intersecting channel by defined by 10-rings of oxygen atoms in all three dimension array [69].

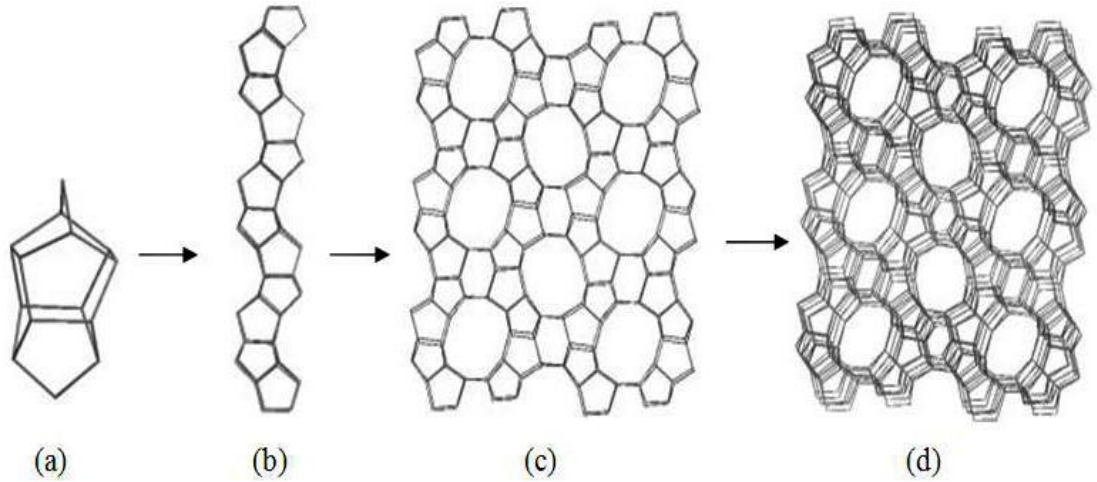

Figure 3.6. Framework topology of ZSM-5. The 5-ring polyhedron is connected into chains which form the ZSM-5 structure with the 10-membered openings of the linear channels [58, 49].

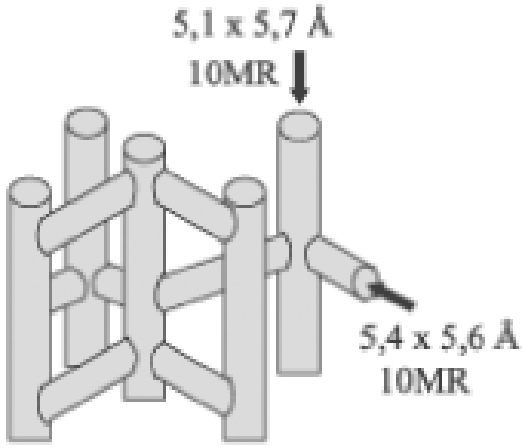

Figure 3.7. Idealize channel system in silicalite [58]

The unit cell of silicalite consists of 96 tetrahedral. They form a 4 connected framework with a system of intersecting channels as shown in the Figure 3.7 above. It depicts from the Figure 3.7 above that it is composed of near circular of zig-zag channels along a axis (free cross-section 5.4+0.2 Å) cross-linked by elliptical, straight channel along b-axis (free cross-section 5.7-5.8 x 5.1-5.2 Å). Both channels are defined by 10 rings. The channels have a free diameter of ~6 Å and, thus, close to the free diameter of the adsorbate molecules used in this study (i.e. methane and nitrogen). Silicalite has high thermal stability and it can be heated up to 1300 °C. Its distinctive features also include hydrothermal stability, hydrophobic and organophilic [9, 19, 28, 32].

3.4 Details of Adsorbates

In this work, various gases were used as either adsorbate (i.e. methane and nitrogen) or probe (i.e. helium for this work) to measure unknown internal volume as mentioned in earlier discussion. In Table 3.3, molecular weight and temperature dependent virial coefficient of all the gases used along with the temperature range it can be used for are given. These values are obtained from DIPPR^{TM} physical properties database. Some of the other physical properties of methane and nitrogen gases are summarized in Table 3.4 below.

Table 3.3. Temperature dependency of second virial coefficient for various gases

Gas	Unit	Helium	Methane	Nitrogen
Temperature range (K)	K	3-519	95-953	6-1400
a_i	kmol/m^3	0.014	0.054	0.046
b_i	kmol.K/m3	-0.354	-27.14	-14.95
c_i	kmol.K^3/m^3	-0.595	-213500	-61130
d_i	kmol.K^8/m^3	361	9.2 x 10^{14}	8.05 x 10^{13}
e_i	kmol.K^9/m^3	-794	-7.85 x 10^{16}	-4.6 x 10^{15}

Table 3.4. Physical properties of gases

Property	Methane	Nitrogen
Molecular weight	16.04	28.01
Kinetic diameter, (cm)	3.82×10^{-8}	3.64×10^{-8}
Critical Diameter (cm) +	3.24×10^{-8}	3.15×10^{-8}
Quadrupole moment ($C.m^2$) *	0	-5×10^{-40}
Permanent dipole moment (C.m)	0	0
Polarizability, (cm3) *~	2.593×10^{-24}	1.7403×10^{-24}
Boiling Point, K	161.48	77.3
Specific gravity (air = 1) (1 atm and 288 K)	0.554	0.967
Critical temperature, K	190.6	126.2
Critical pressure, atm	46.8	34.67
Liquid molar volume at normal boiling point (cm^3/mol)~~	37.7	31.6
Molar heat capacity (298.15 K, 1 atm), J/mol/K	35.9	29.1
Thermal conductivity (1 atm and 273.15 K) W/(mK)	0.033	0.024

*: Molecular thermodynamics of fluid-phase equilibria, J. M. Prausnitz, Prentice-Hall, Inc., Englewood Cliffs, New Jersey (1969)

~ : Table of experimental and calculated static dipole polarizabilities for the electronic ground states of the neutral elements (in atomic units) by Peter Schwerdtfeger, Last Update: February 11, 2014

+: Sydney Ross and James P. Olivier., On Physical Adsorption, (Interscience/Wiley, New York, 1964

~~ T.C. Golden, S. Sircar, Gas adsorption on silicalite. J. Colloid Interf. Sci. 162, 182–188 (1994)

CHAPTER IV

RESULTS AND DISCUSSIONS

Adsorption equilibrium information is an essential requirement for the analysis and design of adsorption separation processes. Adsorption equilibrium data provides information on the capacity and selectivity of an adsorbent for simulation and design of an adsorption process. The closed volumetric system discussed in Chapter III has been used to measure pure component adsorption equilibria of methane (CH_4) and nitrogen (N_2), as well as binary mixtures on silicalite. The following section provides the pure component isotherms and their modelling, binary adsorption equilibrium experimental results and model predictions.

4.1 Pure Component Adsorption Isotherms

The pure component adsorption isotherms for methane and nitrogen were measured using the closed volumetric system at three different temperatures 283.15 K, 308.15 K, and 338.15 K. These results are shown in the regular domain (N vs. P) in Figures 4.1 & 4.2.The data is given in Tables 4.1 and 4.2.

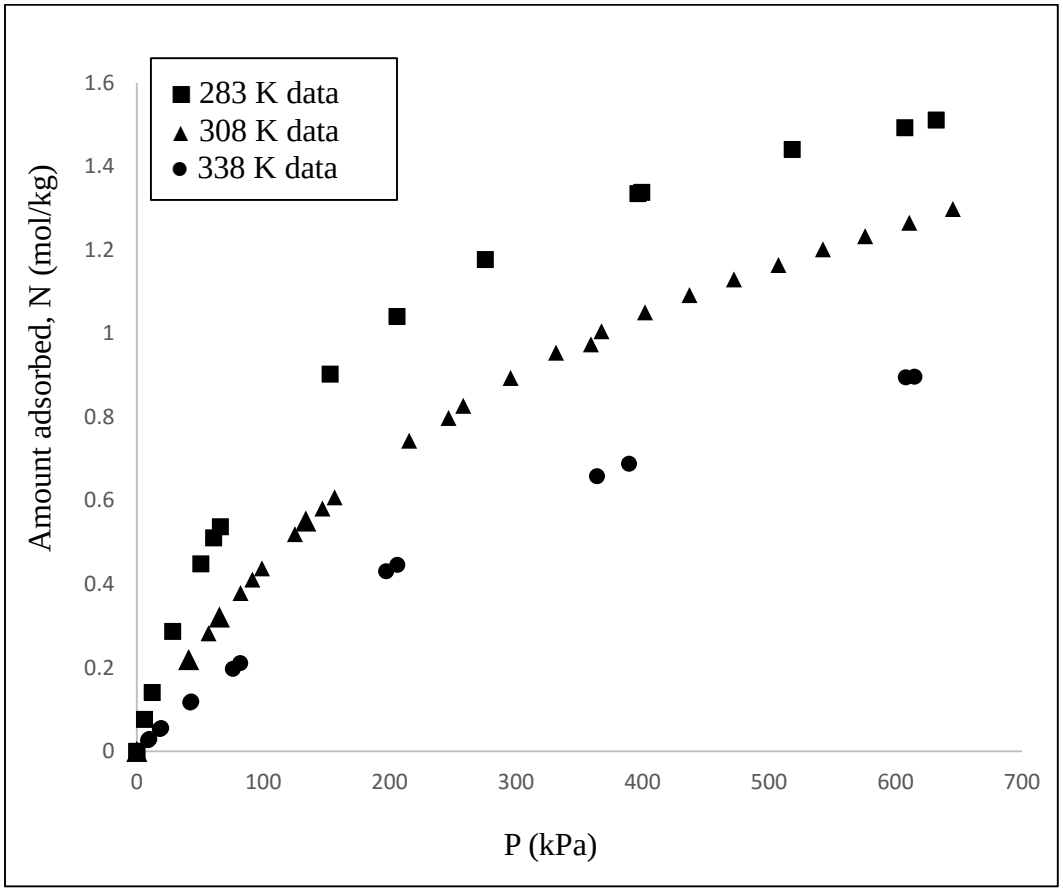

Figure 4.1. Methane adsorption isotherms on silicalite

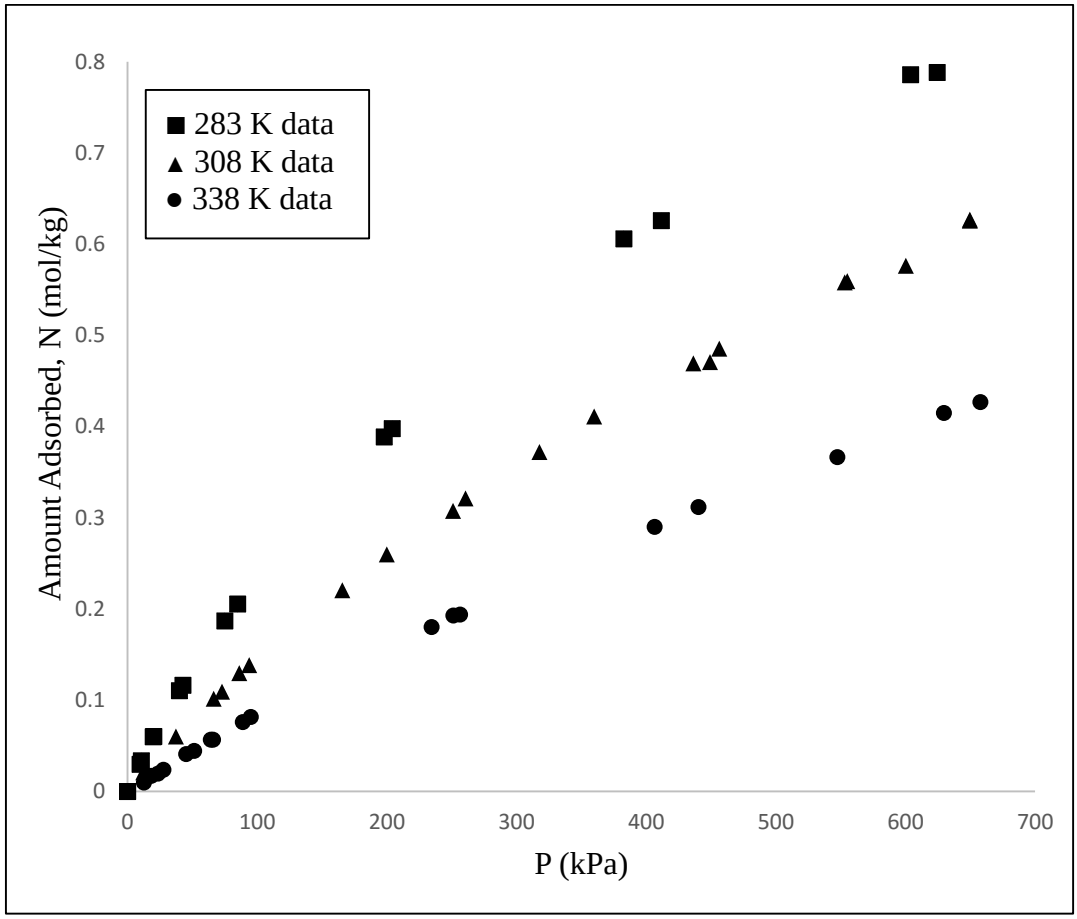

Figure 4.2. Nitrogen adsorption isotherms on silicalite

Table 4.1. Experimental adsorption isotherm data for methane on silicalite

T (K) = 283.15		T (K) = 308.15		T (K) = 338.15	
P (kPa)	N (mol/kg)	P (kPa)	N (mol/kg)	P (kPa)	N (mol/kg)
0	0	0	0	0	0
6.21	0.077	41.03	0.220	9.03	0.027
12.24	0.141	41.27	0.216	10.03	0.030
28.55	0.287	56.75	0.282	18.41	0.054
50.68	0.449	65.5	0.322	19.41	0.056
61.02	0.511	65.71	0.318	42.27	0.117
66.12	0.537	82.19	0.379	43.23	0.120
153.1	0.903	91.36	0.411	75.95	0.198
205.8	1.041	98.95	0.438	81.71	0.211
275.8	1.177	125.2	0.520	197.2	0.431
396.5	1.335	133.8	0.551	206.2	0.447
399.6	1.338	146.9	0.581	364.1	0.658
518.5	1.441	156.5	0.608	389.2	0.688
607.5	1.493	215.5	0.744	608.2	0.895
632.3	1.511	246.5	0.798	615.1	0.896
		258.2	0.827		
		295.8	0.893		
		331.7	0.955		
		359.2	0.974		
		367.5	1.005		
		402.0	1.051		
		437.2	1.092		
		472.3	1.129		
		507.5	1.164		
		542.7	1.202		
		576.1	1.233		
		610.9	1.265		
		645.4	1.298		

Table 4.2. Experimental adsorption isotherm data for nitrogen on silicalite

T (K) = 283.15			T (K) = 308.15			T (K) = 338.15	
P (kPa)	N (mol/kg)		P (kPa)	N (mol/kg)		P (kPa)	N (mol/kg)
0	0		0	0		0	0
9.45	0.030		12	0.021		12.62	0.010
10.55	0.034		37.2	0.060		18.2	0.017
19.79	0.060		66.4	0.102		23.37	0.020
20.24	0.060		72.71	0.109		27.48	0.024
39.92	0.110		86.19	0.130		45.16	0.041
42.75	0.117		93.71	0.138		51.23	0.045
74.95	0.187		165.5	0.221		64.06	0.057
84.74	0.206		200.0	0.260		65.85	0.057
197.9	0.389		251.0	0.308		88.74	0.076
204.1	0.398		260.6	0.321		94.95	0.082
382.7	0.606		317.5	0.372		234.4	0.180
411.6	0.626		359.9	0.411		251.3	0.193
604.0	0.786		436.5	0.469		256.5	0.194
624.4	0.788		449.2	0.471		406.5	0.290
			456.5	0.486		440.3	0.312
			553.0	0.558		480.9	0.328
			555.1	0.560		547.5	0.367
			600.2	0.577		629.5	0.415
			649.5	0.626		632.6	0.406
			649.5	0.627		657.8	0.427

The uncertainty in the isotherm was calculated using propagation of error analysis (Appendix A). It must be noted that apart from the volume of the various sections the only other measured variables for pure component isotherms are temperature and pressure before and after equilibrium. All the experiments in pure component isotherm were performed by successive charges. Six to seven data points were obtained to complete one isotherm after each activation. Because of that reason, the maximum uncertainty is for the last few points on isotherm after activation, due to accumulation of error. For the majority of the remaining points the uncertainty is lower. This uncertainty can be reduced, and more accurate measurements would be possible, if the sample were activated after each measurement.

Table 4.3. Uncertainty in pure component adsorption isotherms obtained from volumetric system

Gas	Minimum Error		Maximum Error		Average Error	
	Absolute (mol/kg)	%	Absolute (mol/kg)	%	Absolute (mol/kg)	%
Methane	0.002	0.6	0.079	6.9	0.027	2.8
Nitrogen	0.000	0.1	0.015	2.6	0.001	1.1

4.2 Modeling of Pure Component Adsorption Isotherms

It is always convenient to be able to represent pure component adsorption isotherms by an equation to facilitate binary adsorption predictions. Two models can be used to determine the adsorption isotherm equation parameters: the Langmuir model and the Virial model.

4.2.1 Langmuir Adsorption Isotherm Regression Results

Langmuir parameters can be obtained from experimental data by linear regression with the adsorption isotherm expression seen in Equation (2.52). The model fits are shown in Figures 4.3 and 4.4 below as dotted lines. The parameter values obtained by linear regression are given in Table 4.4 below. Once Langmuir parameters are estimated, the assessment of goodness-of-fit is discussed t-statistics and also standard error of the parameters. This would normally be an excellent representation of data with the model in the regression domain as (P/N) VS. P.

Table 4.4. Langmuir parameters for methane, nitrogen on silicalite

Parameters	Units	Methane			Nitrogen		
		Value	Std. Error (%)	t-stat	Value	Std. Error (%)	t-stat
T = 283.15 K							
N^{∞}	mol/kg	1.8796	1.3	65.48	1.3163	6.9	48.41
b	1/kPa	0.0062	0.0	134.53	0.0022	0.0	31.89
T = 308.15 K							
N^{∞}	mol/kg	1.9516	1.5	116.74	1.4273	8.4	73.31
b	1/kPa	0.0029	0.0	113.89	0.0011	0.022	31.79
T = 338.15 K							
N^{∞}	mol/kg	1.7433	1.8	188.31	1.5408	15.9	71.20
b	1/kPa	0.0016	0.0	90.94	0.0005	0.0465	13.95

The Langmuir model is not appropriate for process simulations, since it does not explicitly express how the parameters change with temperature. Temperature variations are inevitable in any realistic application due to the exothermic nature of adsorption. Since one of the purposes of the work is to enable process simulation, the Langmuir model will not be further considered. The Langmuir model results can be used for very dilute system where the change in amount adsorbed is small.

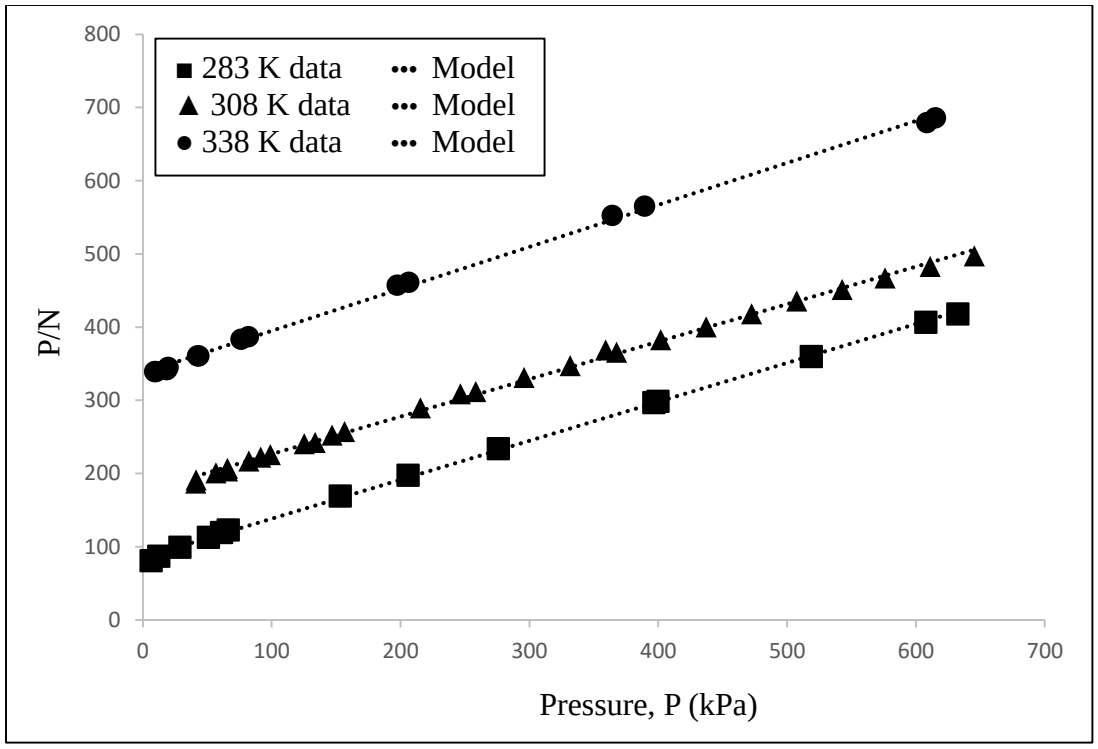

Figure 4.3. Model Predictions and Experimental Data for Pure methane

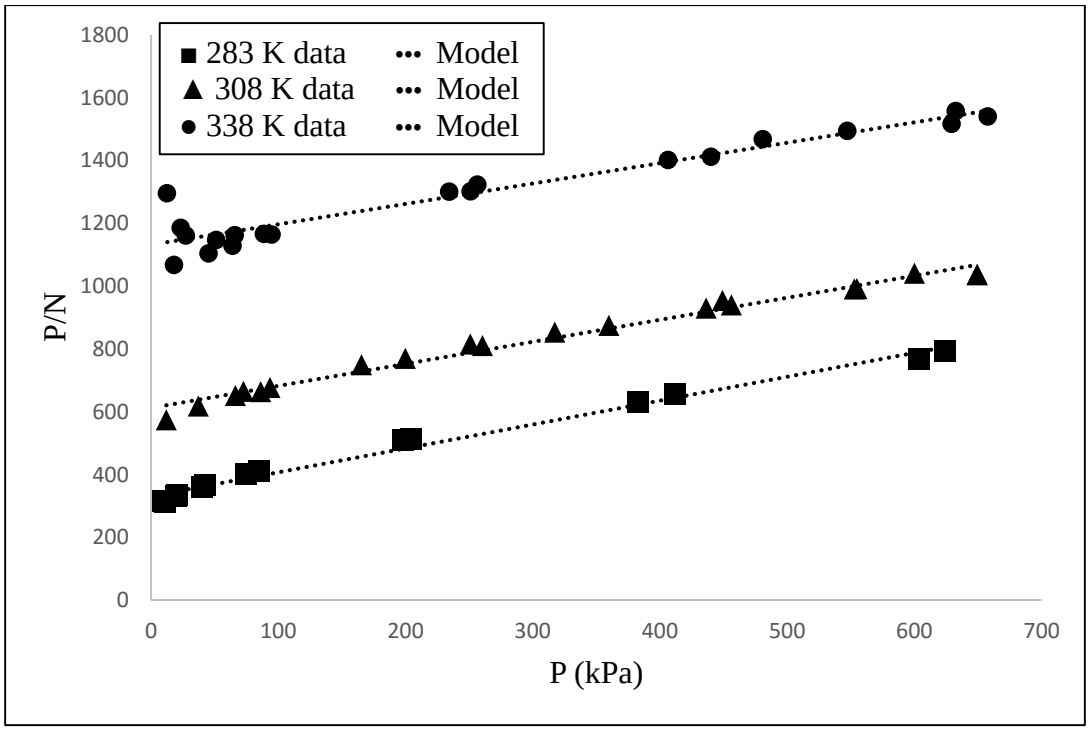

Figure 4.4. Model Predictions and Experimental Data for Pure nitrogen

4.2.2 Virial Adsorption Isotherm Regression Results

Multi-parametric linear regressions analysis were performed on the entire pure component data set for each component to determine the Virial model coefficients and their variation with temperature. A statistic software, Sigmastat, was used. Isotherm data at all temperatures were used in a single multiple linear regression with model equations (Equation (2.58)). The best fitting model was chosen by the F-statistics of the overall regression by forward stepwise technique with a significance level of 0.05. The estimated Virial coefficients obtained from the data analysis for the adsorption of methane and nitrogen in silicalite are presented in Table 4.5 along with standard error of parameters.

Table 4.5. Virial parameters for methane and nitrogen on silicalite

Gas	Methane			Nitrogen		
Parameter	Value	Std. error %	t-stat	Value	Std. error %	t-stat
k_0	13.41	0.08	158.32	13.71	0.09	151.11
k_1	-2584.7	28	-94.07	-2265.4	29	-78.18
b_0	0.21	0.14	0.98	-2.15	0.37	-5.88
b_1	236.7	43	6.70	1057.56	127	8.35
c_0	-0.46	0.1	-6.42	-	-	-
c_1	-	-	-	-223.73	146	-1.54
d_0	0.32	0.04	8.98	-	-	-
d_1	-	-	-	107.13	127	126.63

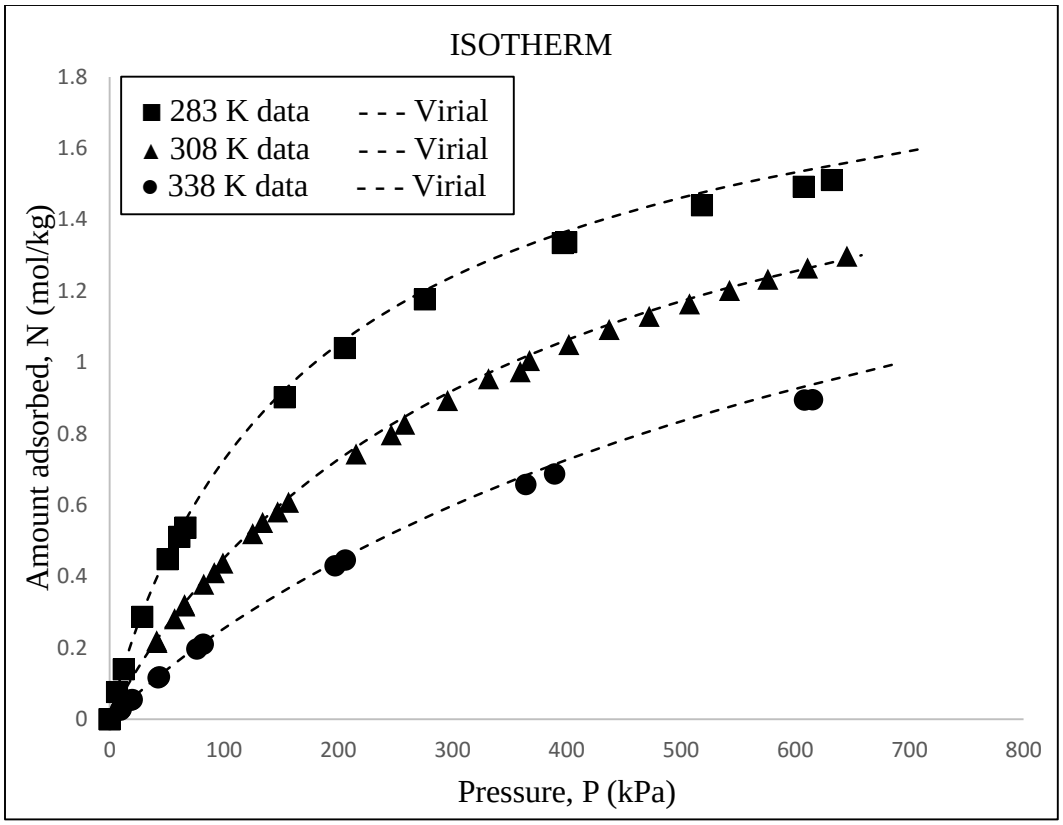

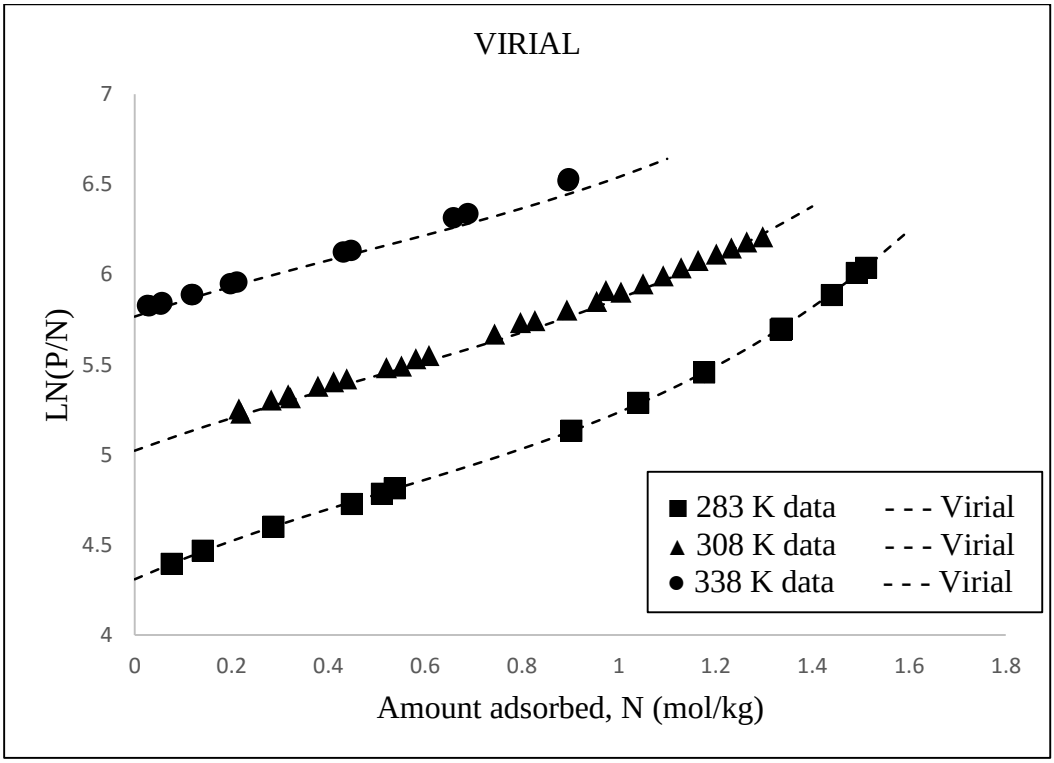

Figure 4.5. Virial Regressions and experimental data for pure methane

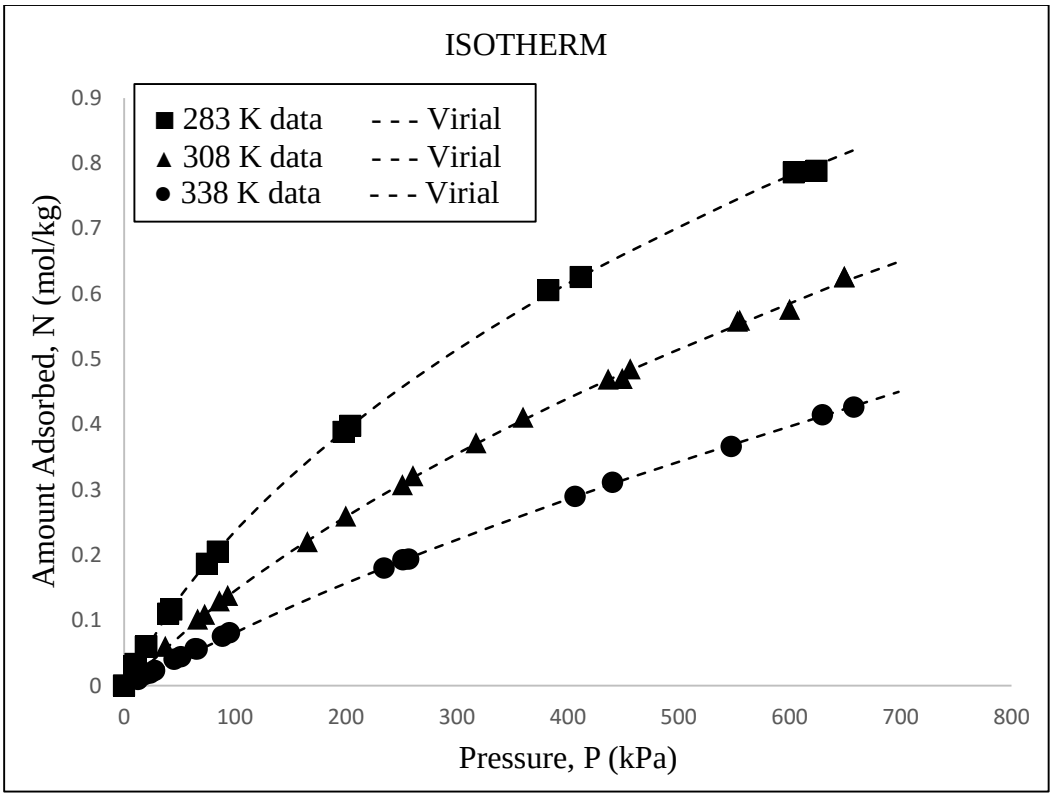

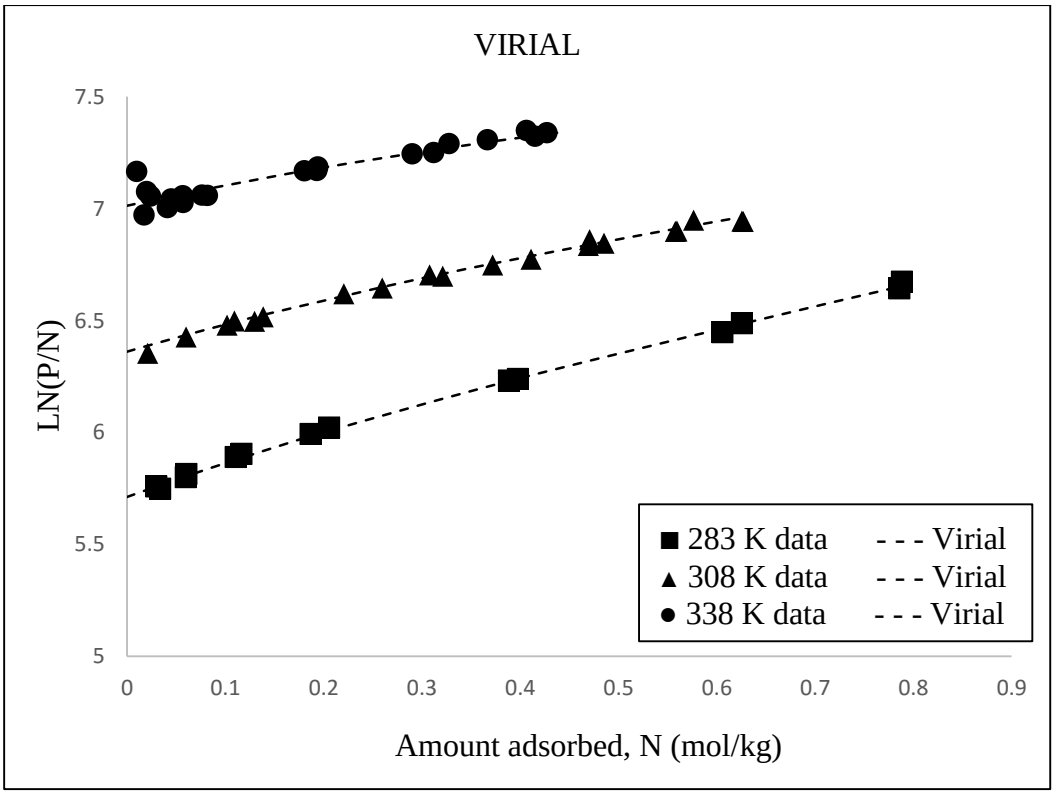

Figure 4.6. Virial Regressions and experimental data for pure nitrogen

4.2.3 Comparison between both the Models

Virial adsorption isotherm model (Equation (2.58)) and Langmuir adsorption isotherm model (Equation (2.52)) both have different structures and contains different parameters. Generally, model accuracy to reproduce data increases with increase in number of parameters. Therefore, comparison of a different models having different number of parameters is not a straightforward task to do. One method commonly used in literature to compare function is Error sum of squares (SSE). SSE is defined as,

$$SSE = \sum_{i}^{\infty} (y_i - \hat{y}_i)^2 \tag{4.1}$$

The SSE is a function of residues, the difference between each calculated observation and sample mean. In our case calculated observation is amount of moles adsorbed ($N_i{}^{model}$) at the same pressure as that of the experimental pressure. As there is no group in data set, mean can be replaced with the same experimental measured amount adsorbed ($N_i{}^{exp}$).

$$SSE = \sum_{i}^{\infty} (N_i{}^{model} - N_i{}^{exp})^2 \tag{4.2}$$

Table 4.6. Comparison of Residual Sum of Squares Error for two different regression models

RESIDUAL SUM OF SQUARES x 10^5				
Temperature (K)	Methane		Nitrogen	
	Langmuir	Virial	Langmuir	Virial
283.15 K	132.65	7.48	200.90	14.22
308.15 K	265.68	822.15	131.93	35.84
338.15 K	28.65	2.24	15.76	16.74

As it can be seen from the Table 4.6, Virial EOS (Equation (2.85)) is usually superior in representing pure isotherm data because of its extreme flexibility and parameters used in model are essentially covering behavior of the real gas without making any assumptions. More importantly the fitted model provides a direct way of calculating isosteric heat which is discussed in next section.

4.3 Isosteric Heat of Adsorption

Isosteric heat of adsorption represents the energetics of any adsorption system. At zero pressure (or coverage), the value of isosteric heat of adsorption directly indicates the affinity of the solid for gas molecules. These vertical interactions are also a proxy for the potential energy between a single molecule and the entire surface. (Properly weighted by the energy itself through Boltzmann distribution). Therefore for a known solid-fluid potential function, one can calculate the isosteric heat of adsorption at zero coverage rather easily with molecular simulation.

In addition the form in which isosteric heat varies with pressure (or coverage) also carries important information about either (1) molecule to molecule interaction in a confined pore system also referred to as the "lateral" interaction, or (2) a combined effect caused by the heterogeneous behavior of gas-solid pair. Two aspects affect how isosteric heat changes with pressure (or coverage) is in opposite direction. Molecule to molecule interactions (regardless of even if being on a surface) should always increase isosteric heat. Heterogeneity always cause a decrease in isosteric heat.

The isosteric heat of adsorption is calculated using virial constants as discussed earlier in Section 2.10 for both the gases. In Figure 4.7 the isosteric heat variation is showed against the loading for methane and nitrogen gases.

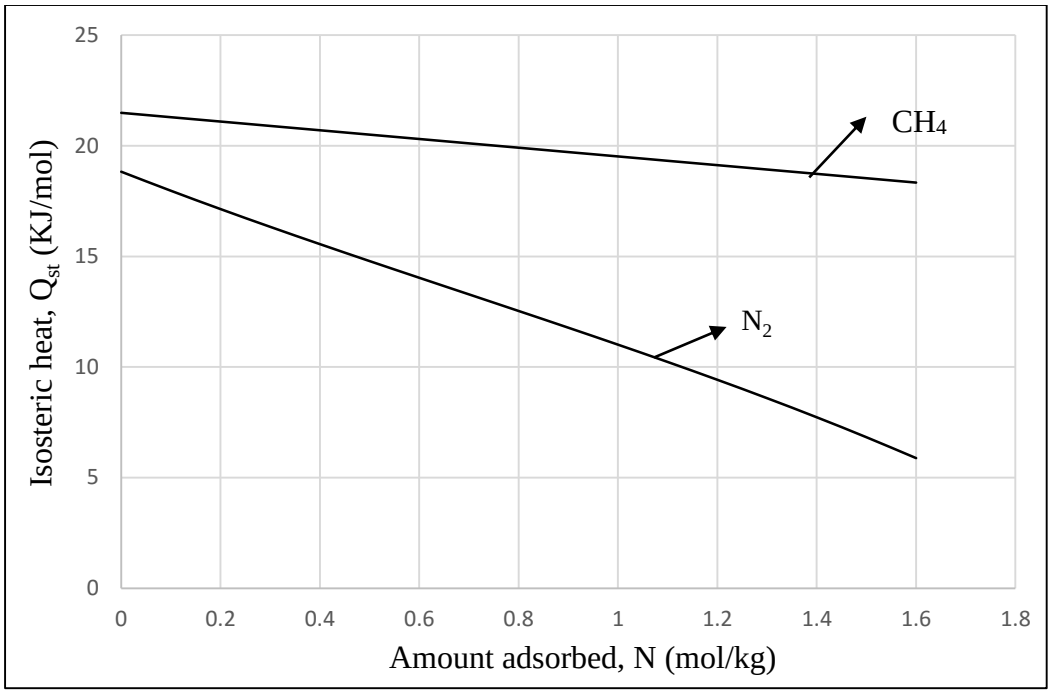

Figure 4.7. Isosteric heat of adsorption for CH_4 and N_2 on silicalite

The limiting isosteric heats of adsorption at zero coverage are 21.5 kJ/mole for methane and 18.8 kJ/mole for nitrogen, which indicate a very strong adsorption of methane compare to nitrogen. The silicalite is showing heterogeneity for both methane and nitrogen as indicated by the negative slope of isosteric heat. It is no surprise that methane isosteric heat changes only about 10% (up to 1.5 mol/kg) while the change in nitrogen isosteric heat is much larger due to its large quadrupole moment.

4.4 Spreading Pressure

The Spreading pressure is calculated as outlined in the Section 2.11 earlier. The plot below shown is obtain using virial model. A plot for spreading pressures against the

gas phase pressure for pure methane and nitrogen adsorption in silicalite at 308.15 K is shown in the Figure 4.8,

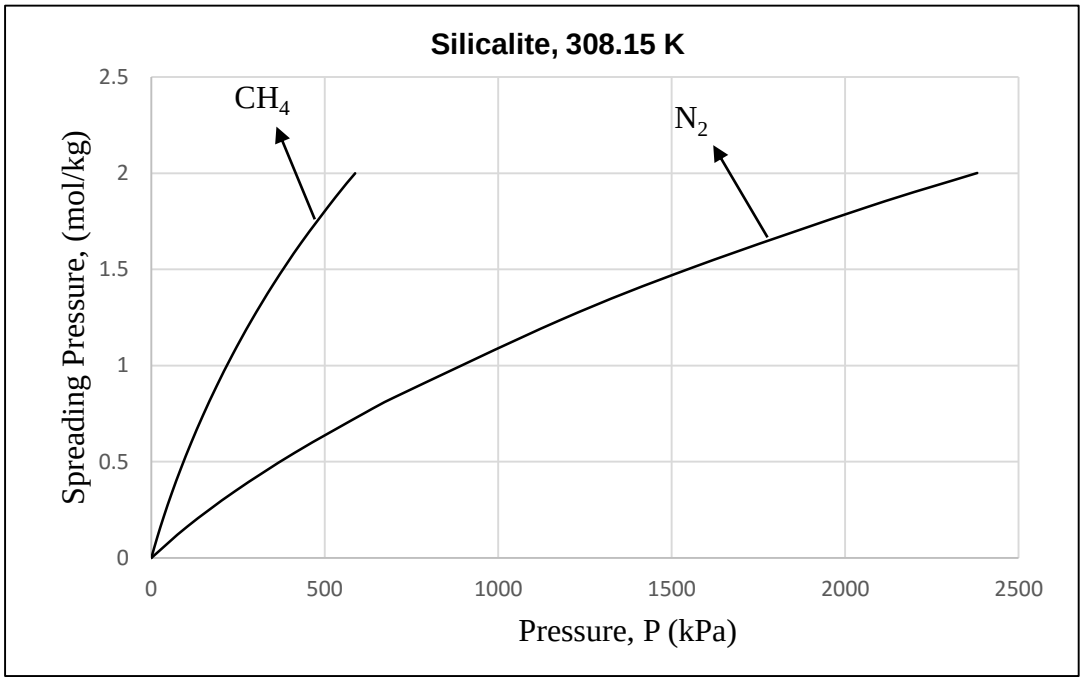

Figure 4.8. Spreading pressure of methane & nitrogen on silicalite at 308.15 K

As one can see from the Figure 4.8, the spreading pressure for methane increases very rapidly with pressure. Since methane is a heavier component the nitrogen spreading pressure increases slowly with pressure. As illustrated in the Figure 4.8, the standard state pressure for the lighter component (i.e. nitrogen) is usually much higher. Thus, based on preliminary estimation of the spreading pressure from the Virial EOS, the adsorbent is 3.81 times more selective for methane over nitrogen at 308.15 K temperature. The point to emphasis here is that lighter component isotherm data in this diagram is extrapolated up to standard state pressure of 2000 kPa while Virial parameters are only obtained upto 600 kPa.

4.5 Binary Adsorption Isotherm Results

In this section the binary adsorption isotherms of CH_4 + N_2 mixture on silicalite at 308.15 K temperature are presented. The analysis of data along with the thermodynamic consistency check. The experimental data is also compared with the predictions from Ideal solution adsorbed theory (IAST) using virial model which represents pure component equilibrium.

4.5.1 Measurement of Binary Adsorption Equilibria

Although it is not possible to control the final equilibrium properties of gases precisely but they can be measure accurately using volumetric system described in Chapter III. Before starting the experiments, the charge condition were estimated through IAST calculations and charge amount is thus calculated accordingly. Then the gases were equilibrated with the solid adsorbent in a closed system. In this work all the data points measured in binary experimental work were obtained at an approximately constant equilibrium pressure (~504 kPa) and an approximately constant equilibrium gas phase composition (60% methane and 40% nitrogen).

The binary equilibrium data was measured using the experimental protocol outlined in Section 3.2.2.4. Apart from the internal volumes of the experimental apparatus (required for material balances), temperature and pressure in various sections of the apparatus at

equilibrium provide the information required for the calculation of total amount adsorbed directly. To determine the surface composition, the equilibrium gas phase composition must be determined. The composition of the gas at equilibrium was measured using a GC (gas chromatographic unit). GC calibration results for the gas mixtures under consideration are given in Appendix B.

4.5.2 Binary Equilibrium Data

The adsorbed phase properties, such as the partial amounts adsorbed, are calculated from the experimental measurements at a given temperature T, gas phase pressure, and composition y_i as described in experimental section. The results are given in Tables 4.7,

Table 4.7. Binary equilibrium data for CH_4 + N_2 mixture on silicalite at 308.15 K

CH_4 + N_2 mixture (Constant pressure region)					
P (kPa)	y_1	N_t, mol/kg	N_1, mol/kg	N_2, mol/kg	$S_{1,2}$
504.7	0.087	0.632	0.284	0.348	8.563
504.7	0.089	0.631	0.249	0.382	6.648
504.7	0.205	0.705	0.351	0.353	3.865
503.3	0.309	0.809	0.455	0.354	2.871
505	0.399	0.88	0.501	0.379	1.992
504.3	0.517	0.94	0.646	0.294	2.054
504.7*	0.605	0.996	0.683	0.312	1.43
502.6	0.705	1.043	0.795	0.248	1.34
504.7	0.803	1.07	0.918	0.151	1.486
504	0.916	1.148	1.036	0.111	0.847
504.7	0.916	1.137	1.126	0.011	9.157
CH_4 + N_2 mixture (Constant composition region)					
140.6	0.619	0.441	0.372	0.069	3.286
241.3	0.619	0.641	0.542	0.099	3.348
360.2	0.618	0.851	0.616	0.235	1.617
504.7*	0.605	0.996	0.683	0.312	1.43

* Common point on both planes.

4.5.3 Analysis of Binary Equilibrium Data

In the following section various thermodynamic diagrams for the experimental data are presented, along with some examples and relevant discussion. In each Figure the IAST predictions are also shown (as solid lines) for reference purpose.

4.5.3.1 X-Y Plot

`

The x-y plot gives a quick overview of the adsorption behavior of a binary mixture. Unlike the vapor liquid equilibrium, due to the extra degree of freedom for adsorption equilibria, the xy- plot is a function of both temperature and pressure. Figure 4.9 shows x-y plots for the methane-nitrogen systems at constant temperature (308.15 K) and pressure (504 kPa). The solid is selective to methane over nitrogen as indicated by both data and IAST.

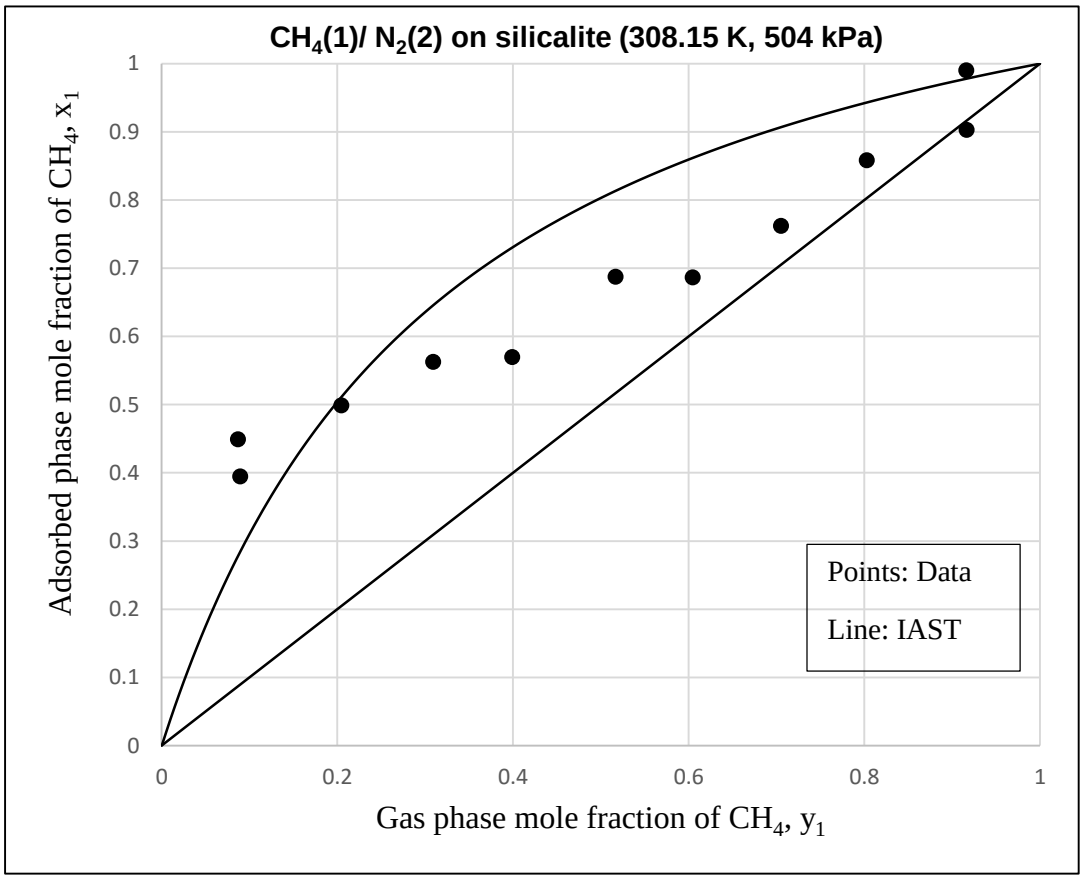

Figure 4.9. X-Y plot of CH_4 + N_2 mixture at 308.15 K and 504 kPa.

4.5.3.2 Variation in Amount Adsorbed With Gas Phase Composition

Figure 4.10 shows the total amount adsorbed from a gas mixture at 308.15 K and 504 kPa. The only thermodynamic requirement for this plot is that, at the ends of the phase diagram as the composition approaches unity, the total amount must reach the pure component amount of the corresponding species. For example, the point A corresponds to pure the nitrogen amount adsorbed at the same temperature and pressure. Since the virial

isotherm represents pure component data so closely, it can be stated that the limits indicated by IAST predictions correspond to the pure components behavior. Similarly point B corresponds to the pure methane amount adsorbed.

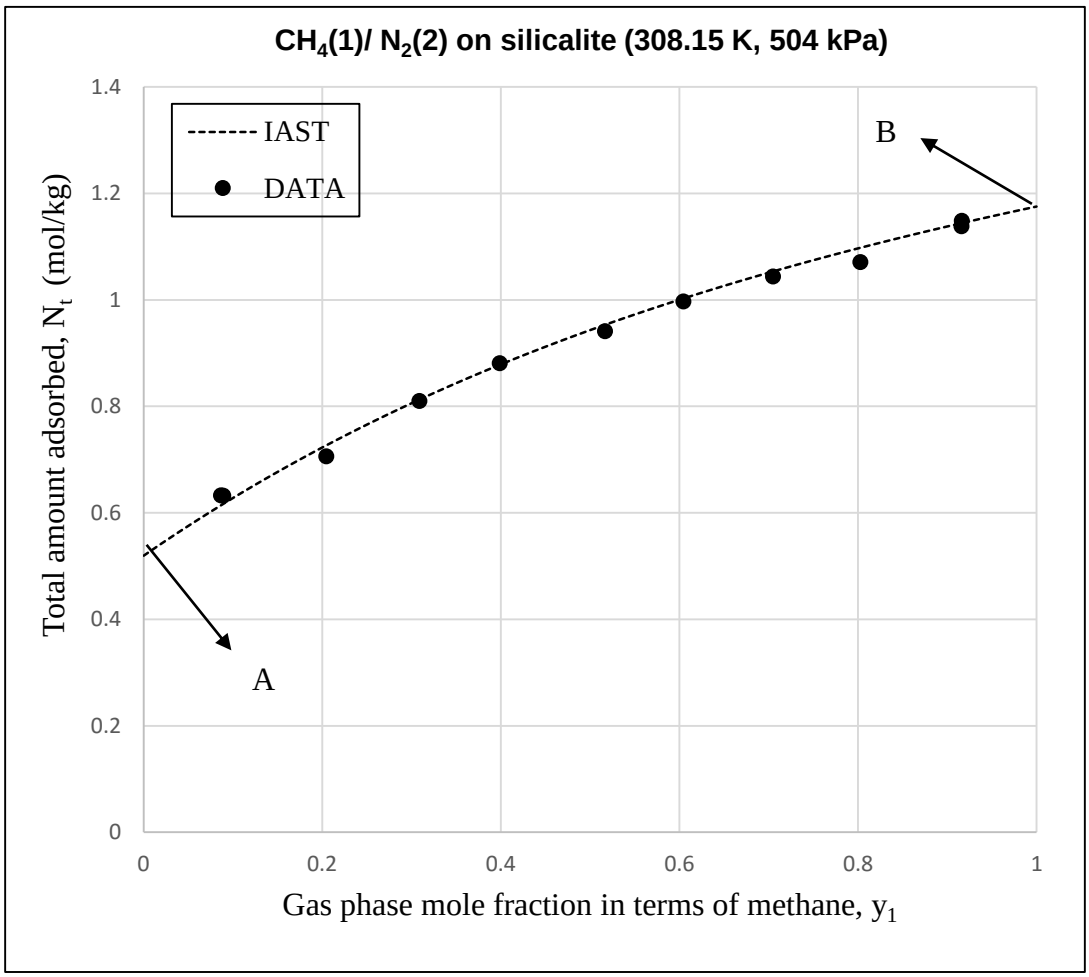

Figure 4.10. Total amount adsorbed with gas phase mole fraction of methane at 308.15 K

Figures 4.11 and 4.12 below show the partial amount adsorbed for each individual species from the mixture. Once again, the intercept at $y_1 = 1.0$ (point B) in Figure 4.11 and at $y_1 = 0.0$ (point A) in Figure 4.12, are related to the pure components. At the limits, data seem to approach IAST predictions with a large deviation for the lighter component (i.e. nitrogen). What is more important to note is that the shape of the data and IAST predictions, are within the accuracy of experimental data. For the methane-nitrogen system on silicalite show an azeotrope at high methane concentrations. It was expected that IAST cannot predict an azeotrope since the adsorbed phase is assumed to be mixed ideally. As one can see from the Figure 4.11, the partial amount adsorbed for methane will increase as methane mole fraction increase conversely the partial amount adsorbed for nitrogen will decrease with the increase in methane mole fraction. Similarly, the partial amount adsorbed for any species must approach zero as its composition goes to zero (Points C and D).

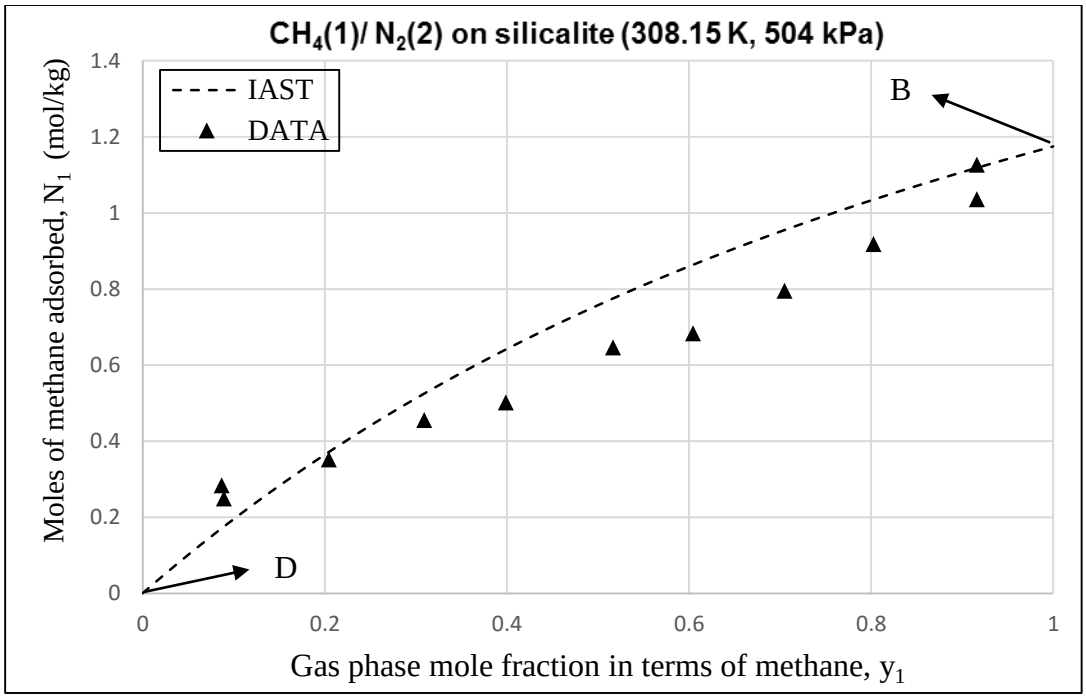

Figure 4.11. Amount adsorbed in terms of methane with change in gas phase mole fraction of methane at 308.15 K

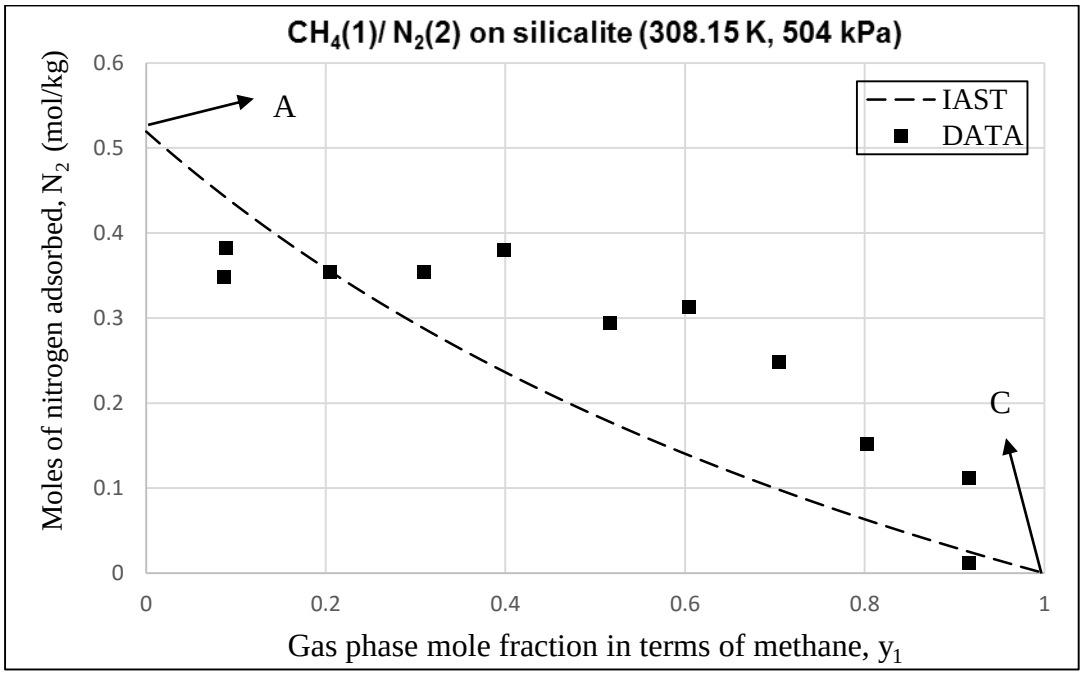

Figure 4.12. Amount adsorbed in terms of nitrogen with change in gas phase mole fraction of methane at 308.15 K

4.5.3.3 Variation in Amount Adsorbed With Equilibrium Gas Phase Pressure

The results shown in the previous section showed the effect of composition on the amount adsorbed at constant pressure and temperature. In this section we will examine the effect of pressure on the amount adsorbed at constant temperature and composition ($y_1 = 0.6$). Figure 4.13 shows the change in the total amount adsorbed (N_t) with pressure and Figure 4.14 and 4.15 present the partial amount adsorbed of methane and nitrogen respectively (in this case N_1& N_2) when composition and temperature is kept constant.

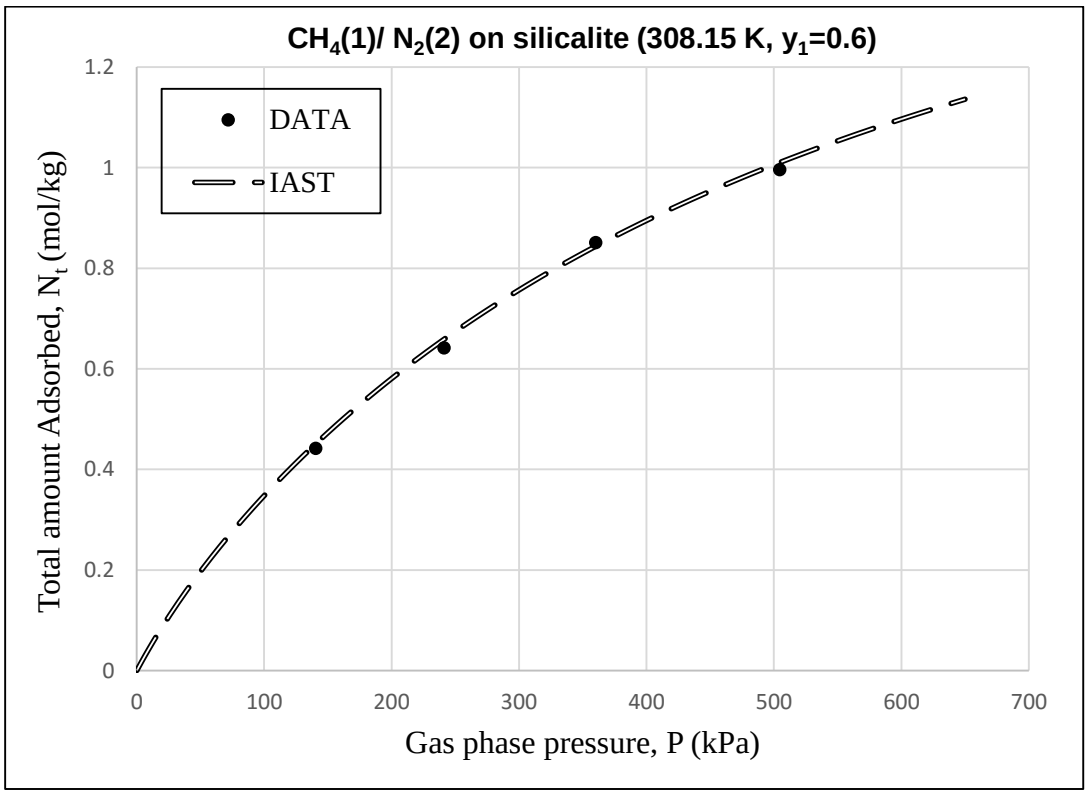

Figure 4.13: Variation in total amount adsorbed with change in gas phase pressure at constant composition and temperature.

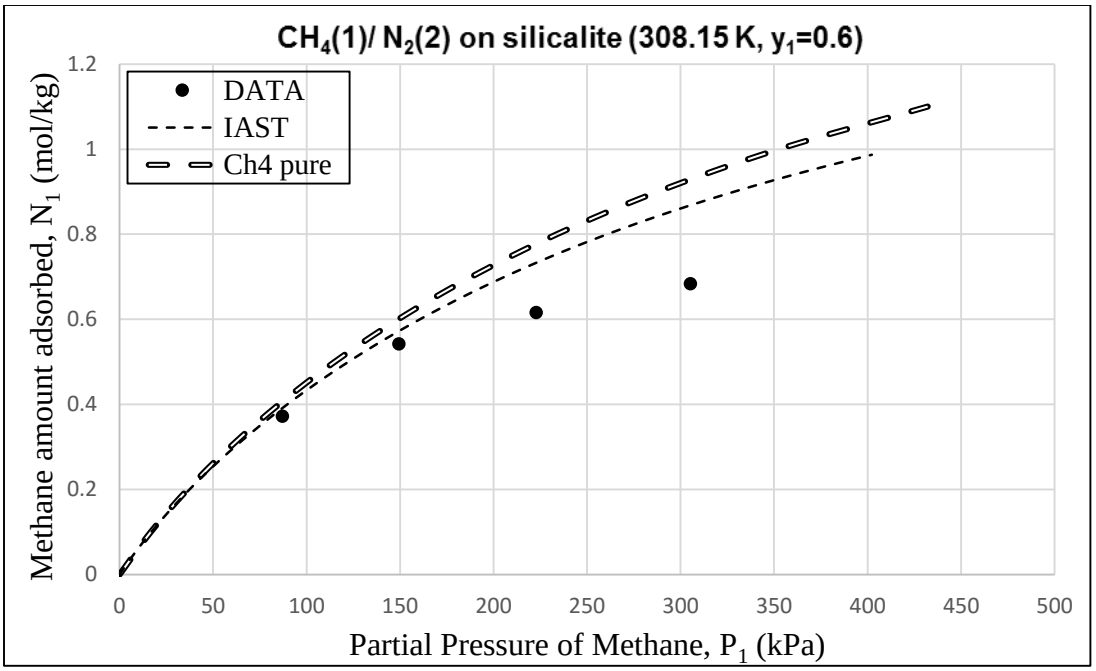

Figure 4.14: Partial amount adsorbed of Methane with change in partial pressure at constant composition and temperature

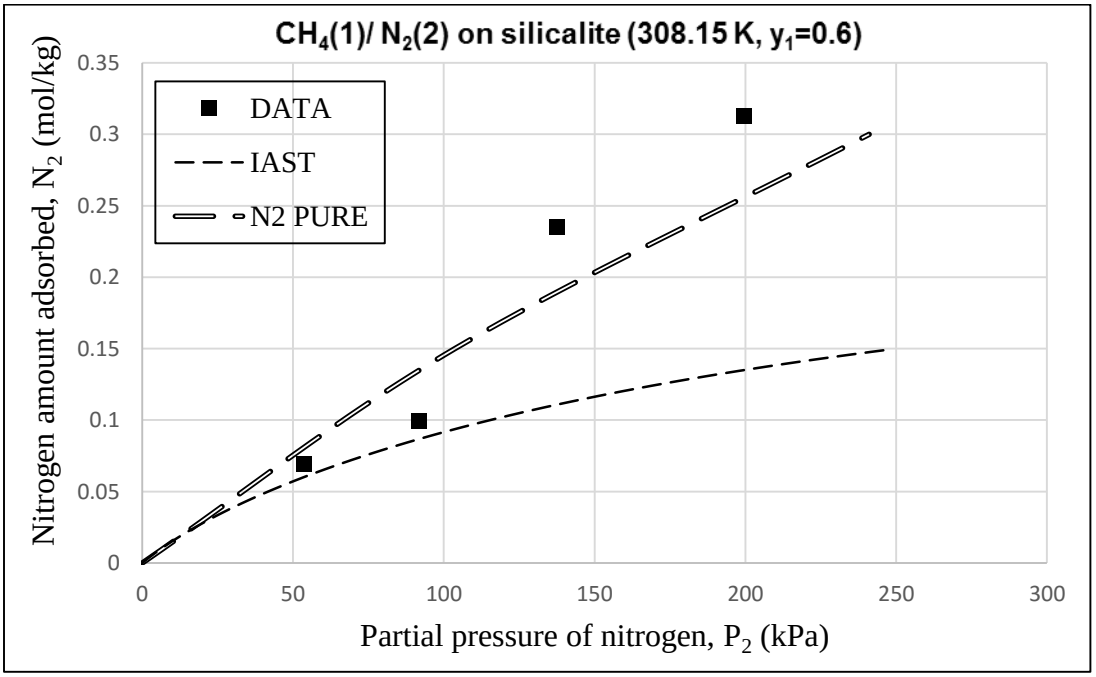

Figure 4.15: Partial amount adsorbed of nitrogen with change in partial pressure at constant composition and temperature

Figures 4.14 and 4.15 show the partial amount of methane and nitrogen adsorbed with the change in partial pressure. For comparison purpose, the pure component adsorption isotherms for methane and nitrogen (at 308.15 K) are also shown. As expected, the partial amount adsorbed in the mixture adsorption isotherm is lower than that of the individual pure component at the same gas pressure. In other words, partial amount adsorbed of a component from a binary mixture must be lower than that of the pure component at the same chemical potential (partial pressure) [62]. All the amounts adsorbed for pure component, partial and total amount adsorbed in terms of mixture adsorption must starts from zero at zero gas phase pressure.

4.5.3.4 Variation in Selectivity with Equilibrium Gas Phase Pressure

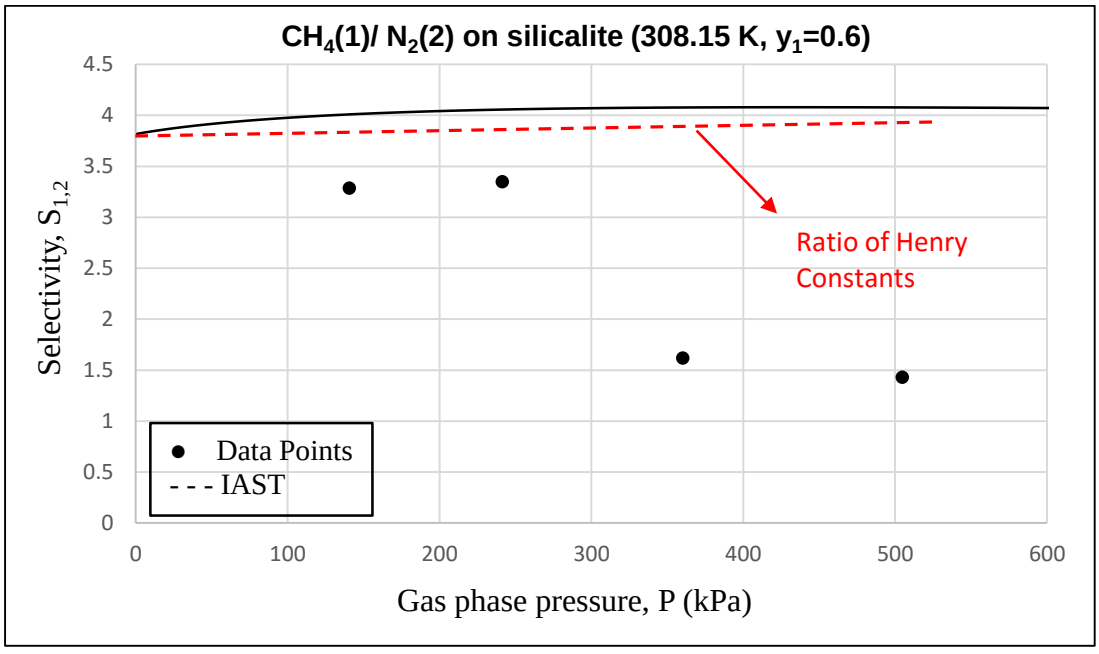

Figure 4.16. Selectivity in terms of methane with the change in pressure

Figure 4.16 shows the surface selectivity of methane over nitrogen as function of pressure. Thermodynamics detects that all systems must approach ideal behavior as pressure (or coverage) approaches zero. This is one of the hardest test to perform especially when the data is so scarce, but data seems to approach the ratio of pure component Henry's constants (i.e. 3.81 for our system) as expected [62, 65].

4.5.3.5 Surface Response Plot for Total Amount Adsorbed

Combining isothermal pressure at equilibrium and constant composition data, the corresponding amount adsorbed can be shown on a 3D graph. Figure 4.17 is a plot of the total amount adsorbed for CH_4 + N_2 mixture with the change in pressure and gas phase composition, at a constant temperature (308.15 K).

In Figure 4.17, the IAST predictions are shown as mesh lines, data points measured in constant composition set ($y_{Ch_4} = 0.60$) (along with line J-K-L-M) and data points measured in constant pressure set (P = 504 kPa) (along with line D-H) are shown as solid circles. The path ABCD and EFGH are pure component isotherms for methane and nitrogen, respectively.

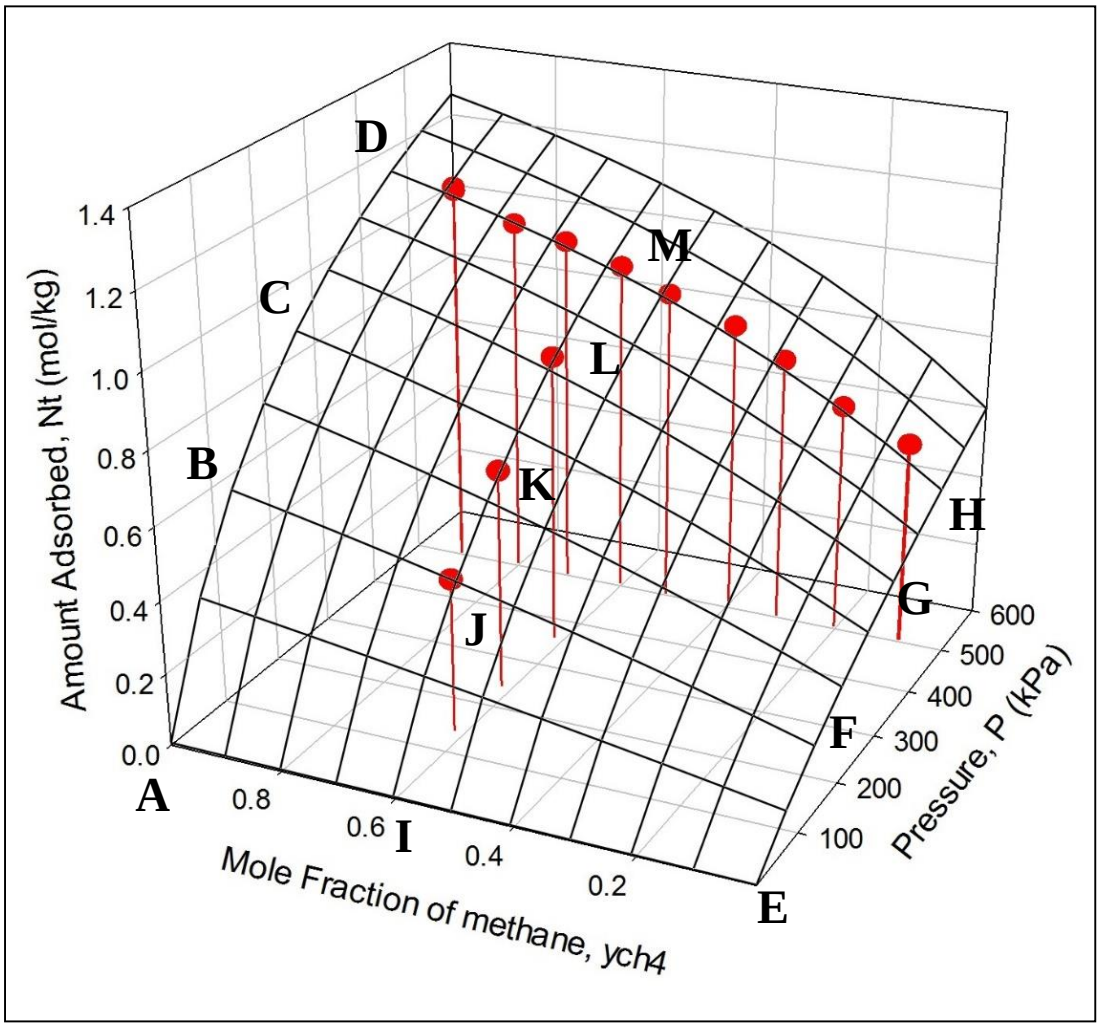

Figure 4.17. Change in total amount adsorbed with gas phase pressure and composition for CH_4+N_2 mixture on silicalite at 308.15 K

It is clear from the 3D graph that experimental data for the total amount adsorbed are being predicted by IAST quite accurately.

4.5.3.6 3D Plot for Selectivity

Selectivity data can also be represented in a 3D diagram for easier visualization.

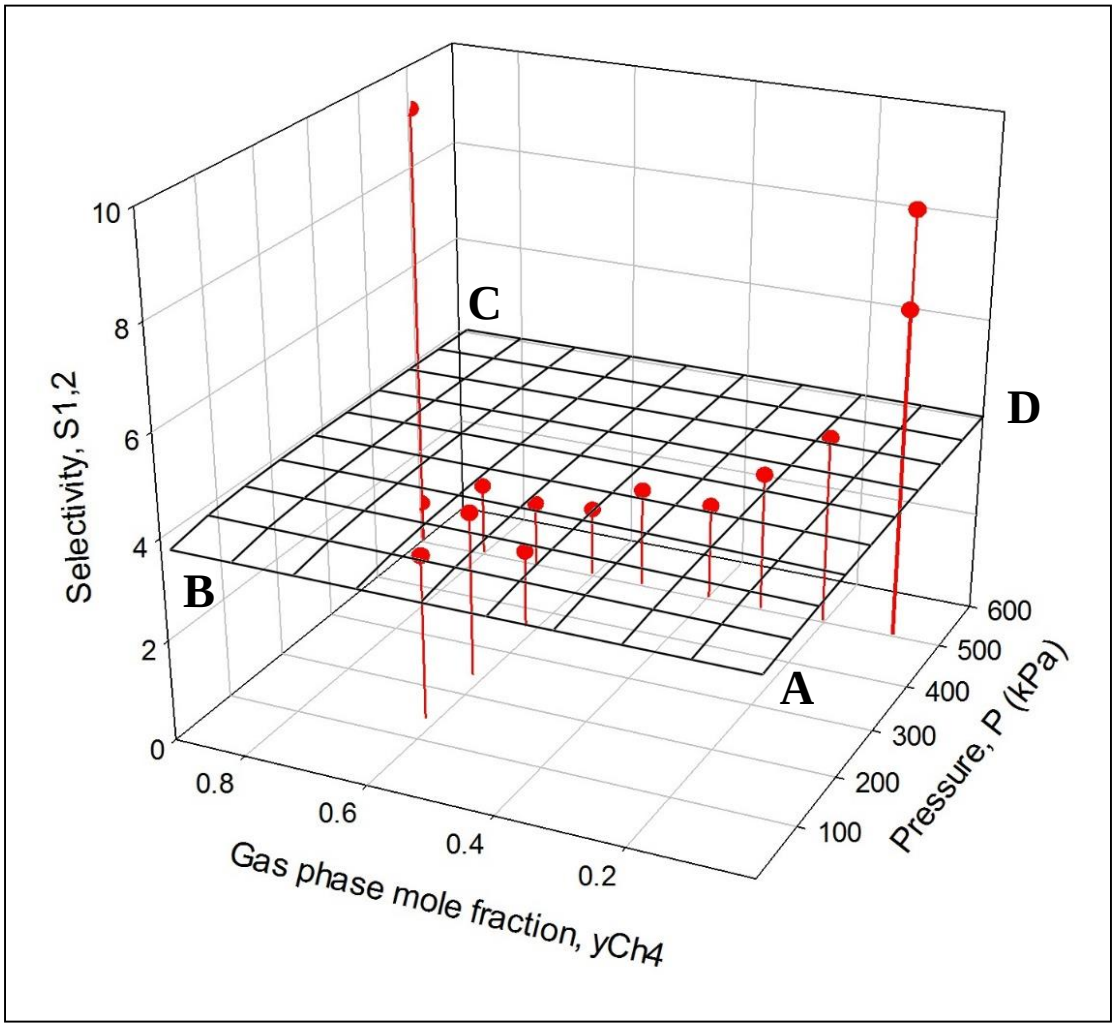

Figure 4.18. Change in selectivity with gas phase composition and pressure for CH_4+N_2 mixture on silicalite at 308.15 K

4.5.3.7 Variation in Selectivity with Equilibrium Gas Phase Composition

For better clarity, the variation in selectivity of methane over nitrogen with the change in gas phase composition is shown in Figure 4.19 for a CH_4+N_2 mixture at constant pressure (504 kPa) and constant temperature (308.15 K). At a constant pressure according to IAST prediction, the selectivity remains almost constant with the change in composition. In Figure 4.19 the dashed line reflects the selectivity for methane over nitrogen for the system as predicted by IAST while symbols represent the actual experimental data.

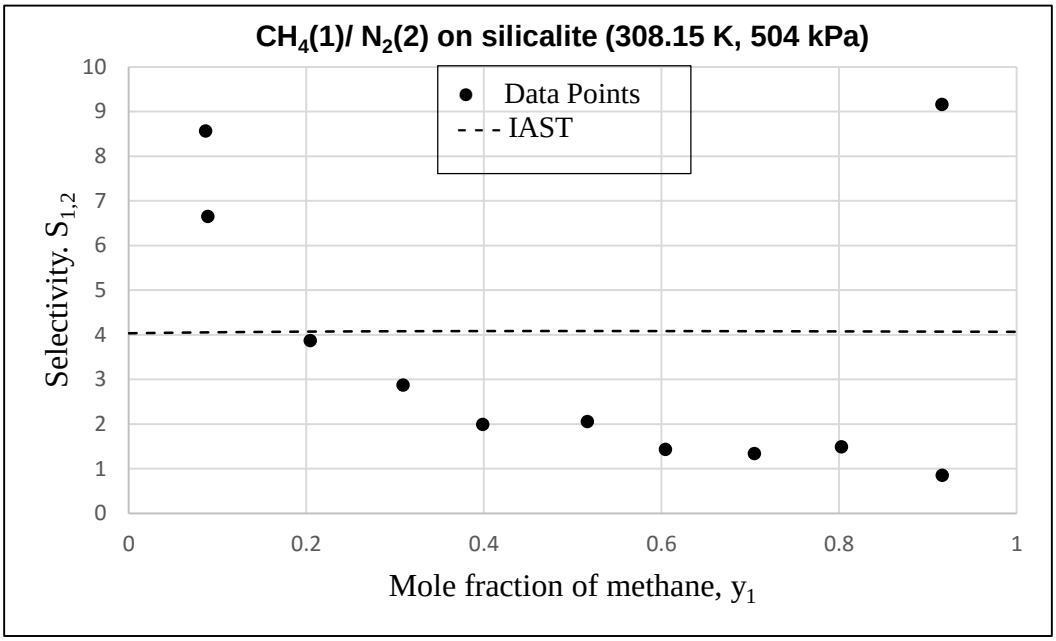

Figure 4.19. Selectivity in terms of methane with the change in gas phase composition

In comparing the partial amount adsorbed for both gas species (Figures 4.14 and 4.15), a high scattering for nitrogen is appreciable to compared to that of methane. This is because of the accuracy in determining properties of light component is always poorer than

heavy component. Since the difference between charge and final amount in a volumetric system for the lighter component is always smaller in the material balance than that of the heavier component, by definition of light. The accuracy of light component properties also has a large impact on the selectivity. The IAST predictions support this observation. As shown in Figure 4.14, IAST predicts the partial amount of methane adsorbed fairly accurately while underestimating the amount of nitrogen adsorbed (Figure 4.15). As a result, IAST predicts the total amount adsorbed fairly accurately in Figure 4.13 and Figure 4.17 which is predominantly controlled by the adsorption of heavy component. While overestimating the selectivity in Figures 4.16 and 4.19 which is predominantly controlled by the adsorption of light component [62, 65].

4.5.3.8 Thermodynamic Consistency

The spreading pressure plays a pivotal role in adsorption thermodynamics. It is a state property indicating the change in the chemical potential of the solid due to adsorption of a guest molecule.

The spreading pressure is related to a measurable quantity at isothermal condition by,

$$d\psi = \sum N_i \, dlnP_i \quad \text{(Constant T)} \tag{4.3}$$

Thermodynamic consistency check of binary data involves the integration of Equation (4.3) for spreading pressure over a closed path. This must be zero since spreading pressure

is a state property. In this work, two paths were used: The first is over a constant gas composition path spreading pressure is given by,

$$\psi = \int_0^P \frac{N_t}{P}\, dp \qquad \text{(Constant y and T)} \qquad (4.4)$$

Figure 4.20 shows the integrand for the data and IAST predictions under this conditions. The second is over a constant pressure path, where spreading pressure can be written as,

$$\psi = \psi(T, P, y_1 = 1) + \int_{y_1=1}^{y_1} \left(\frac{N_1}{y_1} - \frac{N_2}{y_2}\right) dy_1 \qquad \text{(Constant P and T)} \qquad (4.5)$$

Where $\psi(T, P, y_1 = 1)$ is the spreading pressure of component 1 (methane in this case) at the same pressure and temperature as the mixture. Figure 4.21 shows the integrand for the data and IAST predictions under this condition.

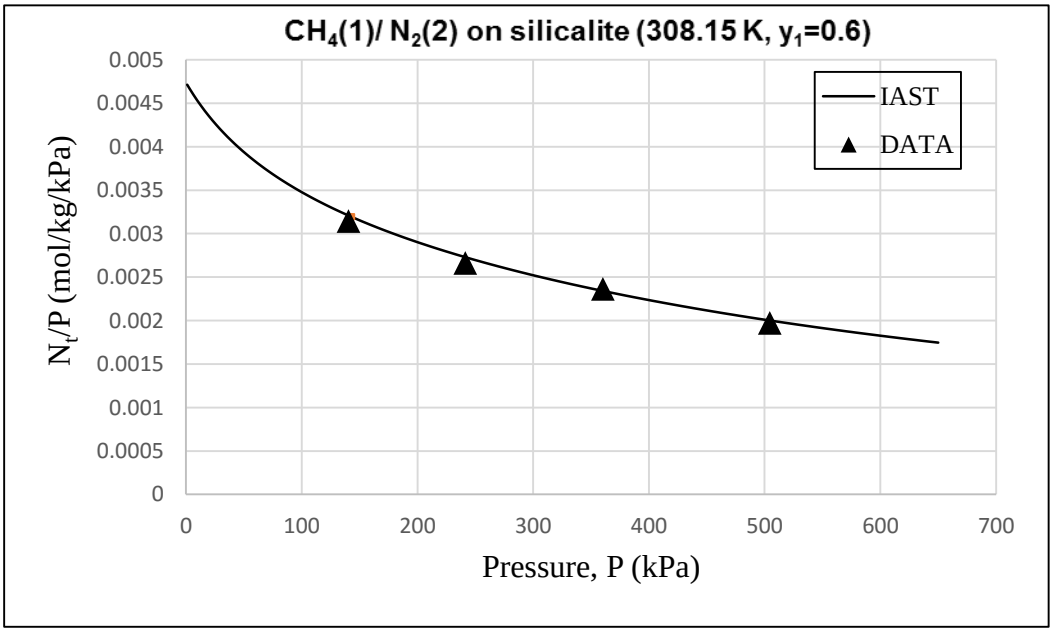

Figure 4.20. The integrand in spreading pressure calculations for binary adsorption at constant composition and temperature.

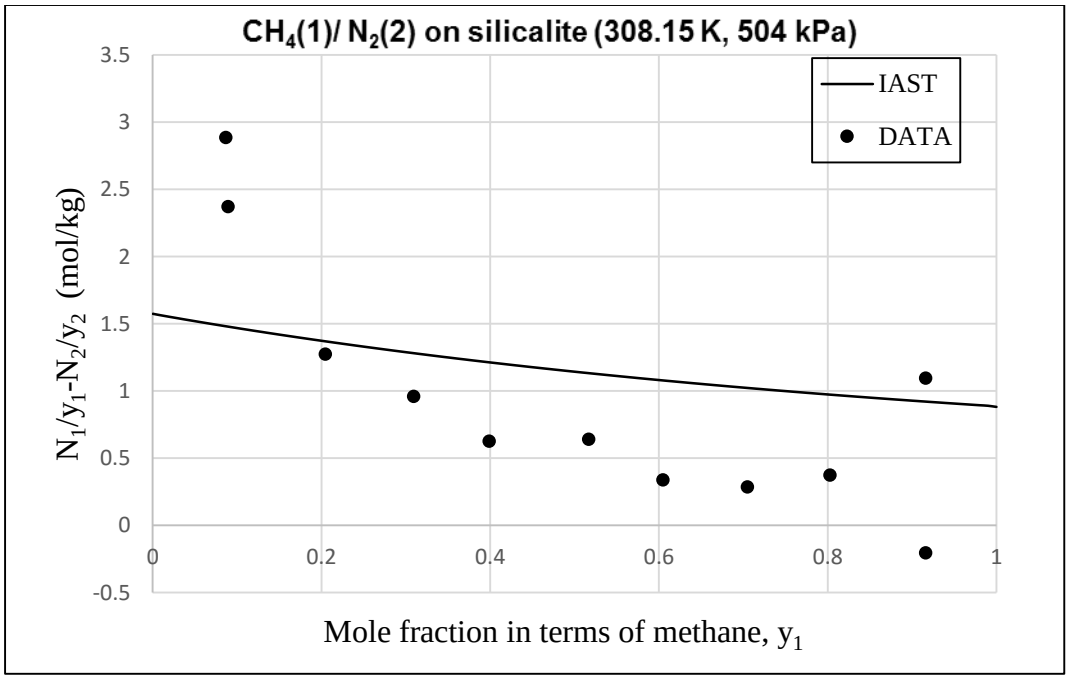

Figure 4.21: The integrand in spreading pressure calculations for binary adsorption at constant pressure and temperature.

These two equations (Equations (4.4) and (4.5)), combined with the corresponding pure component versions cover all possible paths. Such as pure component integration over ABCD, binary constant pressure integration over DM, binary constant composition integration over IJKLM, and again over a constant pressure region IA, which is by definition zero.

Typically the highest uncertainty path over this integration involves the binary constant pressure path shown in Figure 4.21, where the uncertainty at the limits of composition reaches its highest value at the pure light component (at $y_1 = 0.0$). This inevitable uncertainty is a shortcoming of the experimental technique used (i.e. volumetric system). Therefore, rigorous thermodynamic consistency check by integration of these curves is questionable.

On the other hand, the quick method of necessary thermodynamic consistency exist as described by Talu and Myers [65]. The method states that all thermodynamic consistent data and/or model should have the same integral value (i.e. area under the curve) for the function shown in Figure 4.21. Therefore mathematically, the curve displayed for model (i.e. IAST) and data (points) must intersect at least once. Therefore, it can be stated with confidence that the data collected satisfies thermodynamic consistency within its accuracy.

4.6 Literature Review and Comparison

In this section pure component adsorption isotherms on silicalite pellets collected in this study for methane and nitrogen are compared with existing literature data Experimental data are represented by the virial isotherm curves while points represent data from the literature. For the comparison the physical form of adsorbent must be consolidated first. Some literature report data on silicalite crystals while others, like this study, report data with formed particles. Assuming that the particle forming (pelletizing) with clay binders do not change micropore adsorption equilibrium characteristics, the difference should only be a scale difference due to added weight of binder material. Therefore all the literature data are corrected by a binder correction factor assuming that the adsorbent material has 20% binder in it (which does not take part in adsorption). These corrections affected the literature results by 20% as most of the literature data are obtained with silicalite crystals, without binder, except the one by Tezel et al. [37, 38, 45] and Abdul-Rehman et al. [1] where the silicalite with 20% binder was the material used. Although it

is not possible to find isotherm comparisons at exactly the same temperature as the ones presented here, qualitative comparisons can still be made as adsorption capacity increases as temperature decreases.

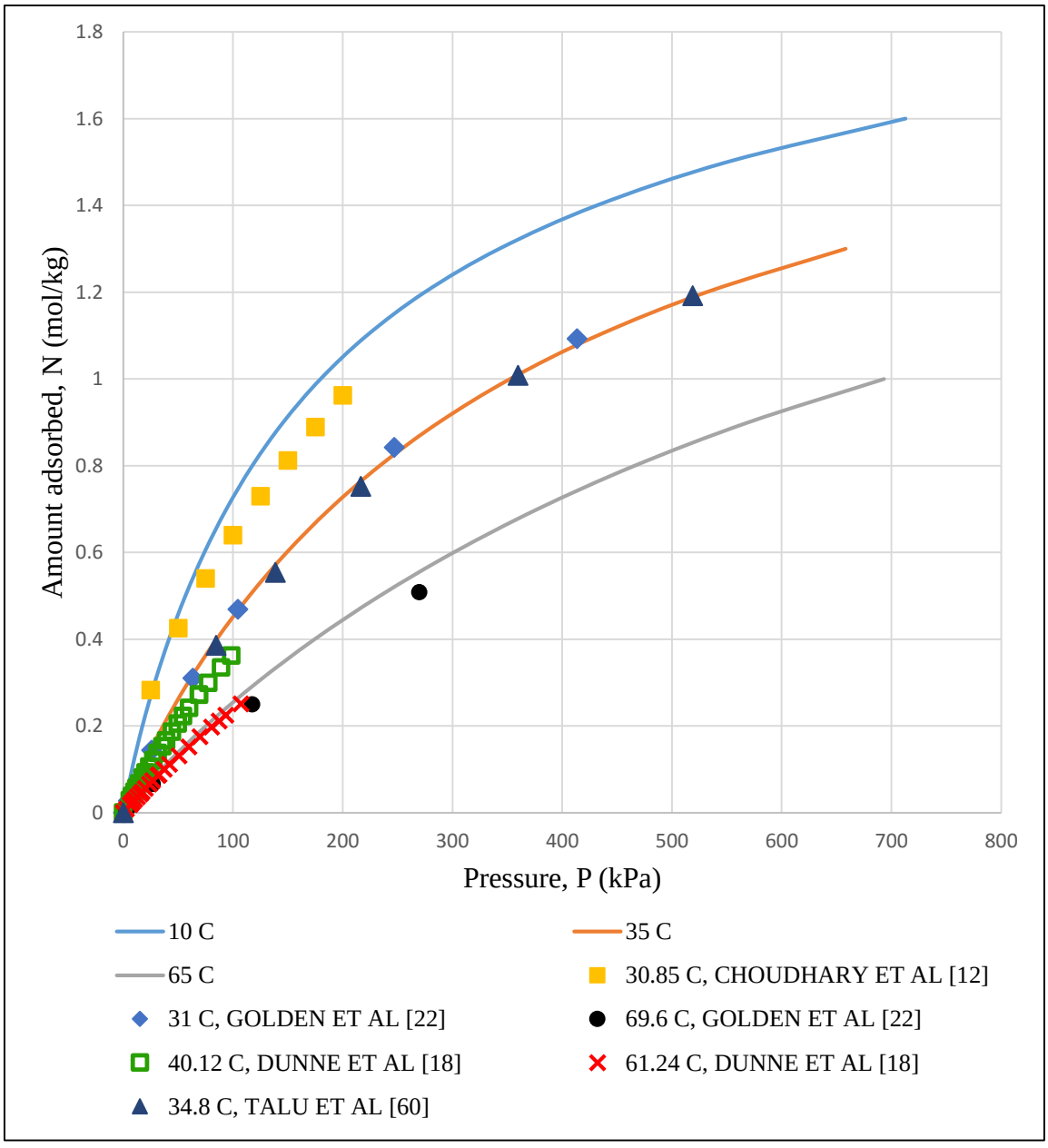

Figure 4.22. Pure methane adsorption isotherms on silicalite and comparison with literature data.

As it is shown in Figure 4.22, the experimental data collected in this study for methane are represented by virial isotherm curves at three different temperatures (i.e. 10°C, 35°C, and 65°C) and points represents data from the literature. Talu et al. [60] have measured methane isotherm at three different temperature (i.e. 3.8 °C, 34.8 °C, and 79.6 °C) on silicalite crystals. After binder correction the results at 34.8 °C by Talu et al. [60] are in well agreement with the data collected in this study at 35 °C. As is apparent in Figure 4.22, results collected by Choudhary et al. [12] at 30.85 °C, adsorption isotherm is well above the result collected in this study at 35 °C, which might be because of the different silicalite supplier. Results collected by Golden and Sircar [22], and Dunne et al. [18] on silicalite crystals after binder correction are in good quantitatively agreement considering different temperatures. All the datasets are following the trend that uptake will decrease as temperature increases. Results collected by Abdul-Rehman et al. [1] and Rees et al. [54] are not shown in the comparison because the isotherm measurements were too far from the measurements made in this study.

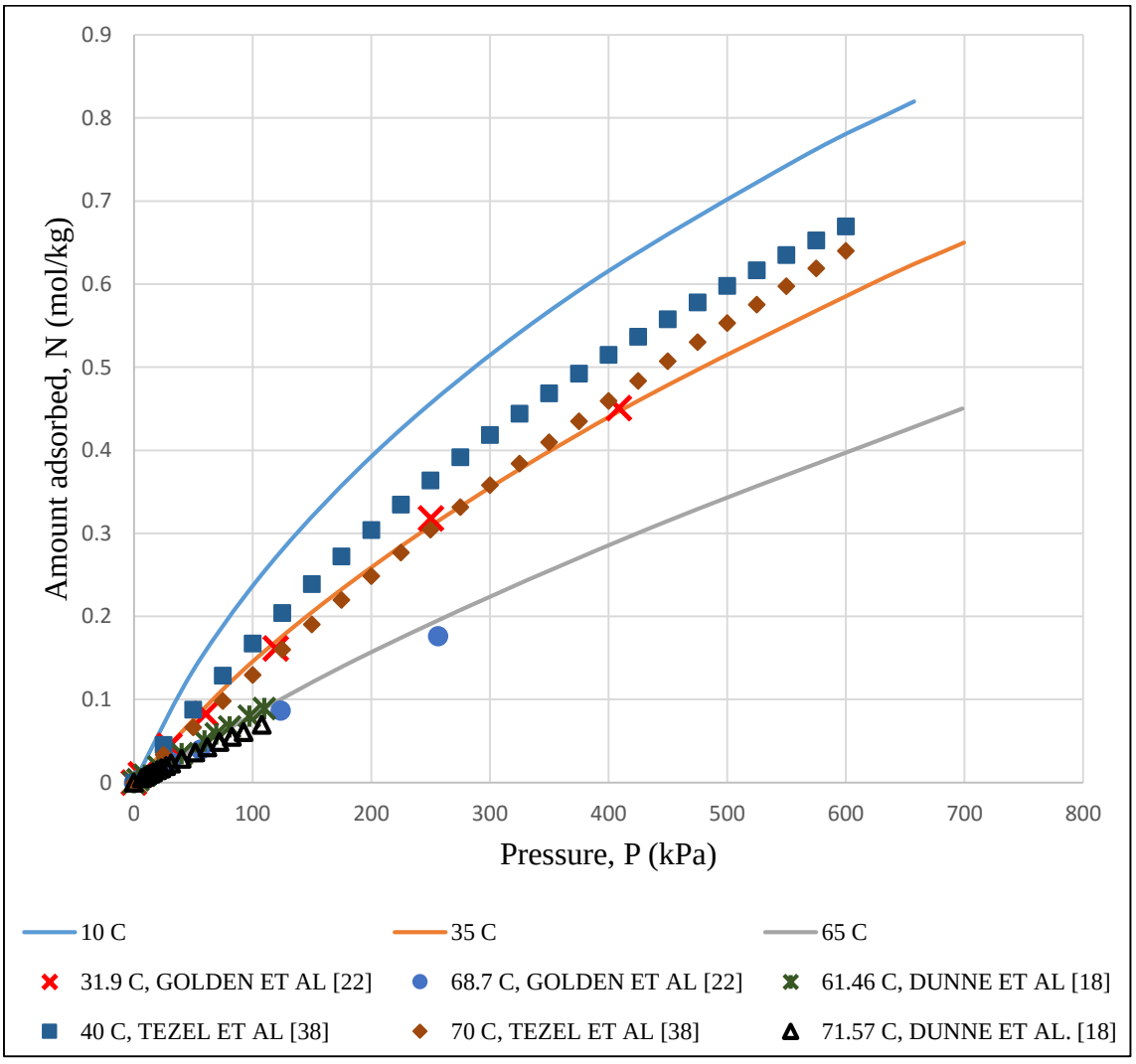

Figure 4.23. Pure nitrogen adsorption isotherms on silicalite and comparison with literature data.

Figure 4.23 shows the experimental data collected in this study for nitrogen as represented by virial isotherm curves at three different temperatures (i.e. 10°C, 35°C, and 65°C) while points represents data from the literature. Tezel et al. [38] measured nitrogen adsorption at three different temperatures (i.e. 40 °C, 70 °C, and 100 °C) on silicalite pellets using a volumetric technique. Their uptake for all the isotherms are very high compared to the uptake measured in this study. Golden et al. [22] reported this measurement at two different temperatures, 31.9 °C and 68.7 °C on silicalite crystals. When their results are compared after binder correction with the results collected from this study, it can be seen that adsorption capacities are in good qualitative agreement for nitrogen, considering different temperatures. Dunne et al. [18] measured isotherm up-to relatively low pressure (i.e. up to 100 kPa) at two different temperatures, 61.46 °C and 71.57 °C on silicalite crystals; and their results are also in good qualitative agreement with the those measured in this study at 65 °C.

As it can be seen from Figures 4.22 and 4.23, the experimental data match very well with data from the literature for methane, while data reported by Tezel et al. [38] shows a much higher adsorption capacity than any other literature data for nitrogen. The difference can be speculated to be attributable to the adsorbent being purchased from different supplier.

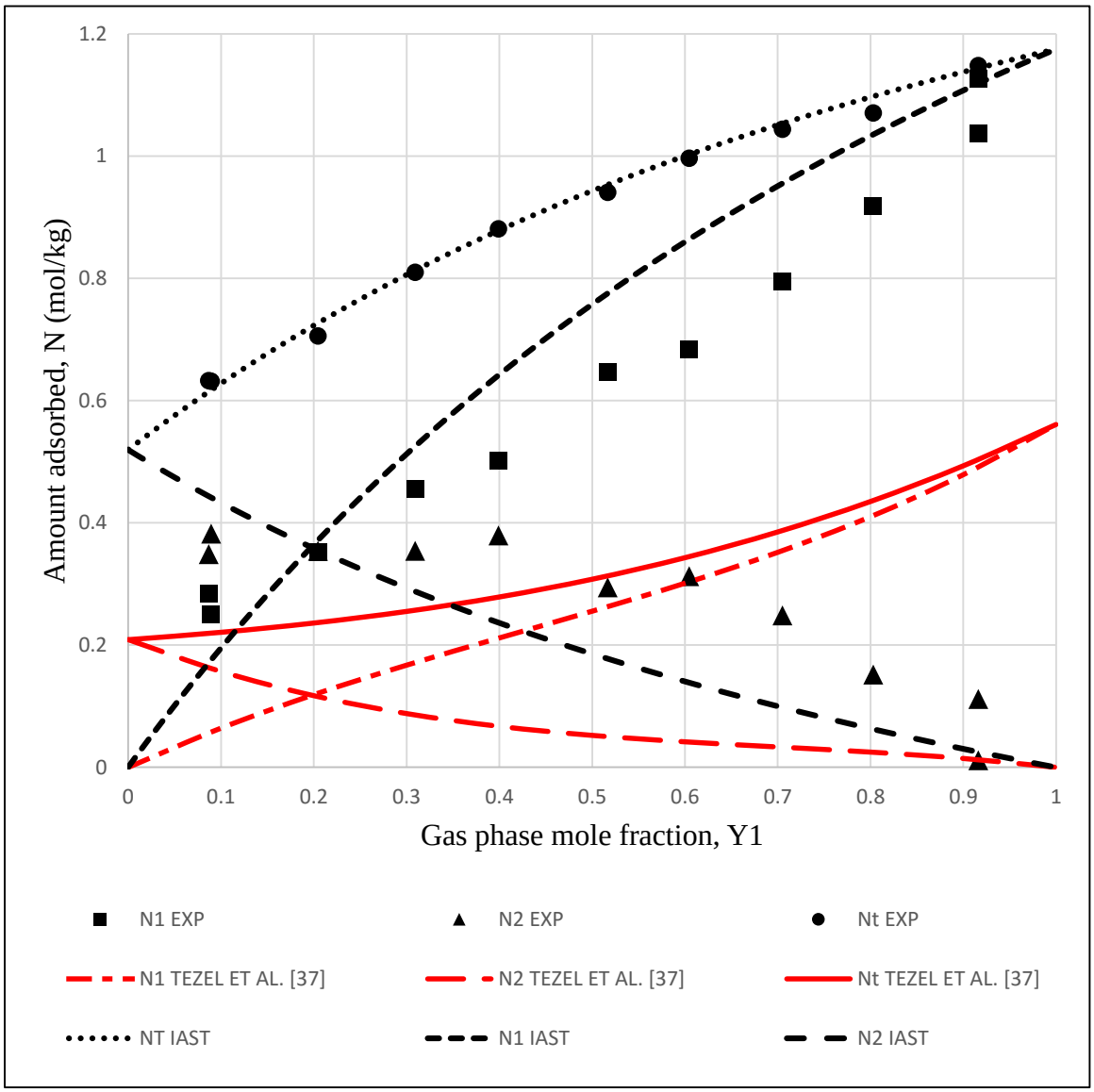

Figure 4.24. Amount adsorbed with change in gas phase composition data and their comparison with Tezel et al. [37]

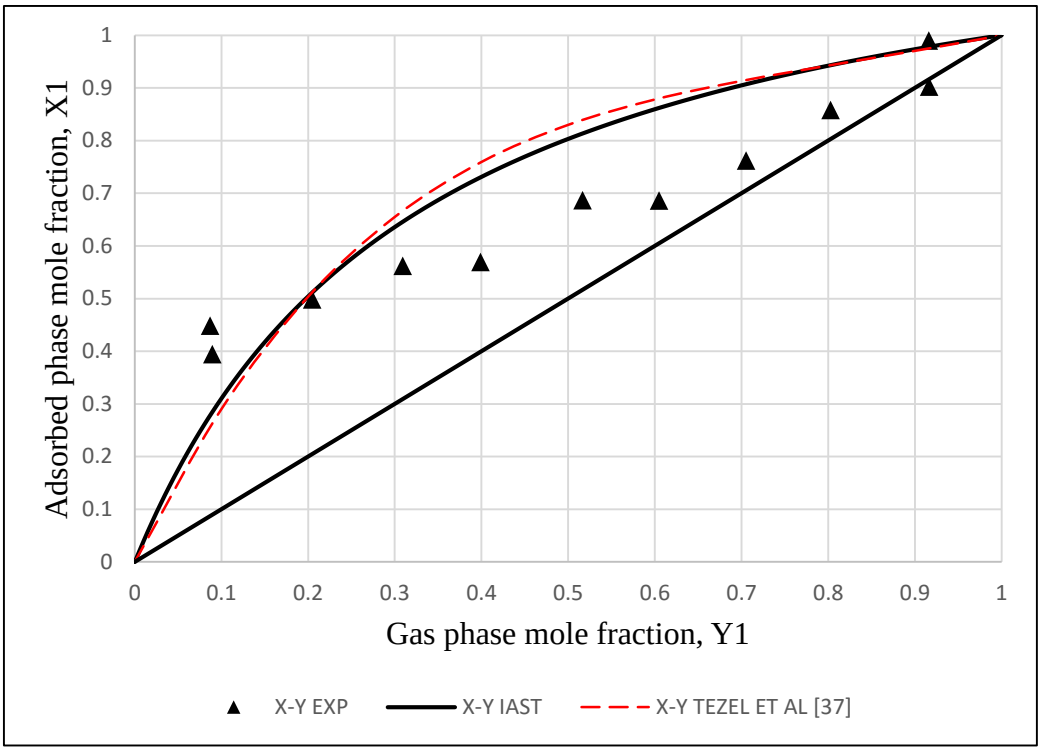

Figure 4.25. X-Y diagram and comparison with Tezel et al. [37]

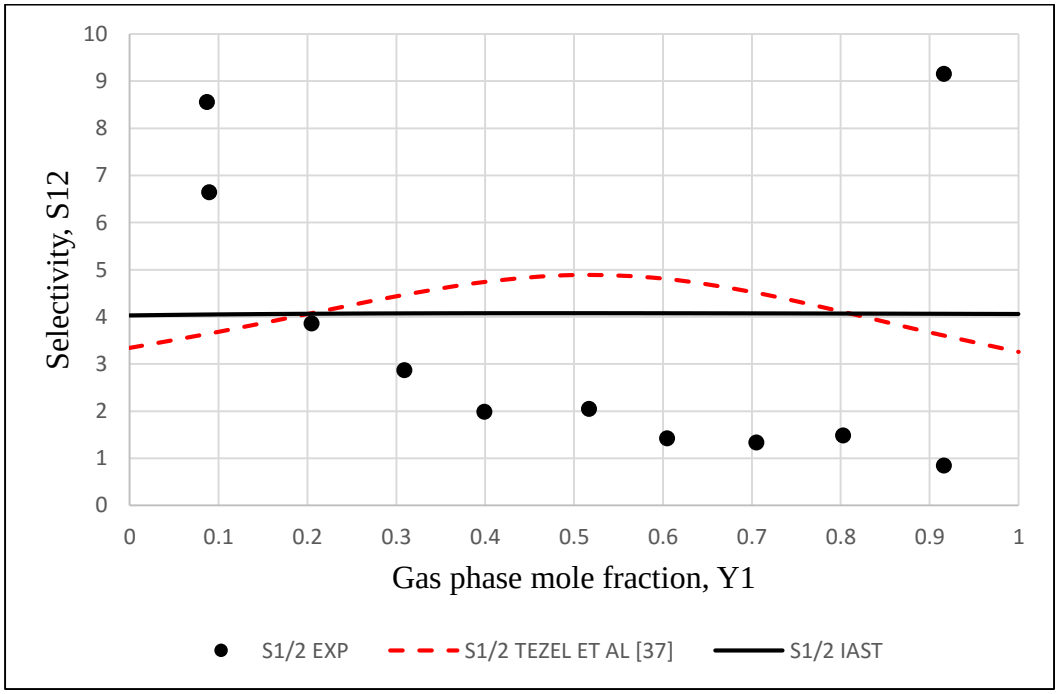

Figure 4.26. Selectivity Vs Gas phase mole fraction and comparison with Tezel et al. [37]

As it can be seen in Figure 4.24, it was expected that total amount adsorbed, N_t, partial amount adsorsorbed for both methane and nitrogen are higher in this study compared to reported by Tezel et al. [37], as their experiment was conducted at a fairly lower Pressure (i.e. 100 kPa Vs. 504 kPa). As pressure increases, the total and partial amounts adsorbed increase. The temperature was nearly similar in both the studies. The total and partial amount adsorbed for the heavy component (i.e. methane) curves are convex to horizontal axis when plotted against gas phase mole fraction for heavy component which is highly usual. While experimental total amount adsorbed from this study is concave to horizontal axis and following IAST predictions very well. From Figure 4.25, it reflects that the data points that Tezel et al. [37] collected for the adsorbed phase and gas phase composition are very close to those predicted by IAST. Data points are slightly scattered in this study compared to IAST predictions which is due to experimental shortcoming in mixing the gases properly before introducing them to the solid adsorbent. From Figure 4.26, it reflects that the experimental selectivity in Tezel et al. [37] shows maximum in the range of y_1 between 0.5 and 0.6; which is unusual. The predicted selectivity in this study on the other hand remains constant all over the composition range. The point to emphasize here is that the adsorption behavior of a methane and nitrogen mixture on silicalite adsorbent was studied by concentration pulse chromatography in Tezel et al. [37], while in this study a volumetric technique was used for binary measurements.

CHAPTER V
SUMMARY AND CONCLUSIONS

5.1 Pure Component Adsorption Equilibrium Measurements Using Volumetric System

A standard volumetric technique was used to measure pure component adsorption isotherms of methane and nitrogen on silicalite adsorbent at three different temperatures (283.15 K, 308.15 K, and 338.15 K). Since methane has no dipole or quadrupole moment, its stronger adsorption is due to a high degree of polarizability than that of nitrogen. The adsorption capacity on silicalite adsorbents increases with decreasing temperature for both of the adsorbates, since physical adsorption is always an exothermic process. Pure component adsorption isotherms were modeled using virial model for both gases. Henry's constants are of utmost thermodynamic importance in modeling all adsorption equilibria.

In general, a better estimate of the Henry constant can be obtained from the Virial model. Isotherms for both gases were successfully modeled using a Virial isotherm model with four parameters. Henry's constant for methane was found to be 3.81 times stronger than that of nitrogen at 308.15 K temperature.

Isosteric heat of adsorption is also an important property as it affects the energy of the adsorbed phase. The limiting isosteric heats of adsorption at zero coverage for methane and nitrogen indicate a stronger adsorption of methane compared to that of nitrogen. The silicalite is showing heterogeneity for both methane and nitrogen as indicated by the negative slope of isosteric heat (Figure 4.7).

5.2 Binary Adsorption Equilibrium Measurements Using Volumetric System

Because of the extra degree of thermodynamic freedom in adsorption, even the simplest multi-component adsorption equilibrium measurement is difficult and time consuming. Binary equilibria of methane and nitrogen mixtures covering the whole concentration range was measured at 308.15 K and 504 kPa. The equilibrium data was subjected to thermodynamic consistency tests. IAST predictions closely matched experimentally measured total amount adsorbed results for the complete range of concentration. The reason is total amount adsorbed is predominantly controlled by the adsorption of heavy component (i.e. methane). The change in the partial amount adsorbed

with pressure for both the species is following IAST in the beginning but they deviate from predictions at high pressure.

Adsorption selectivity is a thermodynamic variable of interest analogous to relative volatility of vapor-liquid equilibria. The measurement of selectivity in adsorption equilibria is a challenging task since errors in the measurements are greatly magnified as selectivity is predominantly controlled by the adsorption of lighter component. The main reason for the difficulty is the fact that surface phase properties are only measurable as changes in gas phase, whereas in the VLE the equilibrium properties are directly measurable in both phases. The uncertainty in selectivity measurements are higher compared to those of the total amount adsorbed. Particularly because large error is introduced in measurement of the partial amount adsorbed for the lighter species. The binary experiments indicated constant equilibrium separation factors for methane-nitrogen separation throughout the composition range. According to the pure gas and binary mixture isotherm data on silicalite, methane is adsorbed more compare to nitrogen and therefore, it cannot be considered as a good candidate for natural gas upgrading.

REFERENCES

[1] Abdul-Rehman, H.; Hasanain, M.; Loughlin, K. Quaternary, ternary, binary, and pure component sorption on zeolites. 1. Light alkanes on Linde S-115 silicalite at moderate to high pressures. *Ind. Eng. Chem. Res.* **1990**, *29*, 1525-1535.

[2] Adamson, A. W.; Gast, A. P. Physical chemistry of surfaces. **1967**.

[3] Barrer, R. M. *Zeolites and clay minerals as sorbents and molecular sieves;* Academic press: 1978.

[4] BCS Incorporated; Oak Ridge National Laboratory. *Materials for Separation Technologies: Energy and Emission Reduction Opportunities* **2013**, retrieved from: https://www1.eere.energy.gov/manufacturing/industries_technologies/imf/pdfs/separationsreport.pdf

[5] Boer, J. H. *Dynamical character of adsorption* **1968**.

[6] Broughton, D. Adsorption isotherms for binary gas mixtures. *Industrial & Engineering Chemistry* **1948**, *40*, 1506-1508.

[7] Brunauer, S.; Deming, L. S.; Deming, W. E.; Teller, E. On a theory of the van der Waals adsorption of gases. *J. Am. Chem. Soc.* **1940**, 62, 1723-1732.

[8] Cavenati, S.; Grande, C. A.; Rodrigues, A. E. Adsorption equilibrium of methane, carbon dioxide, and nitrogen on zeolite 13X at high pressures. *Journal of Chemical & Engineering Data* **2004**, *49*, 1095-1101.

[9] Cavenati, S.; Grande, C. A.; Rodrigues, A. E. Upgrade of methane from landfill gas by pressure swing adsorption. *Energy Fuels* **2005**, *19*, 2545-2555.

[10] Chakraborty, A.; Saha, B.; Koyama, S.; Ng, K. Specific heat capacity of a single component adsorbent-adsorbate system. *Appl. Phys. Lett.* **2007**, *90*.

[11] Chica, A. Zeolites: promised materials for the sustainable production of hydrogen. *ISRN Chemical Engineering* **2013**, *2013*.

[12] Choudhary, V. R.; Mayadevi, S. Adsorption of methane, ethane, ethylene, and carbon dioxide on silicalite-l. *Zeolites* **1996**, *17*, 501-507.

[13] Dąbrowski, A. Adsorption—from theory to practice. *Adv. Colloid Interface Sci.* **2001**, *93*, 135-224.

[14] Dąbrowski, A.; Curie, S. *Adsorption and its applications in industry and environmental protection;* Elsevier Amsterdam: 1999.

[15] De Saussure, N. T. *Gilbert's Ann. Phys.* **1814**, 47,113.

[16] De Saussure, N. T. *Ann. Phil.* **1815**, 6, 241.

[17] Do, D. D. *Adsorption Analysis: Equilibria and Kinetics :(With CD Containing Computer Matlab Programs);* World Scientific: 1998; Vol. 2.

[18] Dunne, J.; Mariwala, R.; Rao, M.; Sircar, S.; Gorte, R.; Myers, A. Calorimetric heats of adsorption and adsorption isotherms. 1. O2, N2, Ar, CO2, CH4, C2H6, and SF6 on silicalite. *Langmuir* **1996**, *12*, 5888-5895.

[19] Flanigen, E. M.; Bennett, J.; Grose, R.; Cohen, J.; Patton, R.; Kirchner, R. Silicalite, a new hydrophobic crystalline silica molecular sieve. *Nature* **1978**, *271*, 512-516.

[20] Flank, W. H. *Adsorption and ion exchange with synthetic zeolites;* American Chemical Society: 1980.

[21] Gibbs, J. W.; Bumstead, H. A.; Longley, W. R. *The collected works of J. Willard Gibbs;* Longmans, Green and Company: 1928; Vol. 1.

[22] Golden, T.; Sircar, S. Gas adsorption on silicalite. *J. Colloid Interface Sci.* **1994**, *162*, 182-188.

[23] Gregg, S. J.; Sing, K. S. W.; Salzberg, H. Adsorption surface area and porosity. *J. Electrochem. Soc.* **1967**, *114*, 279C-279C.

[24] Gumma, S. *On measurement, analysis and modeling of mixed gas adsorption equilibria* **2003**.

[25] Gumma, S.; Talu, O. Gibbs dividing surface and helium adsorption. *Adsorption* **2003**, *9*, 17-28.

[26] Hill, T. L. *An introduction to statistical thermodynamics;* Courier Corporation: 2012.

[27] Humphrey, J.; Keller, I. GE, 1997. Separation Process Technology. *McGraw Hill, New York, NY*.

[28] Kärger, J.; Ruthven, D. M. *Diffusion in zeolites and other microporous solids;* Wiley New York: 1992.

[29] Kayser, H. *Wied. Ann. Phys.* **1881**, 12, 526.

[30] Kayser, H. *Wied. Ann. Phys.* **1881**, 14, 450.

[31] Knaebel, K. S.; Reinhold, H. E. Landfill gas: from rubbish to resource. *Adsorption* **2003**, *9*, 87-94.

[32] Kokotailo, G.; Lawton, S.; Olson, D. Structure of synthetic zeolite ZSM-5. *Nature* **1978**, *272*, 437-438.

[33] Langmuir, I. The adsorption of gases on plane surfaces of glass, mica and platinum. *J. Am. Chem. Soc.* **1918**, *40*, 1361-1403.

[34] Langmuir, I. The constitution and fundamental properties of solids and liquids. Part II. Liquids. [1]. *J. Am. Chem. Soc.* **1917**, *39*, 1848-1906.

[35] Langmuir, I. The constitution and fundamental properties of solids and liquids. Part I. Solids. *J. Am. Chem. Soc.* **1916**, *38*, 2221-2295.

[36] Lennard-Jones, J. Processes of adsorption and diffusion on solid surfaces. *Transactions of the Faraday Society* **1932**, *28*, 333-359.

[37] Li, P.; Handan Tezel, F. Pure and binary adsorption of methane and nitrogen by silicalite. *Journal of Chemical & Engineering Data* **2008**, *54*, 8-15.

[38] Li, P.; Tezel, F. H. Pure and binary adsorption equilibria of carbon dioxide and nitrogen on silicalite. *Journal of Chemical & Engineering Data* **2008**, *53*, 2479-2487.

[39] Lowitz, T. *Crell's Chem. Ann.* **1786**, 1, 211.

[40] Lowitz, T. *Crell's Chem. Ann.* **1788**, 2, 36.

[41] Lutz, W. Zeolite Y: Synthesis, Modification, and Properties—A Case Revisited. *Advances in Materials Science and Engineering*, **2014**.

[42] Masters, A. F.; Maschmeyer, T. Zeolites–From curiosity to cornerstone. *Microporous and Mesoporous Materials* **2011**, *142*, 423-438.

[43] Mathias, P. M.; Kumar, R.; Moyer, J. D.; Schork, J. M.; Srinivasan, S. R.; Auvil, S. R.; Talu, O. Correlation of multicomponent gas adsorption by the dual-site Langmuir model. Application to nitrogen/oxygen adsorption on 5A-zeolite. *Ind Eng Chem Res* **1996**, *35*, 2477-2483.

[44] McBain, J. W. XCIX. The mechanism of the adsorption ("sorption") of hydrogen by carbon. *The London, Edinburgh, and Dublin Philosophical Magazine and Journal of Science* 1909, *18*, 916-935.

[45] Mulgundmath, V.; Tezel, F.; Hou, F.; Golden, T. Binary adsorption behavior of methane and nitrogen gases. *Journal of porous materials* **2012**, *19*, 455-464.

[46] Myers, A. Thermodynamics of adsorption in porous materials. *AIChE J.* **2002**, *48*, 145-160.

[47] Myers, A.; Prausnitz, J. M. Thermodynamics of mixed-gas adsorption. *AIChE J.* **1965**, *11*, 121-127.

[48] O'Brien, J. A.; Myers, A. L. Rapid calculations of multicomponent adsorption equilibria from pure isotherm data. *Industrial & Engineering Chemistry Process Design and Development* **1985**, *24*, 1188-1191.

[49] Olson, D.; Kokotailo, G.; Lawton, S.; Meier, W. Crystal structure and structure-related properties of ZSM-5. *J. Phys. Chem.* **1981**, *85*, 2238-2243.

[50] Polanyi, M. Adsorption von Gasen (Dampfen) durch ein festes nichtfluchtiges Adsorbens. *Verhandlungen der Deutschen Physekalischen Gesellschaft* **1916**, *18*, 55-80.

[51] Polanyi, M. Über die Adsorption vom Standpunkt des dritten Wärmesatzes. *Verh.Dtsch.Phys.Ges* **1914**, *16*, 1012-1016.

[52] Prausnitz, J. M.; Lichtenthaler, R. N.; de Azevedo, E. G. *Molecular thermodynamics of fluid-phase equilibria;* Pearson Education: 1998.

[53] Rahman, K. A.; Loh, W. S.; Ng, K. C. Heat of adsorption and adsorbed phase specific heat capacity of methane/activated carbon system. *Procedia Engineering* **2013**, *56*, 118-125.

[54] Rees, L.; Brückner, P.; Hampson, J. Sorption of N2, CH4 and CO2 in silicalite-1. *Gas separation & purification* **1991**, *5*, 67-75.

[55] Rouquerol, J.; Rouquerol, F.; Llewellyn, P.; Maurin, G.; Sing, K. S. *Adsorption by powders and porous solids: principles, methodology and applications;* Academic press: 2013.

[56] Ruthven, D. M. *Principles of adsorption and adsorption processes;* John Wiley & Sons: 1984.

[57] Sircar, S. Excess properties and thermodynamics of multicomponent gas adsorption. *Journal of the Chemical Society, Faraday Transactions 1: Physical Chemistry in Condensed Phases* **1985**, *81*, 1527-1540.

[58] Spencer, N. D.; Moore, J. H. *Encyclopedia of chemical physics and physical chemistry: Applications;* Taylor & Francis: 2001; Vol. 3.

[59] Steele, W. A. *The interaction of gases with solid surfaces;* Pergamon Press: 1974; Vol. 3.

[60] Sun, M. S.; Shah, D.; Xu, H. H.; Talu, O. Adsorption Equilibria of C1 to C4 Alkanes, CO2, and SF6 on Silicalite. *The Journal of Physical Chemistry B* **1998**, *102*, 1466-1473.

[61] Suzuki, M. Adsorption engineering. *Tokyo: Kodansha* **1990**, *551*, 128-132.

[62] Talu, O. Needs, status, techniques and problems with binary gas adsorption experiments. *Adv. Colloid Interface Sci.* **1998**, *76*, 227-269.

[63] Talu, O. *Thermodynamics of multicomponent gas adsorption equilibria of non-ideal mixtures;* Arizona State University: 1984.

[64] Talu, O.; Myers, A. L. Molecular simulation of adsorption: Gibbs dividing surface and comparison with experiment. *AIChE J.* **2001**, *47*, 1160-1168.

[65] Talu, O.; Myers, A. L. Rigorous thermodynamic treatment of gas adsorption. *AIChE J.* **1988**, *34*, 1887-1893.

[66] Thomas, W. J.; Crittenden, B. D. *Adsorption technology and design;* Butterworth-Heinemann: 1998.

[67] U.S. Environmental Protection Agency; Office of Air and Radiation; Climate Change Division. *An Overview of Landfill Gas energy in the United States [PowerPoint slides]* **2013**, retrieved from: https://www3.epa.gov/lmop/documents/pdfs/overview.pdf

[68] Van Ness, H. Adsorption of gases on solids. Review of role of thermodynamics. *Industrial & Engineering Chemistry Fundamentals* **1969**, *8*, 464-473.

[69] Weitkamp, J. Zeolites and catalysis. *Solid State Ionics* **2000**, *131*, 175-188.

[70] Yang, R. T. *Adsorbents: fundamentals and applications;* John Wiley & Sons: 2003.

[71] Yang, R. T. *Gas separation by adsorption processes;* Butterworth-Heinemann: 2013.

APPENDIX

APPENDIX A

Error Analysis and Uncertainties in Primary Data Measurement

The purpose of this analysis is to estimate the impact of uncertainties in experimental measurements on the uncertainty of thermodynamic properties. The pure component isotherm for methane and nitrogen in silicalite was collected on closed volumetric system. The measurements involved in the pure component adsorption isotherm that appeared in Equations 3.3 & 3.4; 3.10 & 3.11 are:

I. Pressure measured by a transducer at different steps of the procedure,
II. Volumes in different parts of the apparatus which are measured by a combination of mercury displacement and helium expansion techniques,
III. Temperature which is controlled by an external bath and measured by a thermocouple in the column,

There are numerous ways to estimate the impact of uncertainty in primary measurements on the final calculated results. Propagation of error is one such technique which calculates the most-probable error bounds on the final results. If a property X is calculated by a mathematical expression;

$$X = f(Y, Z, \dots) \tag{A.1}$$

Where the measurements Y, Z, and so on are subject to uncertainty of DY, DZ, then the uncertainty DX can be calculated as [62];

$$\Delta X = \sqrt{\left\{\left(\frac{df}{dY}\right)\Big|_Z * \Delta Y\right\}^2 + \left\{\left(\frac{df}{dZ}\right)\Big|_Y * \Delta Z\right\}^2} \dots \tag{A.2}$$

APPENDIX B

Calibration Data for Gas Chromatograph

The composition of the bulk gas phase at equilibrium in binary adsorption experiments using a volumetric system is analyzed using a gas chromatograph. The following section summarizes the results of a typical GC calibration. Other binary mixtures while doing actual experiments would yielded similar results.

The K-factor for any GC output is given by Equation (3.6) and is related to the composition of the mixture being analyzed through Equation (3.8). The following Table B.1 lists the results of a typical GC calibration for a binary mixture of CH_4+N_2 at constant injection pressure of 15 psi and by varying gas phase compositions. The column y_{CH4} indicates the actual (as measured from material balances) mole-fraction of the methane in the calibration gas mixture. The third column indicate the percentage area fraction under the peaks for the gas mixture that is calculated for.

Table B.1. Results of GC Calibration for CH_4+N_2 Mixture on Silicalite

Y_{CH4}	K-factor (mean)	$\%A_{CH4}$	Std. Dev	Std. Dev+	Std. Dev-
7.0%	1.195	5.9%	0.009	1.205	1.186
10.0%	1.200	8.5%	0.015	1.215	1.185
30.0%	1.299	24.8%	0.002	1.301	1.297
50.0%	1.347	42.6%	0.001	1.348	1.346
70.0%	1.370	63.0%	0.011	1.382	1.358
90.0%	1.396	86.6%	0.010	1.406	1.386

APPENDIX C

Matlab Code for Binary Prediction from IAST

```
%%%%%%%%%%%%%%%%%%%%%%%%%%%%%%%%%%%%%%%%%%%%%%%%%%%%%%%%%%%%%%%%%%%%%%%%%


% prahar.m
clc % clear screen
% transfer parameters

global y1 P k b c d s12 s21
fprintf ('\n *** Ideal Adsorbed Solution Theory *** \n');


k1=5.022; % CH4--35 °C,
b1=0.98;
c1=-0.457;
d1=0.32;

k2=6.361324; % N2--35 °C
b2=1.278962;
c2=-0.72605;
d2=0.347659;

% set parameters
k = [k1; k2];
b = [b1; b2];
c = [c1; c2];
d = [d1; d2];

% set known conditions
y1 = 0.01; % an initial value
P = 1; % just an initial value

% set problem
fun = 'prahar_f';
n1o = 0.01;
n2o = 0.01;
x1 = 0.01;
x2 = 1 - x1;
P1o = 10;
P2o = 1;

% set initial guess
x0 = [x1; n1o; n2o; P1o; P2o];

% % uncomment to check !
% F0 = feval(fun, x0)
% Fnorm = norm(F0)
```

```
options =optimset('Display','off');

% solve for a given y1 value
y1_initial = y1;
y1_final = 1.0;
y1_values = linspace (y1_initial, y1_final, 20)';

% solve for a given P value
P_initial = P;
P_final = 600;
P_values = linspace (P_initial, P_final, 20)';

% initialize
Results = [];
for e = 1:1:length(y1_values)
y1=y1_values(e);
for counter = 1:1:length(P_values)
P = P_values(counter);
x = fsolve (fun, x0, options);
F = feval(fun, x);
Fnorm = norm(F);

% recover variables
x1 = x(1);
x2 = 1-x1;
n1o = x(2);
n2o = x(3);
P1o = x(4);
P2o = x(5);

% total amount adsorbed
nt= n1o*n2o/(x1*n2o+x2*n1o);

% % selectivity
 s12= x1*(1-y1)/(x2*y1); % s1,2
 s21= (x2*y1)/x1*(1-y1); % s2,1

Results = [Results; P, y1, nt, x1, n1o, P1o, x2, n2o, P2o, s12, s21,
Fnorm];

% reset initial condition
x0 = x;
end
x0=[0.01;0.1;0.1;10;1]; % the initial assumption
end


figure(1)% 3D Total amount adsorbed plot, Nt
display (Results);
x=Results(:,1);y=Results(:,2);z=Results(:,3);

scatter3(x,y,z) % 3-D scatter plot
xlabel('Pressure (kPa)')
ylabel('Gas fraction of CH4 y1')
zlabel('Total amount adsorbed nt (mol/kg)')
```

```
figure(2) %3D selectivity plot, S1/2
display (Results);
x=Results(:,1);y=Results(:,2);z=Results(:,10);

scatter3(x,y,z) % 3-D scatter plot
xlabel('Pressure (kPa)')
ylabel('Gas fraction of CH4 y1')
zlabel('Selectivity of methane over nitrogen, S1/2')



%%%%%%%%%%%%%%%%%%%%%%%%%%%%%%%%%%%%%%%%%%%%%%%%%%%%%%%%%%%%%%%%%%%%%%%%%



% PRAHAR_f
% function for IAST
% PRAHAR S VAIDYA
function F = prahar_f(x)
global y1 P k b c d
% recover parameters
k1 = k(1);
k2 = k(2);
b1 = b(1);
b2 = b(2);
c1 = c(1);
c2 = c(2);
d1 = d(1);
d2 = d(2);
% initialize
F = zeros(size(x));
% recover variables
x1 = x(1);
x2 = 1 - x1;
n1o = x(2);
n2o = x(3);
P1o = x(4);
P2o = x(5);
F(1) = y1 - x1*P1o/P;
F(2) =(1-y1)-(1-x1)*P2o/P;
e1 = k1 + b1*n1o + c1*n1o^2+d1*n1o^3;
F(3) = P1o - n1o * exp(e1);
e2 = k2 + b2*n2o + c2*n2o^2+ d2*n2o^3;
F(4) = P2o - n2o * exp(e2);
ee1 = n1o + b1/2 * n1o^2 +2*c1/3 * n1o^3 +3*d1/4 * n1o^4;
ee2 = n2o + b2/2 * n2o^2 +2*c2/3 * n2o^3 +3*d2/4 * n2o^4;
F(5) = ee1 - ee2;
return
end



%%%%%%%%%%%%%%%%%%%%%%%%%%%%%%%%%%%%%%%%%%%%%%%%%%%%%%%%%%%%%%%%%%%%%%%%%
```